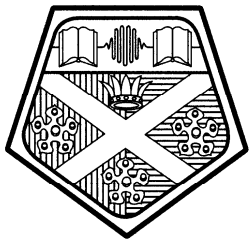

University of
Strathclyde

DEPARTMENT OF PURE AND APPLIED CHEMISTRY

ADSORPTION AND DESTRUCTION OF METHYLENE BLUE AND ACID ORANGE 7 ON TiO_2

by

CHRISTOPHER O'ROURKE

A thesis presented in fulfilment of the requirements for the degree of Master of Philosophy.

JULY 2011

Copyright Statement

This thesis is the result of the author's original research. It has been composed by the author and has not been previously submitted for examination which has led to the award of a degree.

Signed: _____Date:_____

Christopher O'Rourke

Acknowledgements

I would like to thank Professor Andrew Mills for all his support throughout this thesis, especially for his help in generating the in-house macro used to perform the adsorption calculations. I would also like to thank Professor Bourikas for many useful discussions relating to the MUSIC and CD-MUSIC models of the metal oxide-electrolyte interface.

Contents

Abstract

The observed adsorption of methylene blue, MB^+, and acid orange 7, $AO7^-$, on P-25 titania over a range of pH values, pH 2 – 11 and pH 2 – 8 respectively, is reported and the results fitted to a charge distribution, multisite complexation, i.e. CD-MUSIC, model, modified for both monomer and aggregated dye adsorption and (for aggregates) co-adsorption of hydroxyl ions. For the MB^+ system the model predicts that both the apparent dark Langmuir adsorption constant, K_L, and the number of adsorption sites, n_o, increase with increasing pH, and are negligible below pH 6 – 7. For the $AO7^-$ system the model predicts that both, K_L, and, n_o, increase with decreasing pH, and are negligible above pH 6. An adsorption study of $AO7^-$ using paste films where, K_L, and, n_o, were experimentally determined generated similar trends to those calculated for P-25 powder.

The rate of bleaching of MB^+, photocatalysed by titania using UV light, increases over the pH range 4 – 11 in much the same way the amount of adsorbed MB^+, $[MB^+]_{ads}$, increases, indicating that the rate-determining step involves direct hole oxidation of adsorbed MB^+. In contrast, at pH 2, the rate of UVA dye photobleaching appears unduly high but is due to an additional reductive, as well as the usual oxidative, bleaching processes. The initial rate of bleaching of MB^+ via a visible light-driven, dye sensitised process, measured at different pHs correlates with the associated CD-MUSIC-calculated values of $[MB^+]_{ads}$, indicating that only dye molecules that are in direct contact with the surface can undergo photodegradation via a dye-sensitised route.

Although $AO7^-$ adsorption on P-25 titania and paste films is insignificant above pH 6 and increases almost linearly and markedly below this pH, the measured initial rate of bleaching of $AO7^-$, photocatalysed by titania using UV appears to only increase modestly (< factor of 2) over the pH range 2 – 10 studied. In contrast, the rate of bleaching of $AO7^-$ via a visible light driven, dye-sensitised process, shows some correlation with the amount of dye adsorbed. Such a correlation follows from the basic assumption that only dye molecules that are in direct contact with the surface can undergo photodegradation via a dye-sensitised route.

The relevance of this work to the removal of dyes and testing of the efficiency of photocatalytic films is discussed briefly.

1 Introduction

1.1 Semiconductor Photocatalysis

Semiconductor photocatalysis is a significant area of research which has led to various useful commercial products, such as self-cleaning glass (Activ^{TM} Glass), tiles and paint, in which the role of semiconductor photocatalysis is to mineralise noxious organic pollutants. UV light ($\lambda > E_{bg}$) of energy greater than the bandgap energy (E_{bg}) between the valence and conduction band of the photocatalyst, is able to promote valence band electrons into the conduction band creating electron hole pairs in the semiconductor. O_2^- is formed when oxygen reacts with the photogenerated electrons and the holes react with surface hydroxyl groups to produce OH• radicals. It is these radicals that attack the organic molecules (pollutants) and oxidise them to species like CO_2, H_2O etc. Figure 1.1 below shows a schematic of these processes.[1]

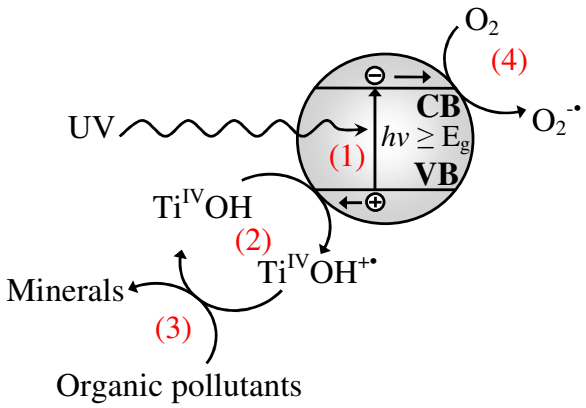

Figure 1.1 Schematic illustration of the major processes associated with the photomineralisation of organics by oxygen, sensitised by a titania semiconductor particle photocatalyst. (1) Ultra-bandgap light generates electron hole pairs. (2) The photogenerated holes which move to the surface can react with the hydroxyl groups present, which generates OH• radicals. (3) These radicals can then oxidise organic pollutants to its mineral form. (4) The electrons which make it to the surface can react with adsorbed oxygen to generate superoxide.

Another possible route of destruction of organics, and of particular relevance to dyes, is via a photosensitised process, where the dye is excited by visible light and injects an electron into the conduction band of the semiconductor to produce an oxidised dye radical. These radicals are unstable and capable of decomposing to bleached products.[2] The injected electron can also promote this process via its subsequent reaction with O_2 to produce a number of different oxidising species, such as hydrogen peroxide. This process is illustrated below in figure 1.2.

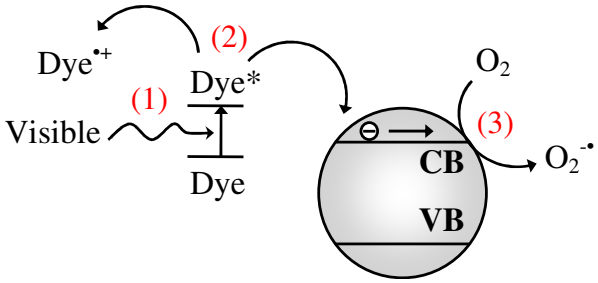

Figure 1.2 Schematic illustration of the major processes associated with the photosensitised destruction of dyes. (1) Electronically excited state of the dye produced by the absorption of visible light. (2) The excited dye injects an electron into the conduction band of the semiconductor to produce an oxidised dye radical which can then decompose to give bleached products. (3) The injected electron can react with oxygen to generate superoxide.

Usually, using UVA light, the photobleaching of dyes is considered to progress mainly through the photocatalytic mineralisation route, rather than the above dye-sensitisation route.

1.1.1 Uses of Semiconductor Photocatalysis

1.1.1.1 Environmental Uses

Approximately 15% of the total world production of dyes is released into the ecosystem as waste.[3] Degradation products of azo-dyes for example are carcinogenic[4] and therefore harmful to the environment, therefore, semiconductor photocatalysis along with some other water-purification methods i.e. biodegradation, chlorination and ozonation are becoming more important since environmental

standards are becoming more stringent (ISO 14001, October 1996)[5]. Semiconductor photocatalysis is an appealing method as it can utilise the light from the sun and it does not involve treating the water with lots of chemicals. In contrast, chemical processes for dye removal can cause secondary pollution and biological degradation can be slow and in some cases, inefficient.[3,6]

1.1.1.2 Commercial Uses

Activ^{TM} glass is self cleaning glass used in windows. The glass has a very thin layer of TiO_2 particles (15 nm) on the side of the glass that is facing outwards. When organic matter begins to collect on the surface of the window, the UV light from the sun will activate the TiO_2 particles and begin to mineralise the matter. The surface then becomes hydrophilic, thus, when it rains all the dirt will be washed away more efficiently than conventional glass in windows since the water will not just form droplets on the surface. The same principle applies to the self-cleaning paint and tiles.[7]

1.1.2 Assessing Photocatalytic Activity of Titania Films

Dyes such as methylene blue and acid orange 7 (shown in figure 1.3(a) and (b) respectively) are very useful reagents when assessing photocatalytic activity, due to the clear colour change observed as the dye is destroyed. This, therefore, gives a good visual demonstration of the working of a photocatalytic material which can be monitored using spectroscopic methods.

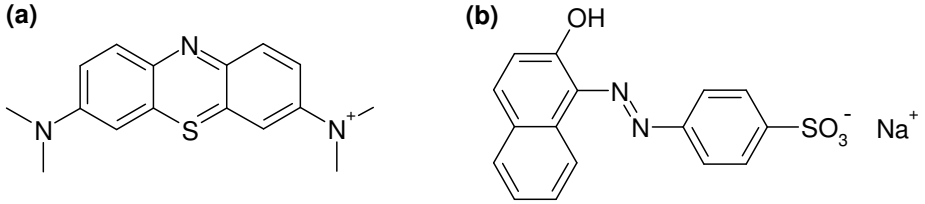

Methylene blue Acid Orange 7

Figure 1.3 The chemical structures of **(a)** methylene blue and **(b)** acid orange 7.

Thus, not surprisingly, the International Organisation of Standardisation have recently published a method for determining the photocatalytic activities of surfaces by monitoring the degradation of methylene blue in solution under artificial UV light (ISO 10678:2010).[8] A surface sample of accurately known geometric area is prepared by firstly cleaning it and irradiating under intense UV light for at least 24 hours. The sample is then conditioned in a solution of methylene blue in water (20 μmol dm^{-3}) for a minimum of 12 hours before transferring into the methylene blue/water test solution (10 μmol dm^{-3}). Figure 1.4 shows the apparatus setup used to perform the irradiations. Figure 1.4(a) shows the use of a cylinder to hold the test solution in contact with the sample surface and figure 1.4(b) shows the samples submerged in test cells. The solution is covered with a glass pane and irradiated from above with an accurately known intensity of UV light and the depletion of the colour of the solution is monitored at regular intervals using UV/Vis spectroscopy. This is done either online, i.e. directly through the test solution or small volumes can be removed, measured and subsequently returned back into the test solution. A blank (dark) experiment is also performed using a UV filter under the same conditions.

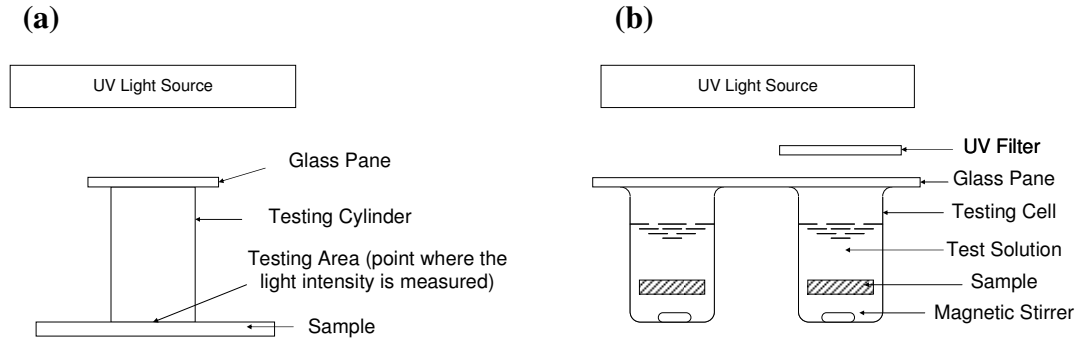

Figure 1.4(a) Schematic diagram of a measuring device with a test cylinder as one test method. **(b)** Schematic diagram of a measuring device with a test cell for another test system (but this time stirred).

It is clear from the literature and the above ISO test that methylene blue is currently a very important dye for assessing photocatalytic activity of films and powders.

1.2 Previous Semiconductor Photocatalysis Work Using Dyes

An in depth review carried out by Rajeshwar *et al.*[9] on photocatalytic treatment of organic dyes notes that the first instance of dye bleaching in the presence of an inorganic semiconductor when irradiated, appears in the early 70's, in which methylene blue was reported to be reduced to its leuco form which is colourless.[10] Methanol was used as a solvent in this study which can act as a sacrificial electron donor (SED). Methylene blue is reduced in the following manner as shown in figure 1.5. The semiconductor is excited by the UV light which produces electron-hole pairs on the surface. A sacrificial electron donor, such as methanol, effectively 'mops up' the holes and therefore allows the photogenerated electrons on the semiconductor surface to subsequently reduce the methylene blue to leuco-methylene blue.

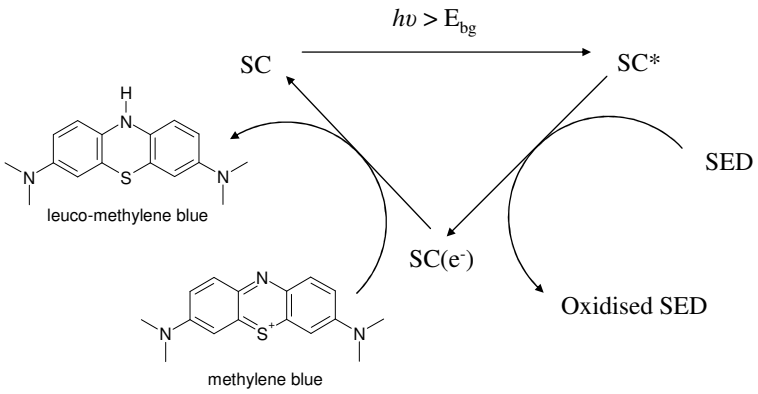

Figure 1.5 Schematic illustration of the processes associated with the conversion of methylene blue to leuco-methylene blue. The semiconductor (SC) is excited by the UV light which produces electron-hole pairs on the semiconductor surface. The sacrificial electron donor 'mops up' the holes by giving up electrons, thus being oxidised. This then allows the generated electrons on the surface to reduce the methylene blue to leuco-methylene blue.

This work was followed by a large number of studies where deliberate attempts were made to photochemically destroy many different organic dyes via a photo-oxidative mineralisation route. One of the most commonly used semiconductors used in such work is Degussa P-25 which is composed of 75% anatase and 25% rutile and has a high specific surface area of 50 m^2 g^{-1}. Whilst methylene blue (a cationic dye) is one of the most well used dyes in this area of chemistry, acid orange 7 (an anionic dye) is

also very popular. As well as studying the destruction of organic dyes, there are also many studies of the adsorption of dyes on semiconductor surfaces and how this affects the photo-destruction rates.

The surface of the semiconductor photocatalyst under test is usually pH, background electrolyte and ionic strength dependant. P-25 has a point of zero charge (p.z.c.) of ca. pH 6.6 which means that below this value, the surface will be positively charged and so repel cationic species, such as methylene blue, but will attract cationic species at pHs > p.z.c. This simple electrostatic model helps explain the observation made in the review by Rejeshwar *et al.*[9], that 'cationic dyes bind on semiconductor surfaces at pH values greater than the p.z.c., whilst anionic dyes show the opposite trend'.

The initial pH of the reaction solution for photocatalytic activity studies are therefore important when using a charged test reagent such as methylene blue or acid orange 7. The observed kinetics of photocatalysis are further complicated by the fact that the photobleaching process often generates acidic species which can alter the pH of the test solution as the photoreaction proceeds.[2] As most studies are performed at 'natural pH', this can be of particular relevance as the solution pH can shift considerably during the course of irradiation if, for example, mineral acids are generated during the course of the reaction. The complete photomineralisation processes by semiconductor photocatalysis of methylene blue and acid orange 7 are summarised by the reaction equations 1.1 and 1.2, respectively.

$$C_{16}H_{18}N_3SCl + 25½O_2 \xrightarrow[h\upsilon \geq E_{bg}]{\text{semiconductor}} HCl + H_2SO_4 + 3HNO_3 + 16CO_2 + 6H_2O \quad (1.1)$$

$$C_{16}H_{11}N_2NaO_4S + 21O_2 \xrightarrow[h\upsilon \geq E_{bg}]{\text{semiconductor}} 16CO_2 + 2HNO_3 + NaHSO_4 + 4H_2O \quad (1.2)$$

The destruction kinetics of such semiconductor/dye-water systems is usually found to follow an apparent first order with respect to the concentration of methylene blue and acid orange 7, which is in agreement with the generally observed Langmuir–

Hinshelwood kinetics. Equation 1.3 shows the Langmuir–Hinshelwood kinetic equation;

$$r = \frac{dC_{eq}}{dt} = \frac{kK_L C_{eq}}{1 + K_L C_{eq}} \tag{1.3}$$

where, r, is the rate of bleaching, k_{max}, is the rate constant, C_{eq}, is the equilibrium concentration of dye solution and, K_L^*, is the apparent Langmuir adsorption constant. At low concentrations the rate of photobleaching becomes proportional to the concentration of methylene blue as shown in equation 1.4.

$$r = \frac{k_{\max} K_L^* C_{eq}}{1 + K_L^* C_{eq}} \approx k_{\max} K_L^* C_{eq} = k_{app} C_{eq} \tag{1.4}$$

And so the observed kinetics become 1st order with respect to the concentration of the dye.

The apparent Langmuir adsorption constant, K_L^*, and rate constant, k_{max}, can be determined from a double reciprocal plot of the measured destruction rates vs. dye concentration using the linear transform of equation 1.3 as shown;

$$\frac{1}{r} = \frac{1}{k_{\max}} + \left(\frac{1}{k_{\max} K_L^*} \right) \frac{1}{C_{eq}} \tag{1.5}$$

where, the reciprocal of the y-intercept is equal to the rate constant, k_{max}. Once, k_{max}, is known, K_L^*, can be obtained from the value of the gradient as shown in equation 1.6.

$$K_L^* = \frac{1}{Gradient \text{ x } k_{\max}} \tag{1.6}$$

In general, it is found that the apparent Langmuir adsorption constant, K_L^*, is related to (but not equal to (usually much greater than)) the dark Langmuir adsorption constant K_L. One way to obtain the dark Langmuir adsorption constant, K_L, is to

perform dark adsorption measurements. In the case of dyes, this involves equilibrating various concentrations of dye solution with the semiconductor. The semiconductor can either be a dispersed powder in solution or coated on a support such as glass. Solutions are left to equilibrate for periods as short as 30 minutes to several hours, depending on the kinetics of the adsorption process. The concentration of the dye in the supernatant is then measured to establish how much dye had adsorbed on the semiconductor surface.

Assuming a Langmuir adsorption model, the fractional coverage, θ, varies as;

$$\theta = \frac{n_{ads}}{n_0} = \frac{K_L C_{eq}}{1 + K_L C_{eq}} \tag{1.7}$$

where, n_{ads}, is the concentration of dye adsorbed, n_0, is the total number of adsorption sites, C_{eq}, is the concentration of the dye solution and, K_L, is the dark Langmuir adsorption constant for the dye.

Rearranging equation (1.7) then gives;

$$\frac{1}{n_{ads}} = \frac{1}{n_0} + \left(\frac{1}{n_0 K_L} \right) \frac{1}{C_{eq}} \tag{1.8}$$

This linear transform of equation 1.7 allows, n_o, and, K_L, to be determined from a double reciprocal plot of the amount of dye adsorbed, n_{ads}, vs. equilibrium dye concentration, C_{eq}. The reciprocal of the value where the line cuts the y-axis is therefore, n_o, and the adsorption constant, K_L, can be determined from the gradient of the line and the determined value for, n_o.

This thesis will concentrate on the adsorption and destruction of methylene blue and acid orange 7 on P-25 and the effect of pH. Tables 1.1 – 1.4 show a selected few key papers in the literature concerning the adsorption and destruction of methylene blue and acid orange 7 using P-25 as the semiconductor. Tables 1.1 and 1.2 list some

previous adsorption studies for methylene blue and acid orange 7 respectively. The results found in these papers will be discussed later on in the introduction and results sections of the experimental chapters.

Table 1.1 Adsorption studies for methylene blue on P-25.

Semiconductor/ Semiconductor Support	pH Range Studied	[MB]/ µmol dm^{-3}	[TiO_2]/ mg dm^{-3}	Comment(s)	Ref.
P-25/ Aqueous suspension	3 - 9	13 - 80	2500	$K_L = 6.25 \times 10^3\ M^{-1}$ (at natural pH)	3
P-25/ Aqueous suspension	3 - 9	13 - 80	2500	$K_L = 6.65 \times 10^3\ M^{-1}$ (at natural pH)	11
P-25/ Non-woven inorganic fibers	3 - 9	84.2	500	Shows $[MB]_{ads}$ increases with increasing pH	12
P-25/ Aqueous suspension	1.85 - 5.32	100	2000	$K_L^* = 2 \times 10^4\ M^{-1}$ (at pH 3.85)	13
P-25/ Aqueous suspension	3.2	6.6 - 36	667	$K_L^* = 1.79 \times 10^4\ M^{-1}$	14
P-25/ Aqueous suspension	2	10	100	Both monomeric and dimeric forms of the dye found to adsorb to the same extent	15
P-25/ Film coated on a borosilicate glass spiral	Natural	1 - 100	75 mg coated	$K_L = 2.98 \times 10^4\ M^{-1}$	16

K_L^* = 'apparent' K_L value from photocatalysis studies and equation 1.6.

Table 1.2 Adsorption studies for acid orange 7 on P-25.

Semiconductor/ Semiconductor Support	pH Range Studied	[AO7]/ µmol dm^{-3}	[TiO_2]/ mg dm^{-3}	Comment(s)	Ref.
P-25/ Aqueous suspension	6	100 - 1000	2000	$K_L = 1.8 \times 10^4$ M^{-1} FTIR adsorption study.	17
P-25/ Aqueous suspension	2 - 10	100 - 3000	2000 and 750	Model AO7 adsorption using a CD-MUSIC model. Shows $[AO7]_{ads}$ is negligible above pH 7 and increases as the pH is lowered. FTIR adsorption study.	18
TiO_2 (anatase) TiO_2 (rutile)	3.5	0 - 5000	1500	$K_L = 4.37 \times 10^3$ M^{-1} (anatase) $K_L = 5.46 \times 10^3$ M^{-1} (rutile)	19
P-25/ Aqueous suspension	2.5 - 7.5	143	500	Isotherms show $[AO7]_{ads}$ increases as pH is decreased. Shows K_L also increases as pH is decreased.	20
P-25/ Aqueous suspension	5	500	5000	$K_L = 2.48 \times 10^2$ M^{-1} (at pH 5)	21
P-25/ Aqueous suspension	2 - 12	0 - 228	2000	Adsorption of AO7 strongly depends on pH. At basic solutions, adsorption is negligible, whereas at low pH's large amounts of dye is adsorbed.	22

Table 1.3 Photodegradation studies for methylene blue on P-25.

Semiconductor/ Semiconductor Support	Irradiation Source	pH Range Studied	[MB]/ µmol dm^{-3}	[TiO_2]/ mg dm^{-3}	Comment(s)	Ref.
P-25/ Aqueous suspension	125 W Hg mercury lamp with filters ($\lambda > 290$ nm & $\lambda > 340$ nm)	3 - 9	72	2500	Follows apparent first order kinetics. Shows faster destruction rates as the pH is increased. Identified intermediate products by GC/MS and LC/MS.	3
P-25/ Aqueous suspension	125 W Hg mercury lamp with filter ($\lambda > 290$)	3 - 9	84.2	500	Increase in photocatalytic activity at basic pH is mainly attributed to an increase in the surface density of TiO^- adsorption sites.	6
P-25/ Aqueous suspension	75 W Hg mercury lamp	1.85 - 5.32	100	2000	Follows apparent first order kinetics. Looked at the N-demethylation of MB. Assessed how rate is dependant on temperature, pH, dissolved [O_2], [MB] and light intensity. Found that rate increases as the pH is increased from pH 1.85 to pH 4.	13
P-25/ Aqueous suspension	125 W Hg mercury lamp	2.8 - 8.0	10	267	Shows an increase in the rate of photobleaching as the pH is increased up to pH7 and then levels off.	14

Table 1.4 Photodegradation studies for acid orange 7 on P-25.

Semiconductor/ Semiconductor Support	Irradiation Source	pH Range Studied	[AO7]/ µmol dm^{-3}	[TiO_2]/ mg dm^{-3}	Comment(s)	Ref.
P-25/ Aqueous suspension	450 W Xe-arc lamp	5.8	850	750	Identified destruction intermediates. Seen that the pH of the test solution decreases as the destruction proceeds due to the formation of acidic intermediates.	2
P-25/ Aqueous suspension	450 W Xe-arc lamp	2 - 12	856	750	Found that degradation of AO7 is much faster in basic solution cf. neutral and acidic	22
Various	Various	--	--	--	Review of the literature on the identification of by-products from degradation studies	23
P-25/ Aqueous suspension	175 W metal halide lamp/ 2 x 6W UV lamps	5.6	114	2000	Found no significant relationship between $[AO7]_{ads}$ and destruction rates.	24

1.2.1 Methylene Blue Adsorption

Methylene blue is a cationic dye which can be readily adsorbed onto titania in alkaline conditions, i.e. pH > 7. The structure of methylene blue is shown below in figure 1.6.

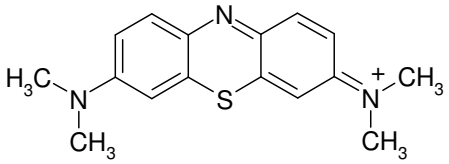

Figure 1.6 Methylene blue monomer.

This is due to the fact that, when the pH is greater than the titania's p.z.c. (ca. pH 6.6) the following equilibrium is setup;

$$Ti\text{-}OH + OH^- \rightleftharpoons TiO^- + H_2O \qquad (1.9)$$

When the titania is in an alkaline environment (i.e. pH > p.z.c.), its surface negative, thus, making it favourable for cationic materials such as methylene blue to adsorb.

Work carried out by Houas *et al.*[3] and Lachheb *et al.*[11] shows that for 'staining' solutions containing 5 – 30 mg dm^{-3} of methylene blue, the time taken for the dye adsorption equilibrium to be reached was no longer than 1 hour when using P-25 titania powder. Their results are shown in figure 1.7, where, q, is the weight of methylene blue adsorbed per gram of photocatalyst at a given soaking time.

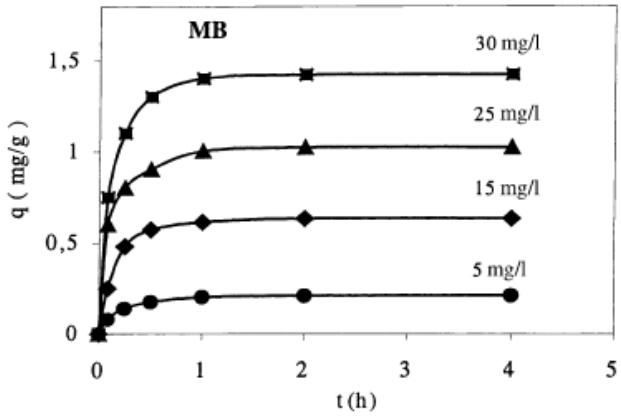

Figure 1.7 Adsorption isotherms of methylene blue onto mesoporous titania at pH 9.[3]

From figure 1.7, the amount of methylene blue adsorbed, n_{ads}, can be determined from the maximum value, i.e. where the isotherm plateaus. The value of, q, at this point can be converted to, n_{ads}, by multiplying the value by the mass of photocatalyst to give the mass of dye in milligrams. This is then divided by the molecular weight of the dye (Mol.Wt. MB^+ = 284.12 g mol^{-1} (without Cl^- or H_2O)) to give the number of moles adsorbed.

A plot of $1/n_{ads}$ vs. $1/C_{eq}$, where, C_{eq}, is the equilibrium concentration of the solution, can yield values for the maximum number of adsorption sites, n_o, and the Langmuir adsorption constant, K_L as described in section 1.2. Figure 1.8 shows the reciprocal plot using the data from figure 1.7.

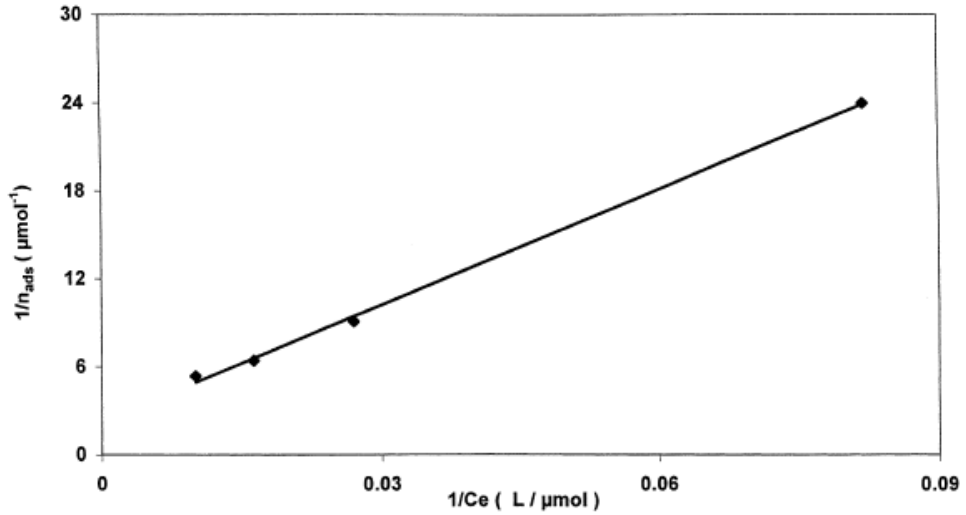

Figure 1.8 Langmurian linear transform for the data in figure 1.7, revealing a K_L of 6.25 x 10^3 M^{-1}.[3]

From the results of Houas *et al.*[3] shown in figures 1.7 and 1.8, the adsorption constant, K_L, for methylene blue was calculated to be 6.25 x 10^3 M^{-1} at natural pH and the value of the total number of adsoption sites, n_o, was calculated to be approximately 8.6 µmol g^{-1}. Houas *et al.*[3] found this value of K_L to be 'in good agreement with that of other pollutants readily soluble in water'.[3]

These results are not however readably comparable with many others in the literature[11-16] which used a different source of TiO_2 and different reaction conditions (most notably pH). Thus, it is not surprising that Rajeshwar *et al.*[7] noted the reported values of, K_L, are generally in the 10^2 – 10^5 M^{-1} range. However, even from this information it is clear that there is a strong interaction of the dye and the surface of the semiconductor. Interestingly, it seems there are no studies in the literature for methylene blue that observe the trends in adsorption constant, K_L, and the maximum number of adsorption sites, n_o, as a function of pH. However, it can be assumed that these values will increase as the pH is increased from the semiconductors p.z.c.

The following data shown in figure 1.9 by Houas *et al.*[3] demonstrates the fact that if the pH is increased, the quantity of methylene blue adsorbed, n_{ads}, increases because the surface of the titania becomes more negatively charged at high pH values as previously shown in equation 1.9.

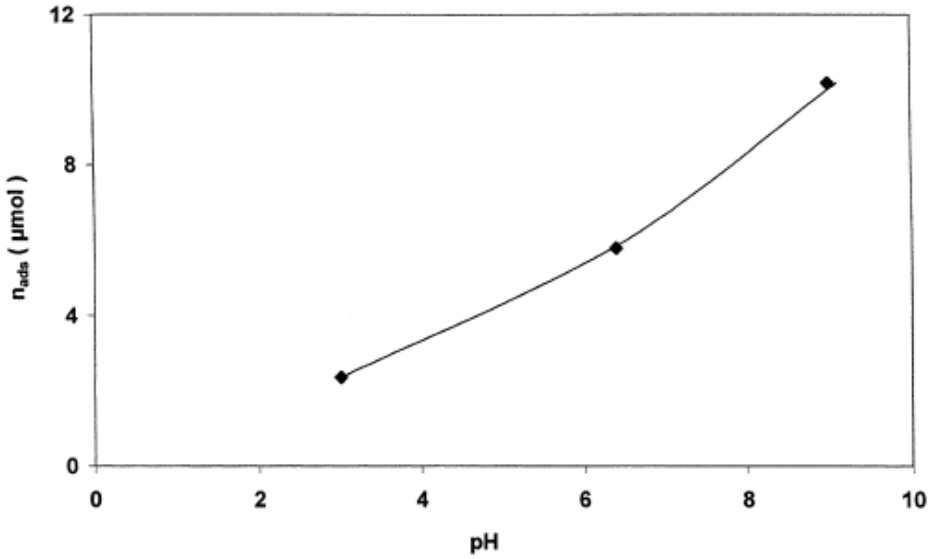

Figure 1.9 Variations of methylene blue adsorption at three different pH values.[3]

It is slightly surprising that these workers found, n_{ads}, to still be appreciable at pH < p.z.c.

1.2.1.1 Photocatalytic Destruction of Methylene Blue

The photocatalytic destruction of methylene blue is achieved by bringing it into contact with a photocatalyst e.g. titania, and irradiating it with a UV light source. The complete destruction/mineralisation is summarised by the following equation;

$$C_{16}H_{18}N_3SCl + 25½O_2 \xrightarrow[h\upsilon \geq E_{bg}]{\text{semiconductor}} HCl + H_2SO_4 + 3HNO_3 + 16CO_2 + 6H_2O \qquad (1.10)$$

Figure 1.10 below shows the proposed *N*-demethylation steps by Zhang *et al.*[13] during the photodegradation of methylene blue, below which, the chemical structures of the *N*-demethylated intermediates at each step and their associated colour are shown. Methyl groups are weak electron donor substituents and can therefore aid the attack of methylene blue by electrophilic OH• radicals or photogenerated holes.

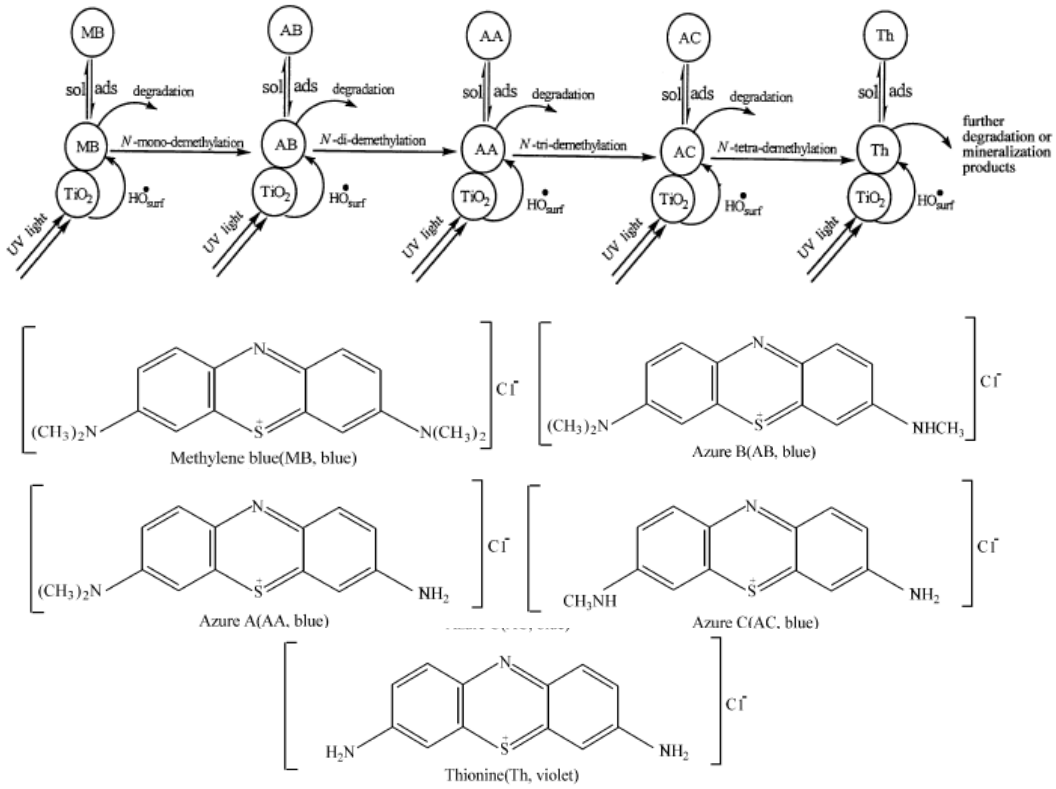

Figure 1.10 Scheme depicting the N-demethylation of methylene blue and the dynamic equilibrium of methylene blue and N-demethylated species between the bulk solution and the TiO_2 particle surface during the photodegredation of methylene blue.[13]

The demethylation of methylene blue causes a blue-shift in the absorption spectrum upon irradiation, as each new demethylated product has a slightly different maximum wavelength, λ_{max}, from methylene blue. Figure 1.11 shows this shift in the maximum wavelength as the irradiation proceeds.

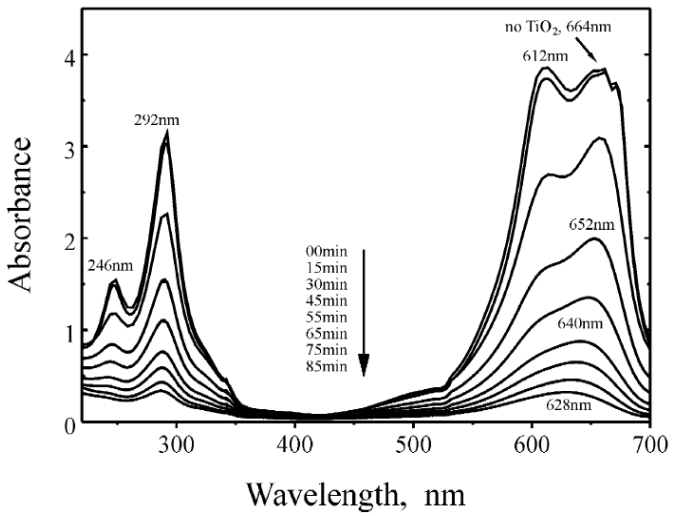

Figure 1.11 Spectral changes of methylene blue in aqueous TiO_2 suspensions under UV illumination.[13]

Research by Houas *et al.*[3] brought about the following proposed degradation pathway for methylene blue as shown in figure 1.12. They analysed the intermediate products during degradation using gas chromatography/mass spectroscopy (GC/MS) and liquid chromatography/mass spectroscopy (LC/MS). The intermediates were then identified by comparison to commercial standards and by interpretation of their fragment ions in the mass spectra. The initial step in the destruction of methylene blue is the cleavage of the C–S^+=C functional group by OH• radicals. Going from C–S^+=C to C–S(=O)–C requires conservation of the double bond conjugation. This therefore induces the opening of the central ring. An alternative rearrangement of the phenothiazine structure is shown in figure 1.13. Although not detected in their study, Houas *et al.*[3] suggested that generated sulfoxide could be attacked by a second OH• radical to form the sulfone and cause the dissociation of the two outer rings. Further attack of OH• radicals create the subsequent sulfonic acid and phenolic metabolites shown in figure 1.12, before being eventually completely mineralised to H_2O, CO_2, etc.

From the pathway shown in figure 1.12, it can be expected that the colour of the methylene blue will disappear a considerable time before the bulk of the organic

matter is completely photomineralised, although Matthews[16] demonstrated that eventually and not too long after the dye is bleached, this process is achieved, as shown in figure 1.14 which compares the disappearance of colour with the generation of CO_2.

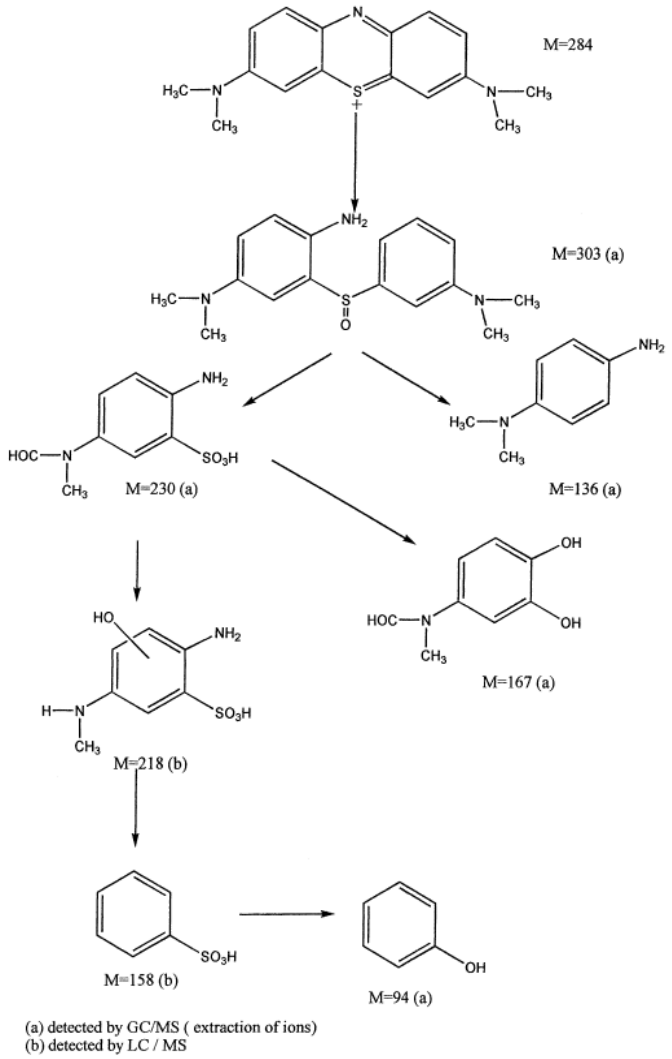

Figure 1.12 Photocatalytic degradation pathway of methylene blue.[3]

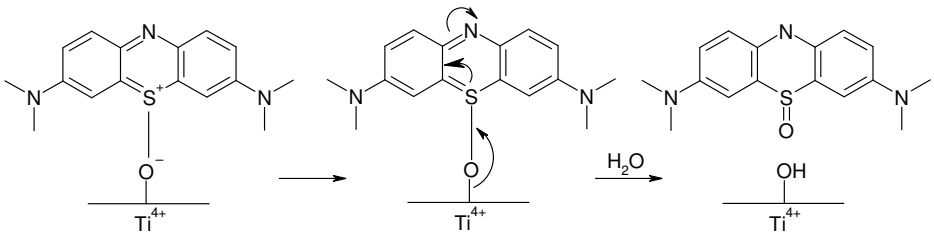

Figure 1.13 Electronic reorganisation during the passage of methylene blue adsorbed to the sulfoxide form.[3]

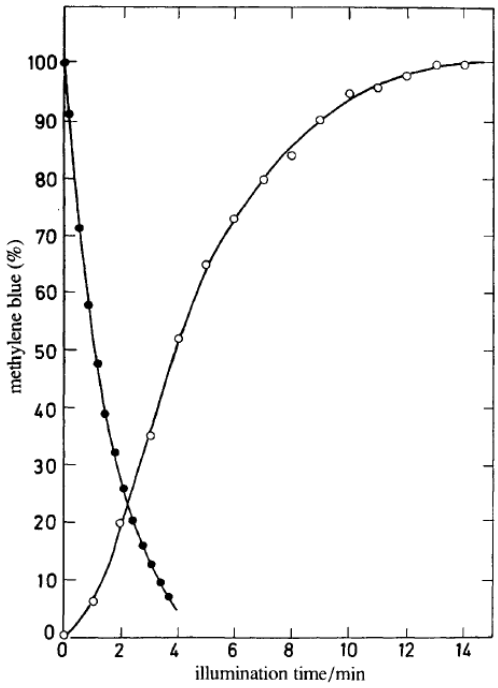

Figure 1.14 Comparison of methylene blue disappearance (●) and CO_2 appearance (○) from a 40 cm^3 10 μmol dm^{-3} solution at pH 3, irradiated using a 20 W NEC blacklight blue fluorescent tube.

1.2.1.2 Kinetics of Methylene Blue Photobleaching

Most literature deals with the destruction of dyes in solution i.e. the semiconductor/dye-water system. The kinetics of this system is usually found to be simple first order with respect to the concentration of methylene blue. The results of Houas *et al.*[3] kinetic study of the disappearance of methylene blue is shown in figure 1.15. The inserted graph shows the depletion of the methylene blue concentration as a function of time. The photolysis data in the inserted graph in figure 1.15 shows very little colour loss in the absence of titania which indicates that methylene blue is UV stable. They found the disappearance to follow apparent first order kinetics in agreement with generally observed Langmuir-Hinshelwood kinetic model under the condition of $K_L^*[MB] < 1$ (see equation 1.4). Figure 1.15 shows the first order transforms of the disappearance of methylene blue. Houas *et al.*[3] studied the destruction of methylene blue using two wavelengths i.e. 290 nm and 340 nm. Their results show that the far UV light (290 nm) is more efficient at destroying the dye as

this light is more strongly absorbed by the semiconductor. The rate constants calculated from the slopes in figure 1.15 are 0.06 min^{-1} and 0.025 min^{-1}, respectively.

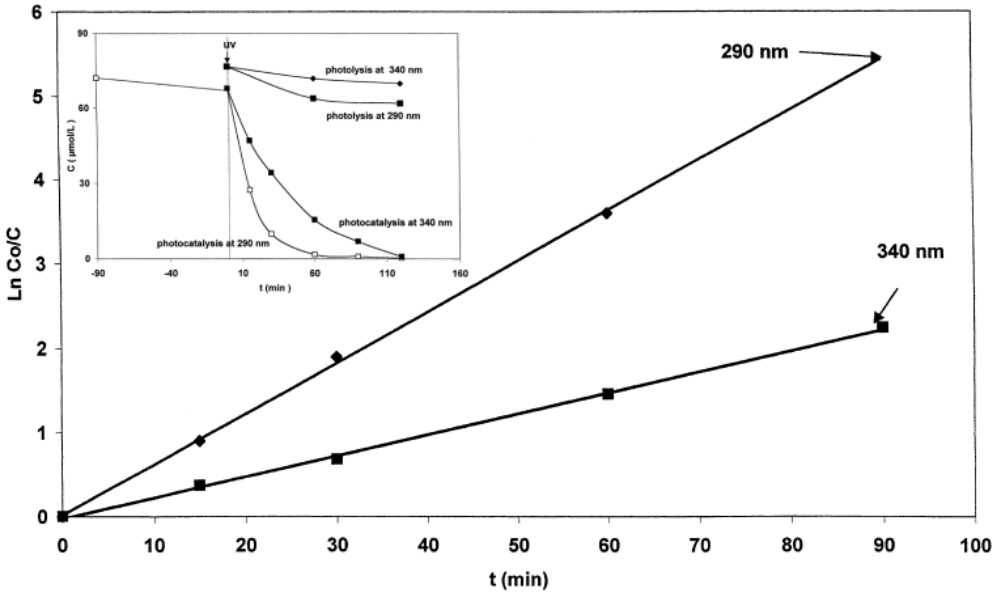

Figure 1.15 First order linear transforms of disappearance of methylene blue by photocatalysis under UV-irradiation at λ = 290 nm and at λ = 340 nm ([MB] = 72 μmol dm^{-3}, [TiO_2] = 2.5 g dm^{-3}) The inserted graph shows the disappearance of methylene blue as concentration vs. time before the linear transform calculation.[3]

A study by Lakshmi *et al.*[14] using P-25 as the source of TiO_2, showed the rate of photocatalytic destruction of methylene blue increases as the pH is increased from pH 2. This was explained by the fact that the positive charge on the surface of the titania will be reduced as the pH is increased, thus allowing the cationic dye to approach closer to the photocatalyst surface and therefore increase the chance of being photo-mineralised. Figure 1.16 shows the results of Lakshmi *et al.*[14] using a 125 W Hg lamp to irradiate solutions containing 1 x 10^{-5} mol dm^{-3} of methylene blue and 267 mg dm^{-3} of P-25.

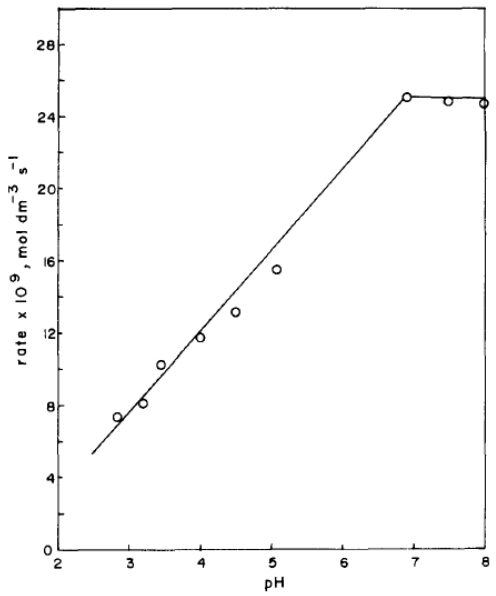

Figure 1.16 Effect of the photocatalytic degradation rate of methylene blue with respect to pH.[14]

Although Lakshmi *et al.*[14] found the rate to increase only until pH 7 where it reached its maximum, a more recent study by Guillard *et al.*[12] using a 125 W Hg lamp and solutions containing 8.42 x 10^{-5} mol dm^{-3} of methylene blue and 500 mg dm^{-3} of P-25, showed, in contrast, the rate increasing up to pH 9 as shown in figure 1.17.

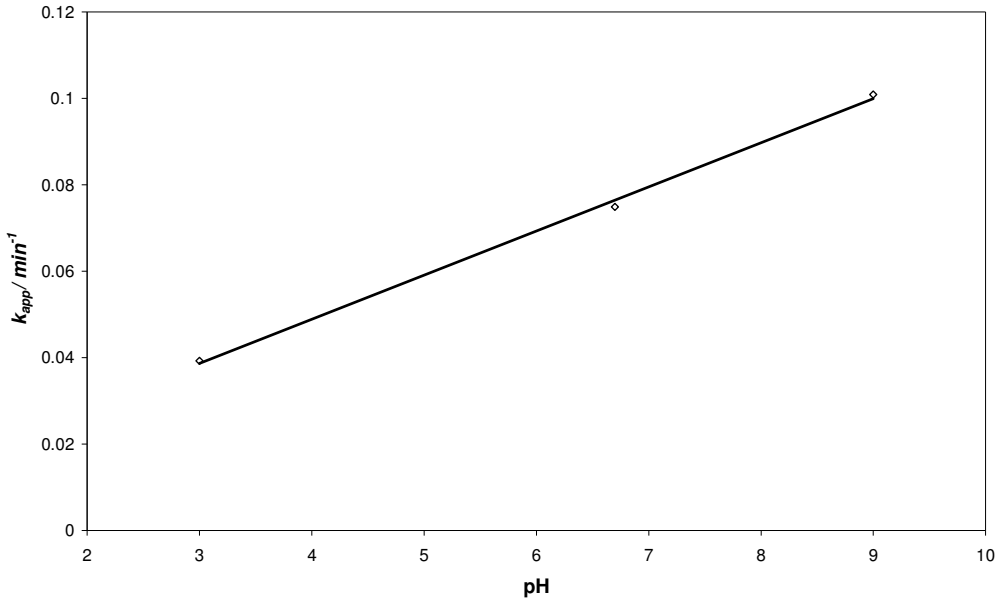

Figure 1.17 Influence of pH on the constant rate of methylene blue (MB) photocatalytic disappearance. Log k_{app} = log r + npH, where, k_{app}, is the pH-independent rate constant, r, is the reaction rate and, n, is the kinetic partial order with respect to proton concentration.[3,12]

It is hard to marry these two very different reports and part of this project is to identify which of the two is nearest to the truth and what reasons may lie for the apparent striking difference.

1.2.2 Acid Orange 7 Adsorption

Acid orange 7 is an anionic dye which can be readily adsorbed onto titania in acidic conditions, i.e. pH < 7. The structure of acid orange 7 is shown in figure 1.18(a). Under acidic conditions the following system shown in equation 1.11 is set up, thus making it favourable for the negatively charged dye to adsorb on the titanias surface.

$$\text{Ti-OH} + \text{H}^+ \rightleftharpoons \text{TiOH}_2^+ \qquad (1.11)$$

Groups such as Bourikas *et al.*[18] have looked at fourier transform infrared (FTIR) analysis of the adsorption of acid orange 7 onto P-25 titania have suggested that the dye adsorbs in a bidentate manner as shown in figure 1.18(b).

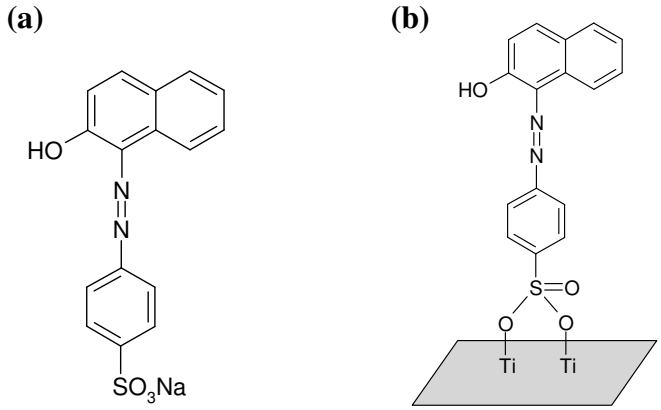

Figure 1.18 (a) Structure of the sodium salt of acid orange 7. **(b)** Proposed adsorption mode of the dye on the surface of titania.

Bourikas *et al.*[18] have performed an impressive study on the adsorption of acid orange 7 on the surface of titania and have modelled this process using the charge distribution multisite surface complexation (CD-MUSIC) model. Details of this model will be discussed later on in this thesis.

Bourikas *et al.*[18] generated adsorption edge plots (shown in figure 1.19) which gives a clear picture of how pH affects the adsorption of the dye on the titania. The solid lines represent the calculated curves from their model. It is observed that, when lowering the pH of the staining solution, more acid orange 7 is adsorbed on the titania at a given soaking solution concentration. Figure 1.19 shows that at around pH 6 – 7, not very much (if any) dye is seen to adsorb which correlates nicely with the p.z.c. of the titania, which is around this pH value (pH 6.6).

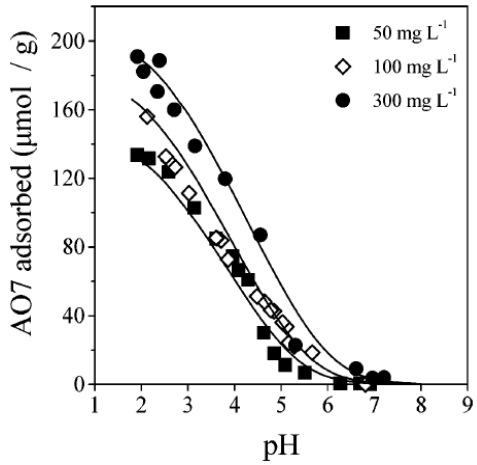

Figure 1.19 Adsorption of acid orange 7 on titanium oxide as a function of pH, at three different initial dye concentrations (50, 100, or 300 mg dm^{-3}; TiO_2 concentration: 750 mg dm^{-3}; room temperature). Data points represent experimental data and solid lines correspond to calculated curves.[18]

Figure 1.20 shows an adsorption isotherm plot reported by Bourikas *et al.*[18] for various staining solution concentrations of acid orange 7 at pH 2, pH 5.7 and pH 10, where, C_{eq}, is the equilibrium concentration of the solution and the amount of dye adsorbed is quoted per gram of semiconductor (P-25). It can be seen that as the equilibrium concentration is raised, the amount of acid orange 7 adsorbed increases until it eventually reaches a plateau. The shape of the isotherms implies localised, Langmuir-type adsorption of the dye on the titania surface.

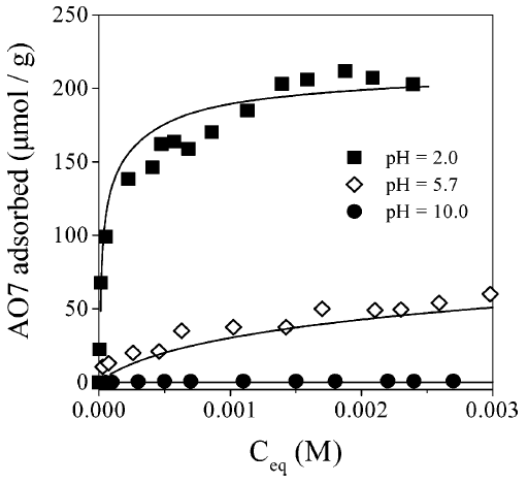

Figure 1.20 Adsorption of acid orange 7 on titanium oxide as a function of the equilibrium concentration, at three different pH values. Data points represent experimental data and solid lines correspond to calculated curves.[18]

As detailed in section 1.2, adsorption constants, K_L, and the maximum number of adsorption sites, n_o, can be determined from these results and the electrostatic 3-plane model used to fit them.[18] Figure 1.21(a) shows the trend in the adsorption constant, K_L, as a function of pH. As expected, the adsorption constant is high at lower pH values where the dye should be attracted most strongly as the surface is highly positively charged, and decreases as the pH value is raised. Figure 1.21(b) shows the variation of the maximum number of adsorption sites as a function of pH.[25]

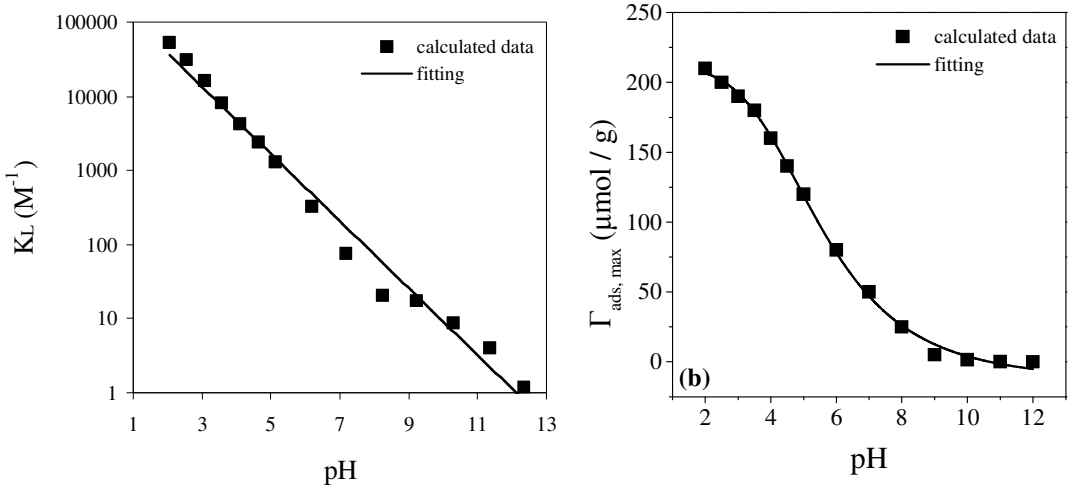

Figure 1.21 (a) The variation of the adsorption constant, *K*, as a function of pH. **(b)** The variation of the maximum number of adsorption sites as a function of pH.[25]

1.2.2.1 Destruction of Acid Orange 7

In a review of the literature Konstantinou *et al.*,[23] proposed the degradation pathways shown in figure 1.22, based on previously identified by-products from degradation studies using techniques such as high performance liquid chromatography (HPLC) and Fourier transform infra red (FTIR) spectroscopy. The proposed pathway suggests that the initial step in the destruction of acid orange 7 is the oxidative attack at the azo linkage to yield 4-hydrazinobenzenesulphonic acid and 2-Naphthol. Twenty two other products were identified upon destruction of acid orange 7.[23] As you can imagine, if the azo linkage is the first point of attack, then any visible colour will disappear immediately upon braking the link. Unlike methylene blue with its N-demethylated derivatives,[13] no coloured intermediates have been reported for acid orange 7 upon destruction.

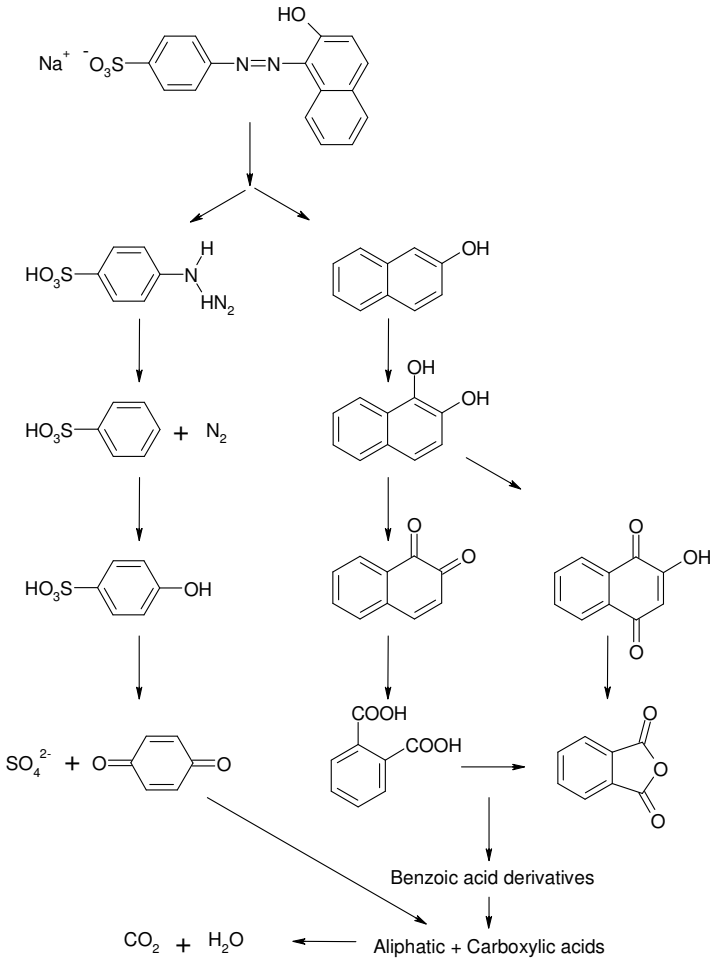

Figure 1.22 Major photocatalytic pathways of acid orange 7.[23]

There are a number of papers that have looked at the destruction of dyes such as acid orange 7 on titania as mentioned in the review by Rajeshwar *et al.*[9] However, a lot of these studies only report the destruction at a single pH (usually natural pH) and not over a wide range to assess how the adsorption of acid orange 7 influences the rate of destruction. Studies on other similar azo dyes, reported in the review by Rajeshwar *et al.*,[9] have shown that generally, the destruction rate is faster when more dye is adsorbed on the surface of the titania. One group that did look at a wide pH range (pH 2 – 12) for the destruction of acid orange 7 is Kiriakidou *et al.*[22] They found that the rate was faster in basic conditions i.e. pH 10 – 12, where no dye should be adsorbed on the titanias surface and between pH 2 – 9 the destruction was not significantly pH dependant. There results can be seen in figure 1.23. The irradiations were however performed using a 450 W solar simulator which complicates the results due to the possibility that the dye bleaching can occur by both semiconductor photocatalysis and dye photosensitisation.

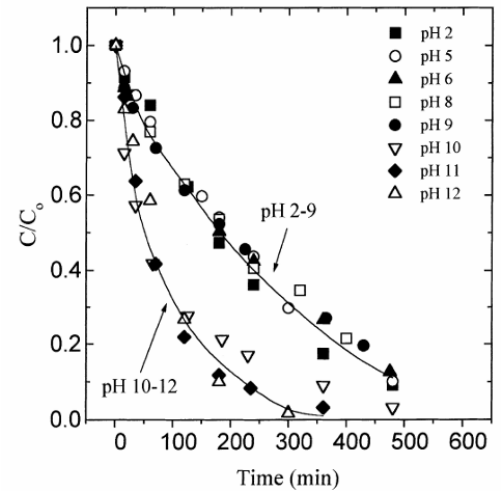

Figure 1.23 Effect of the initial pH on the decolourisation of aqueous solutions of acid orange 7 where [$AO7^-$] = 300 mg dm^{-3} and [TiO_2] = 750 mg dm^{-3}.[22]

Wang *et al.*[24] used both a UV light source as well as a 175 W metal halide lamp from which the light below 400 nm was filtered to assess the destruction of acid orange 7. They reported that there is no significant relationship between the adsorption of acid orange 7 and the photodegradation rate as shown in figure 1.24. Wang *et al.*[24] were

looking at different inorganic anions in their study to see how they competed with acid orange 7 for binding onto the titanias surface. They found a linear dependence on the amount acid orange 7 adsorbed and the rate of photosensitised destruction using visible light as shown in figure 1.24. This is to be expected as the dye has to be in contact with the surface of the titania in order to inject an electron.

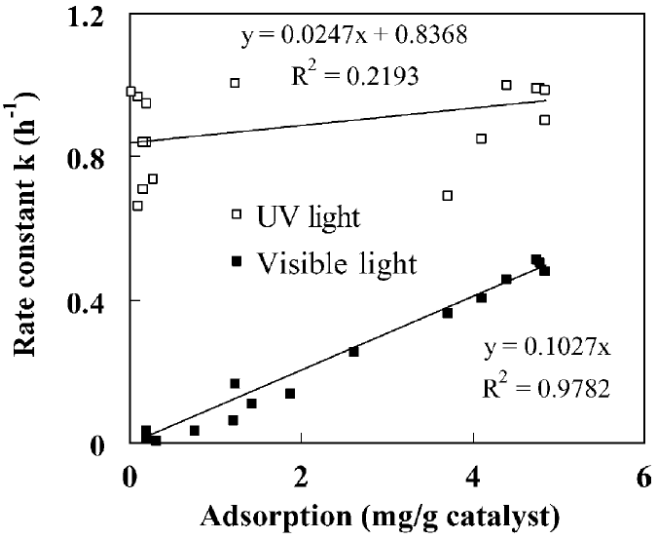

Figure 1.24 The effect of the adsorption on the photodegradation of acid orange 7 in the presence of different inorganic anions (i.e. chloride, sulphate, carbonate, nitrate, and phosphate) under UV or visible light irradiation at pH 5.6, where, [AO7] = 40 mg dm^{-3} and [TiO_2] = 2.0 g dm^{-3}.[24]

1.3 Aims

The aims of this thesis are to assess the adsorption of the commonly used test dyes methylene blue and acid orange 7 onto P-25 titania powder and onto titania paste films as a function of pH and for each to relate this adsorption to the photocatalytic activity exhibited by the semiconductor. Secondly, this thesis aims to model the adsorption of both these dyes onto P-25 using a charge distribution multisite complexation (CD-MUSIC) model and investigate the relationship between the amount of adsorbed dye and the observed rate of dye bleaching.

2 Experimental

2.1 Instrumentation

2.1.1 (UV/Vis) Spectrophotometer

The spectrophotometer used throughout this project was the Cary 300 UV/Vis shown in figure 2.1, produced by Varian, Inc.

Figure 2.1 The Cary 300 UV/Vis spectrophotometer produced by Varian, Inc.

2.1.1.1 UV/Visible Spectrometry Theory[26]

Lambert's Law states that each layer of equal thickness of an absorbing medium absorbs an equal fraction of the radiant energy that passes through it. The intensity of the incident radiation has no effect on the fraction of radiant energy transmitted through a sample as long as the radiation does not cause a physical or chemical change in the sample.

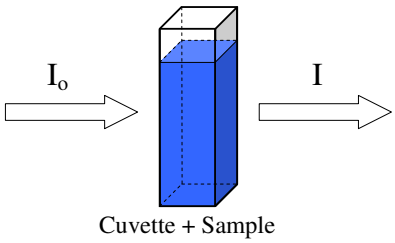

Figure 2.2 Transmittance of light through a sample in a cuvette in a UV/Vis spectrometer.

If the intensity of the incident radiation is I_o and the transmitted light is I as shown in figure 2.2, then the fraction transmitted T is:

$$I/I_o = T \tag{2.1}$$

Therefore, the percentage transmission is

$$\%T = I/I_o \times 100 \tag{2.2}$$

The Beer-Lambert law is as follows,

$$A = \varepsilon \times c \times l \tag{2.3}$$

where ε is the molar absorptivity, c is the concentration of the sample and *l* is the path length of the cuvette.

This law states that the concentration of a substance (c) is directly proportional to the absorbance (A). This is only true if the radiation does not cause a physical or chemical change in the sample and also if the light is monochromatic.

Mathematically, absorbance is related to percentage transmittance by the expression:

$$A = \log_{10}(I_o/I) = \log_{10}(100/T) = \varepsilon \times c \times l \tag{2.4}$$

Figure 2.3 shows the shape of the graphs obtained by plotting % transmittance and absorbance against concentration. It can be clearly seen from figure 2.3 that it is more convenient to work in absorbance than transmittance since there is a linear relationship for absorbance i.e. if the concentration of a sample doubles, the absorbance will double. Absorbance values up to approximately one are measured preferentially as an absorbance of one relates to a transmittance of only 10% of the incident light through the sample. When absorbance values are above one there is very little transmitted light, therefore, the accuracy of the data is questionable.

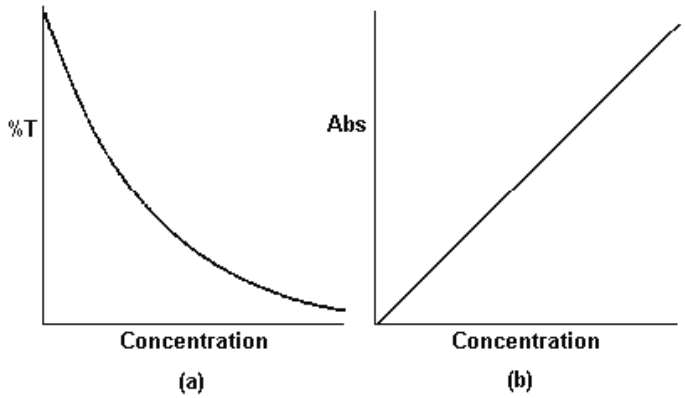

Figure 2.3 (a) % transmittance vs. concentration. (b) Absorbance vs. concentration.

2.1.2 Fourier Transform Infrared Spectroscopy (FTIR)

The infrared spectrophotometer used in this project was a Perkin-Elmer Spectrum One (shown in figure 2.4), which is capable of scanning in the range of 370 – 7800 cm^{-1}. Infrared spectroscopy is a useful technique that allows the determination of functional groups in a molecule. IR spectroscopy works by passing a range of infrared frequencies through a sample and detecting which frequencies the sample absorbs. Each bond in a molecule vibrates at a certain frequency. When the frequency equal to that of a certain bonds vibration is reached in the spectrophotometer, the molecule will absorb the energy and hence reduce the strength of the signal getting to the detector. In order for a molecule to be IR active, there has to be a change in the permanent dipole when vibrating.

It is common to plot % transmittance vs. wavenumber to generate a spectrum, however the % transmittance can be related to absorbance by equation 2.5, as previously mentioned in the UV/Vis theory section 2.1.1.1.

$$A = \log_{10}(100/T) \qquad (2.5)$$

Figure 2.4 The Perkin-Elmer Spectrum One.

2.1.2.1 Attenuated Total Reflectance (FTIR-ATR)[27]

Solid samples are usually ground with potassium bromide to form a powder and then compressed into a disk. The disk is then placed inside the spectrophotometer and the IR beam is passed through the sample. Potassium bromide is not IR active, therefore only the signal from the sample will be observed. Solid samples can also be dissolved in solvent, placed on top of a sodium chloride plate and allowed to evaporate leaving behind a thin film of sample to be analysed.

A much simpler way to measure the IR spectrum of a sample which does not require any special preparation is by the use of attenuated total reflectance (ATR). Figure 2.5(a) shows the Perkin-Elmer Spectrum One with the ATR attachment installed. This attachment works by measuring the changes that occur in a totally internally reflected IR beam when it comes into contact with a sample. The sample is placed in the centre of the round metal plate on top of a crystal and pressure is applied to ensure a good contact. Figure 2.5(b) shows how the IR beam is directed onto the ATR crystal. This internal reflectance creates an evanescent wave that extends beyond the surface of the crystal into the sample which is held in contact with the crystal. When the sample absorbs energy, the evanescent wave is attenuated or altered. The attenuated energy from each evanescent wave is passed out the other end of the crystal to the detector. The sample has to be in good direct contact with the crystal as the evanescent wave only passes 0.5 µm – 5 µm beyond the crystal.

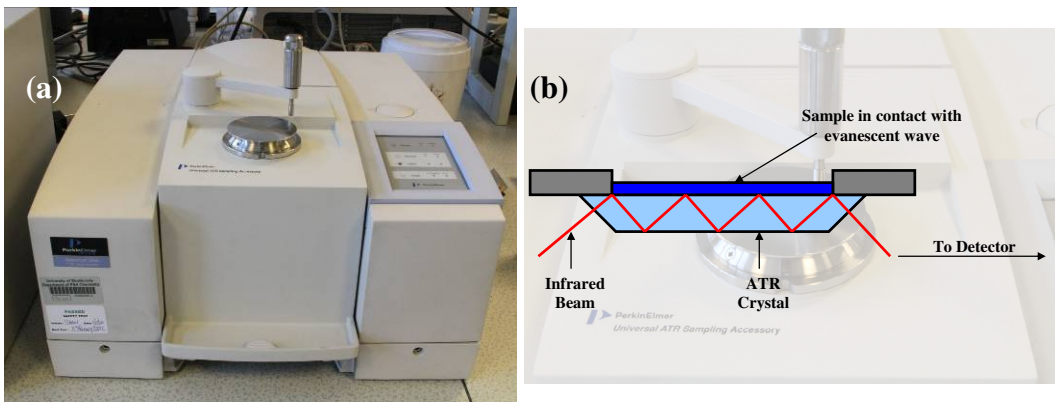

Figure 2.5 (a) The Perkin-Elmer Spectrum One with the ATR attachment installed. **(b)** Pathway of the IR beam through the ATR crystal in contact with the sample.[27]

2.2 Procedures

2.2.1 Materials

Unless otherwise stated, all chemicals used in this project were purchased from Aldrich Chemical Corporation (Gillingham, Dorset, UK) and were used as supplied.

2.2.2 Preparation of TiO_2 Sol-Gel Paste for Thick Film Photocatalysis[28]

Initially all glassware was rinsed with acetone and thoroughly dried using a compressed air stream. 20 mL of titanium (IV) isopropoxide was added to a 100 mL round bottomed flask containing 4.65 g of glacial acetic acid using a syringe as shown in figure 2.6. As titanium (IV) isopropoxide is extremely moisture sensitive, the tip of the needle was kept below the surface of the acetic acid when adding. As a further precaution, argon was flushed through the round bottomed flask. Upon addition, the reaction of the titanium (IV) isopropoxide with the acetic acid was noticeably exothermic.

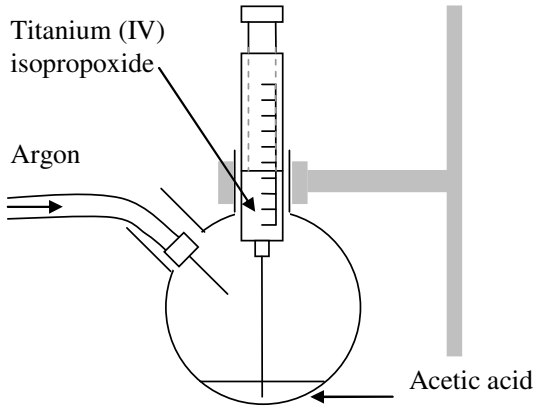

Figure 2.6 Set-up for adding the moisture sensitive titanium (IV) isopropoxide to the glacial acetic acid.

The resulting $Ti(OPr^i)_4$ solution was then transferred by syringe to a 250mL conical flask containing 120 mL of distilled water and 1.08 g of concentrated nitric acid. A magnetic stirrer bar was then added to the flask before covering the top of the flask with Parafilm and piercing a few holes. The flask was then placed in a paraffin oil bath on a stirrer/heating plate as shown in figure 2.7. A Fuzzy Logic temperature controller was used to maintain a temperature of 80°C for 8 hours whilst being continually stirred. After the 8 hours, the solution was allowed to cool down to room temperature before filtering through a 0.45 μm syringe filter to remove any non-dispersed aggregates.

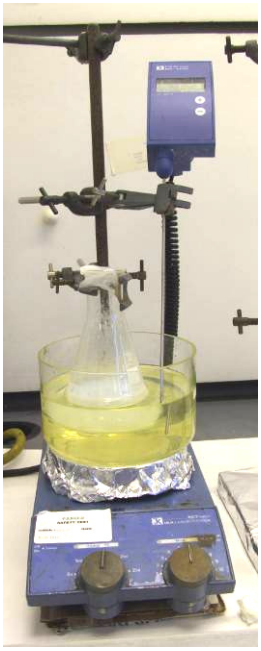

Figure 2.7 Paraffin oil bath setup

80 mL of the filtered solution was transferred into a 125mL Teflon™ liner (shown in figure 2.8(a)) and placed in a digestion bomb. The parts of which are shown in figure 2.8(b). Once constructed as shown in figure 2.8(c), the digestion bomb was then placed inside the furnace and heated to 220°C for 12 hours. The high pressure and temperature conditions inside the vessel encourage crystal growth by increasing the solubility of small particles. This then promotes Ostwald ripening to occur.

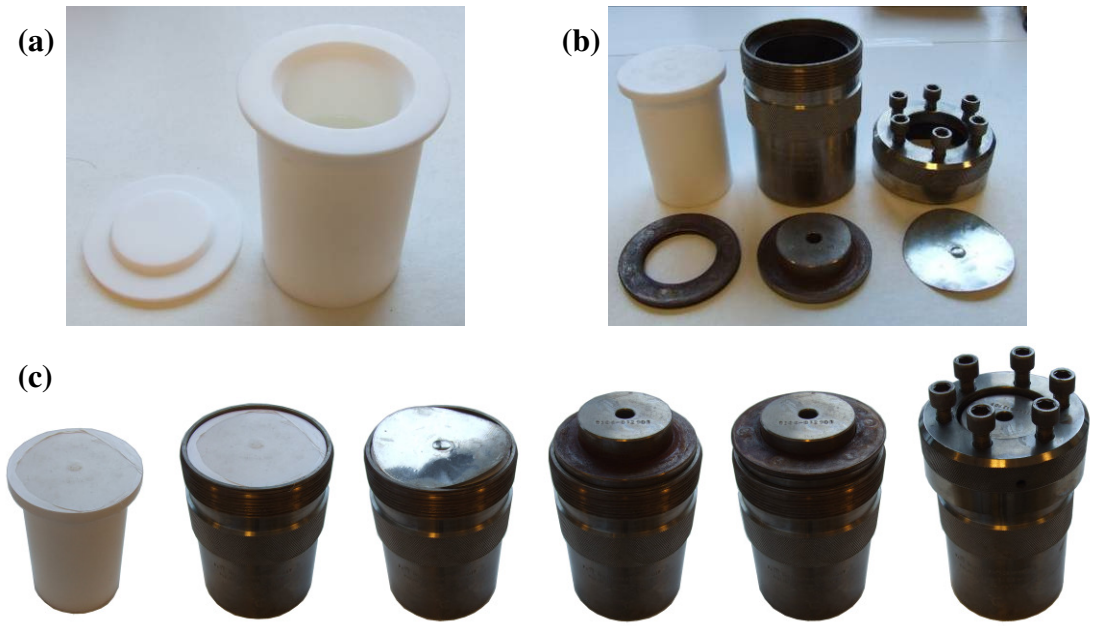

Figure 2.8(a) The 125mL Teflon^{TM} liner **(b)** The parts of the digestion bomb **(c)** Assembly of the digestion bomb.

After cooling, it is observed that the paste has separated into two phases (figure 2.9(a)), therefore, the solution was subjected to ultra-sonic probing to obtain a good dispersion. This was carried out with a Branson Probe 450 sonic horn (figure 2.9(b)) on full power for approximately 30 seconds to ensure a good dispersion and no agglomerates were left in the solution (figure 2.9(c)).

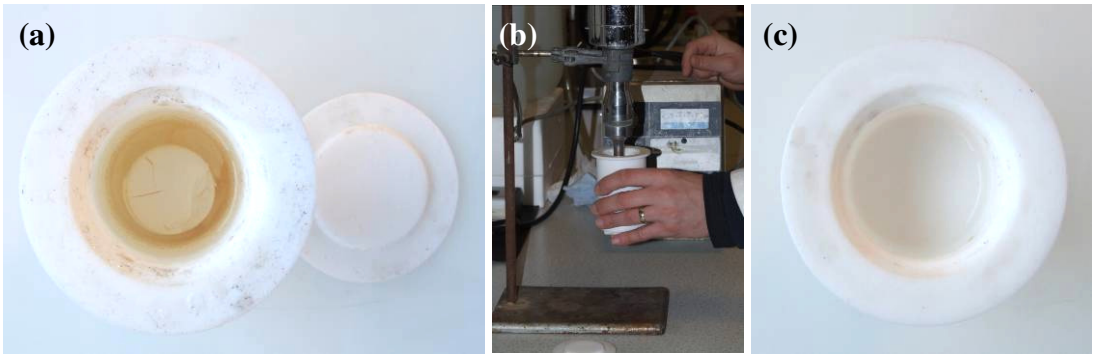

Figure 2.9(a) Inside the liner after 12 hours at 220°C showing the paste separated into two phases (white solid in the centre and the yellowish liquid surrounding it) (b) the liner being raised under the ultra-sonic probe **(c)** A dispersed solution after 30 seconds of ultra-sonic probing.

The solution was then transferred into a 250mL round bottom flask. In order to concentrate the solution to approximately 10 – 12 wt%, the solution was rotary evaporated. The temperature of the water bath was set to 35 – 40°C. After approximately 45 minutes of evaporating, a small amount of the paste was removed and the initial sample weight was recorded before placing in a furnace to evaporate to dryness. Using the initial weight and the dry weight the weight percent could be determined. If the weight percent was not in the region of 10 – 12 wt%, further rotary evaporation was carried out.

When the desired weight percentage of paste had been achieved, the paste was scraped out of the round bottom flask into a pre-weighed 30mL bottle. The weight of the paste was then determined and multiplied by the calculated weight percent giving the weight of solids in the paste. 50 wt% (of the total solids) of polyethylene glycol was then added to the paste as a binder to prevent the formation of small surface cracks when the paste is eventually cast and allowed to dry. The paste was then stirred gently overnight before refrigeration.

2.2.3 Preparation of TiO_2 Coated Glass Slides[28]

TiO_2 paste films supported on glass slides were produced using the paste prepared in section 2.2.2. The square glass slides were cut from microscope slides to a length of 2.5 cm. To ensure the surface of the glass was clean, it was wiped with a little methanol before commencing. The slides were placed in a custom made holder as shown in figure 2.10(a). Three disks could be coated simultaneously. Scotch tape was applied down the sides of the holder as illustrated, overlapping the glass slides by a few millimetres. This created a trough for the TiO_2 paste to be coated. A small quantity of TiO_2 paste was pipetted at the top of the holder and was smeared across. A second pipette was then used to drag the paste down over the slides, as illustrated in figure 2.10(c) and (d). This created a ~ 120 μm thick TiO_2 paste film which was left on the bench to dry for approximately half an hour. After this time, the Scotch tape was carefully removed, the disks were placed on a ceramic slab and then placed in the furnace. The disks were heated to 450°C (with a ramp time of 20 minutes) for half an hour and left to cool slowly to help prevent the TiO_2 flaking. Flaking was only a concern when coating on surfaces other than borosilicate, i.e. quartz or CaF_2 disks. This produced a film approximately 2 μm thick.

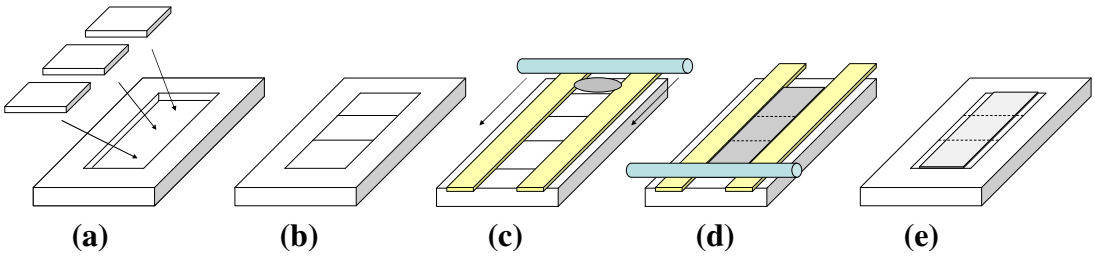

Figure 2.10 (a) The custom made aluminum holder. (b) The glass slides placed in the holder. (c) Scotch tape is applied down the sides creating a trough in which the TiO_2 paste is dragged down using a doctor blade technique. (d) The disk is then left for half an hour for the solvent to evaporate. (e) After half an hour, the tape is removed and the slides are popped out of the holder, ready to be placed in the furnace.

2.2.4 Adsorption of Dye on Syringe Filters

Since syringe filters are used quite a lot in this area of chemistry[2,3,6,11,13,17,18,21,22,24] it was decided to assess the affinity, if any, of the dye to the filter membrane over a range of pH values. Initial work was carried out using 2 μm nylon syringe filters from Gelman. Nylon syringe filters seem to be the membrane of choice according to most chemical suppliers' websites. Firstly, solutions of acid orange and methylene blue (1 x 10^{-4}M) were prepared at a range of pH values with 1 x 10^{-2} M NaCl present. Appropriate dilutions were made in order to achieve a sensible absorbance using a 1 cm cell for each of the starting solutions. Each solution was then drawn up into a 10 mL syringe and the filter was then placed on the tip. The solutions were then passed through the filter and the filtered solutions' spectra was recorded again after the appropriate dilutions were made to the 10 mL. The difference observed upon filtering was used to determine the concentration of dye adsorbed as a function of pH. The same procedure was then repeated using other common types of membrane. The other types chosen were, regenerated cellulose (RC), polyethersulphone (PES), polyvinylidene difluoride (PVDF) and polytetrafluoroethylene (PTFE). All these filters were 2 μm, 13 mm in diameter and manufactured by Cronus®. The structures of all the filter materials used is shown in figure 2.11.

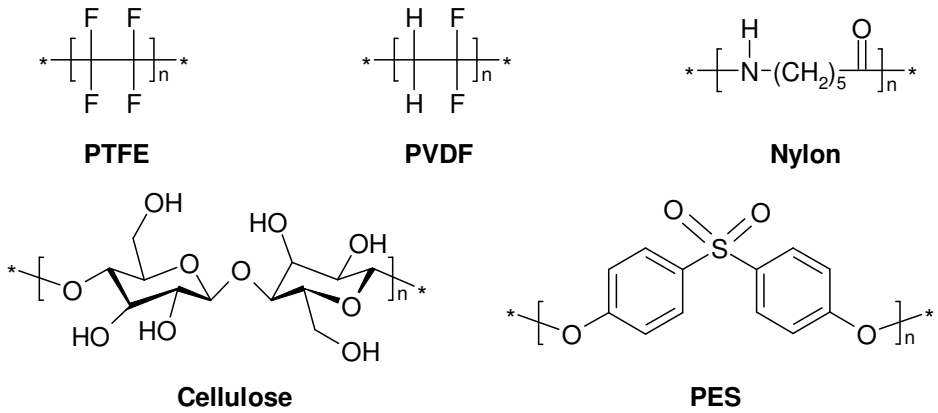

Figure 2.11 Structures of the membranes used in this experiment.

The outcome of testing this range of filters with both acid orange 7 and methylene blue (1 x 10^{-4} M) is shown in figure 2.12. A clear pH dependence is observed for the regenerated cellulose, polyvinylidene difluoride and nylon filters.

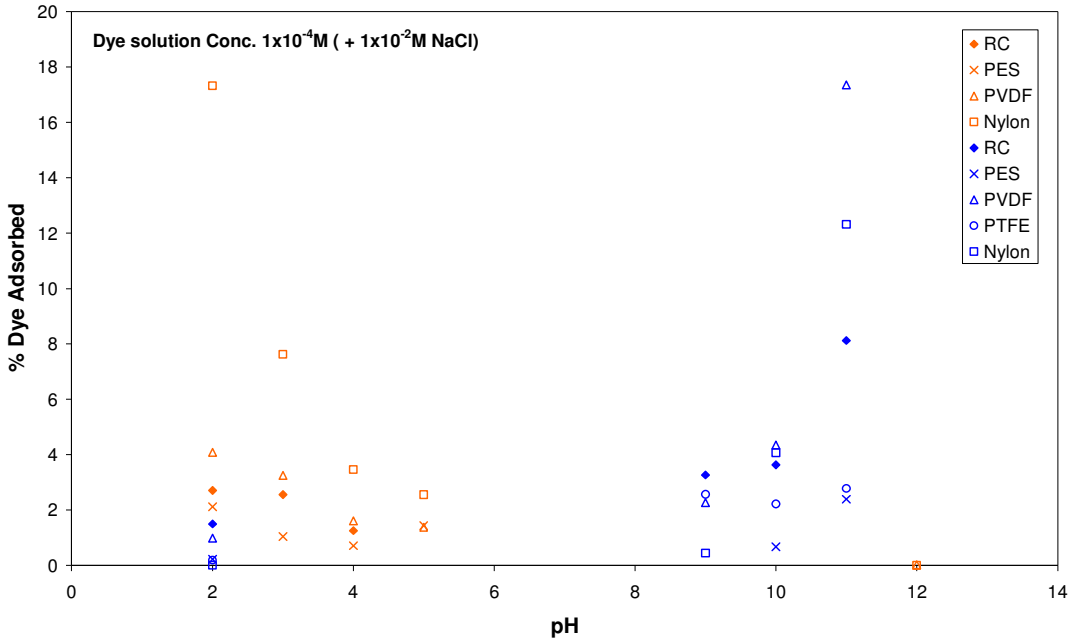

Figure 2.12 Percentage of acid orange 7 and methylene blue dye adsorbed upon filtering through a selection of syringe filters vs. pH for a solution concentration of 1 x 10^{-4} M.

Figure 2.13 shows a clear visual demonstration of how the adsorption of acid orange 7 on nylon filters is pH dependant.

Figure 2.13 Stained filters. (Top) Left to right: pH 0, 2, 3, 4, 5, 6 and 12 stained with 1.5 x 10^{-3} M. (Bottom) Left to right: pH 0, 2, 3, 4, 5, 6 and 12 stained with 1 x 10^{-4} M.

2.2.5 Adsorption of Dye onto P-25 Titania Powder

For the adsorption edge study of both methylene blue and acid orange 7 the concentration of dye and P-25 was chosen to be 300 mg dm^{-3} and 750 mg dm^{-3} respectively. These are similar concentrations used by Bourikas *et al.*[18] 100 mL solutions of dye/P-25 suspensions were prepared and altered to the desired pH using small quantities of 0.1 M NaOH or HNO_3. No background electrolyte (NaCl) was used in this set of experiments.

It was found during the course of this project that syringe filters could create problems when working with dyes as some membranes allow the adsorption of dye depending on the pH of the solution, as shown in section 2.2.4. To overcome this problem, centrifuging was used to separate the P-25 powder from the supernatant. The absorbance of the initial solutions were measured before adding the P-25. The solutions had to be diluted considerably in order to obtain a spectra using a 1 cm cell, this was to ensure an accurate concentration determination, as the diluted solution would be predominantly in the monomer form and so Beer's law can be applied. Thus, typically 2.5 mL of the dye was syringed into a volumetric flask and made up to 100 mL using deionised water, giving a dilution factor of 40. Once all the initial absorbance spectra were recorded, the P-25 was added (75 mg in 100 mL) to the solutions and then placed in a sonic bath for 10 minutes to ensure a good dispersion. The solutions were then left stirring in the dark overnight in sealed bottles. This was to help limit the amount of CO_2 from the atmosphere altering the pH of the solutions around pH7. After 12 hours, 10 mL of each solution were transferred to 15 mL tubes and placed in the centrifuge for 10 minutes at 4000 rpm. Figure 2.14 shows the separated stained P-25 powder after centrifuging methylene blue solutions. When removed from the centrifuge, 2.5 mL of the supernatant were syringed and diluted to 100 mL as described above and the UV/Vis spectrum of the solution obtained. The drop in absorbance (ΔAbs) for each pH was determined by subtracting the final absorbance at λ_{max} from the initial absorbance. These values were then entered into the Beer Lambert equation to calculate the dye concentrations and then multiplied by the dilution factor. To get a final value in μmol g^{-1} of titania, the actual number of

moles of dye in the 100 mL bottle had to be determined by dividing by 10 and then converting to μmol. These values were then finally divided by the amount of P-25 present in the solution (0.075 g).

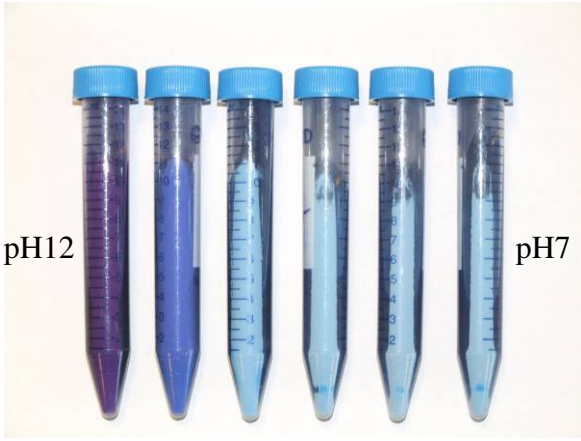

Figure 2.14 (left to right) pH 12 to pH 7 centrifuged P-25/MB solutions.

2.2.6 Adsorption of Dye onto Titania Coated (Paste) Glass Disks

The adsorption of dye over a set period of time (1 hour) was carried out using the setup shown in figure 2.15. Previous studies have shown that the dyes used in this thesis (methylene blue and acid orange 7) reach adsorption equilibrium on TiO_2 paste films within approximately 40 minutes as shown in the inserted graph in figure 2.16.

Each concentration of dye at the desired pH was prepared in a 100 mL beaker containing 1 x 10^{-2} M NaCl. The solution was then stirred to ensure a good mix before inserting the TiO_2 film. The TiO_2 paste film was gently lowered into the solution in a custom made holder and left there whilst the solution was still being stirred for 1 hour in order for the adsorption equilibrium to be reached. After the hour of adsorbing, the disk was generally removed, rinsed with a clean dye free solution of the same pH as the staining solution to remove any excess dye and quickly transferred into the UV/Vis spectrophotometer in order to record the spectrum of the wet film. The film was then dried under a compressed air stream and the spectrum of the dry film was obtained. All adsorption measurements were performed using a single disk for each dye.

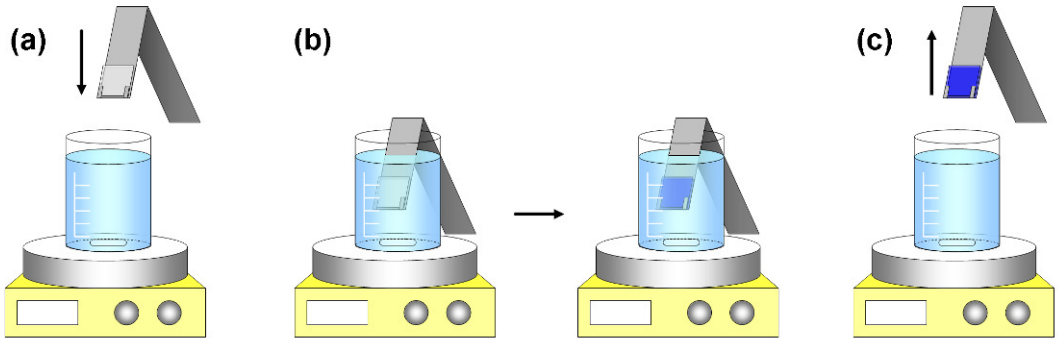

Figure 2.15 (a) The diagram shows the custom holder with a TiO_2 coated slide being lowered into a 100 mL beaker of staining solution. (b) The slide is kept in the continually stirred staining solution for 1 hour whilst adsorption equilibrium is reached. (c) After the hour, the holder is removed and the disk is rinsed with a clean, i.e. no dye, solution of the same pH as the staining solution.

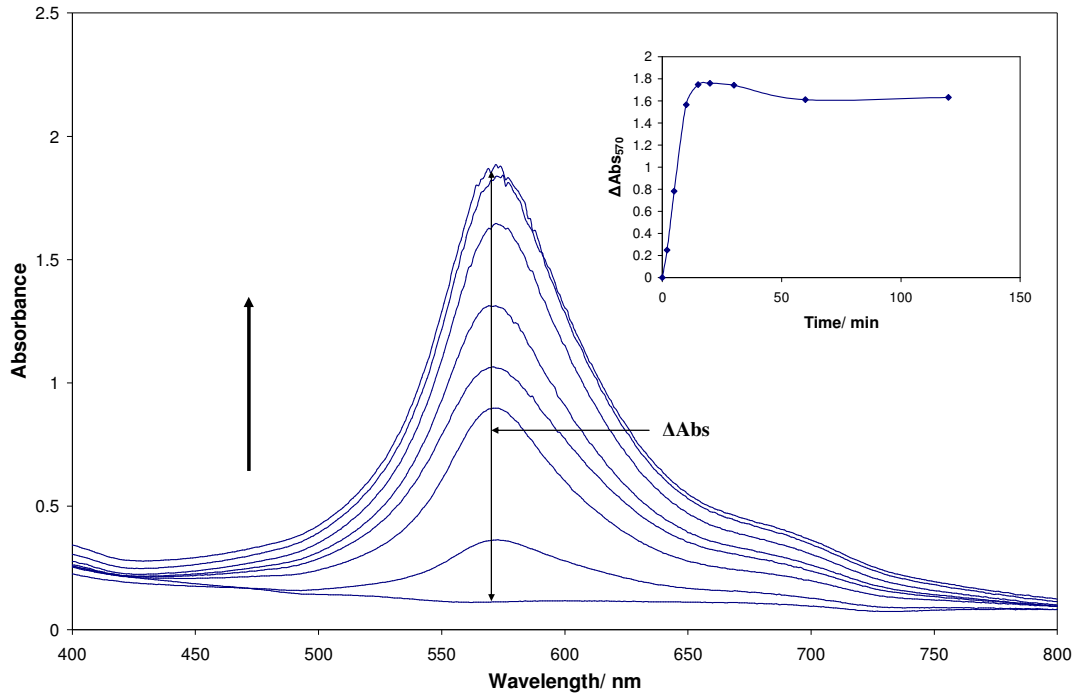

Figure 2.16 Methylene blue spectra increasing as more dye adsorbes over time. The inserted graph shows ΔAbs vs. time obtained from the UV/Vis spectra.

2.2.7 FTIR Study of the Adsorption of Dyes on P-25 and Paste Films

FTIR-ATR was used to obtain the spectra of both methylene blue and acid orange powders of the pure dyes. These spectra were then compared with those of the dye adsorbed onto P-25 in order to see if there are any changes caused by the way the dye is adsorbed onto to the TiO_2 surface. In order to obtain the P-25 stained powder, the same procedure used in section 2.2.5 was carried out. The supernatant was carefully poured out the centrifuge tube and the P-25 compacted at the side of the tube was washed with fresh acid or alkali then scraped out with a spatula and left to dry in the dark before recording its IR spectra. Figure 2.17 shows the dried powder for both dyes along with the dyes themselves and P-25. All of which were measured by FTIR-ATR.

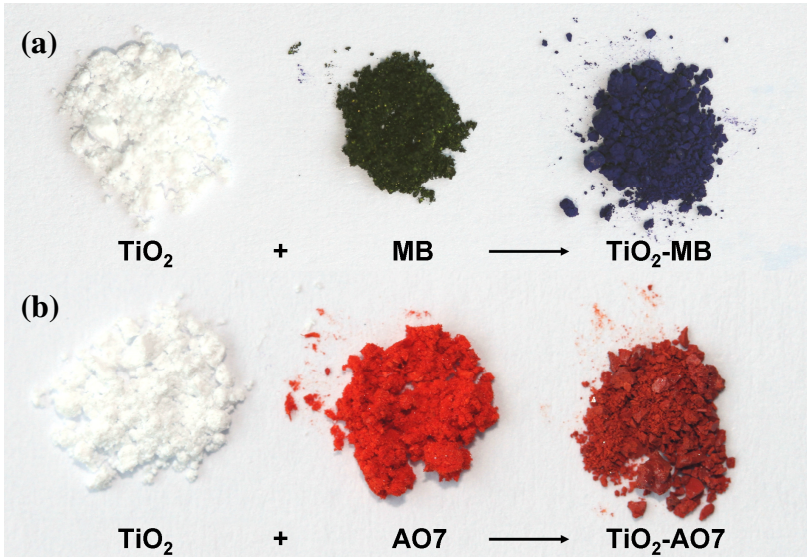

Figure 2.17 (a) (left to right) P-25 powder, methylene blue and methylene blue stained P-25. **(b)** (left to right) P-25 powder, acid orange 7 and acid orange 7 stained P-25 powder.

The FTIR of paste films was a little more difficult to obtain since the support of the paste films was either borosilicate or quartz. This meant that the fingerprint region in FTIR was cut off. In order to overcome this problem, paste films were cast onto calcium fluoride disks and heated to 600°C. The jump from 450°C, used for normal paste films (section 2.2.3), was due to the fact that the paste film did not adhere well

to the disk at this temperature. Although the disk at 600°C was tougher, after soaking in dye solution it still flaked away as shown in figure 2.18 below. The FTIR spectrum could still however be obtained from the little material on the disk.

Figure 2.18 TiO_2 coated calcium fluoride disk after being soaked in acid orange 7 staining solution.

2.2.8 Photocatalytic Destruction of Methylene Blue and Acid Orange

All UV irradiations were conducted using two 8W black light blue (BLB) fluorescent tubes with an output maximum at 365 nm and a typical UV irradiance of 2 mW cm^{-2}. All visible irradiations were carried out using a 150 W Xe-arc lamp (unless otherwise stated) fitted with a 400 nm cut-off filter to remove the UV component of the light. The profiles of the light sources obtained using an Optronic Laboratories OL 750 Spectroradiometer are shown in figure 2.19.

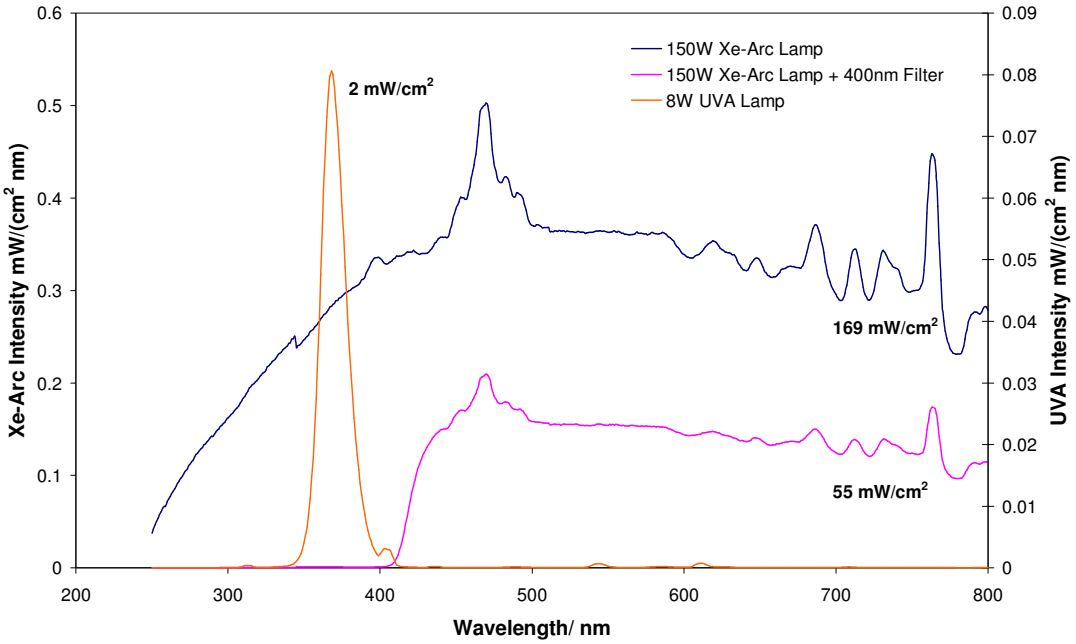

Figure 2.19 Profiles of the 8 W UVA and the 150 W Xe-arc lamp with and without the 400 nm cut-off filter.

2.2.9 pH Study of the Photocatalytic Destruction of Methylene Blue and Acid Orange 7 in Solution Using P-25 Powder Dispersions

100 mL solutions were prepared with a dye concentration that gave an absorbance of 1 A.U in a 1 cm cell ([MB] = 5 mg dm^{-3} and [AO7] = 17 mg dm^{-3}). The pH was altered using small quantities of either 0.1 M NaOH or HNO_3 stock solutions. To these dye solutions, 2 mg of P-25 was added to give a TiO_2 concentration of 20 mg dm^{-3}. This low concentration allowed *in-situ* measurements of the destruction of each dye as the scattering of light by the titania in the spectrophotometer was minimal. Each solution was subjected to ultrasonic treatment for 10 minutes to ensure a good dispersion before being left stirring in the dark for 1 hour to allow adsorption equilibrium to be attained. 3.5 mL of the solution was then syringed into a cuvette, to which a crown stirrer was added.

For the irradiation of P-25 powder dispersions, the filled cuvette was simply placed at a set distance in front of the light source on a magnetic stirrer plate. As the Xe-arc

lamp generates a lot of heat, a water jacket connected up to a Haake circulator bath was used to prevent the solution from heating up. The circulating water was kept at 15°C which kept the cell cool enough and also prevented the build-up of condensation inside the jacket. The cuvettes were placed inside the water jacket as shown in figure 2.20. Regular absorbance readings were obtained during the course of the irradiations to monitor the drop in absorbance at λ_{max} for methylene blue (660 nm) and acid orange 7 (484 nm).

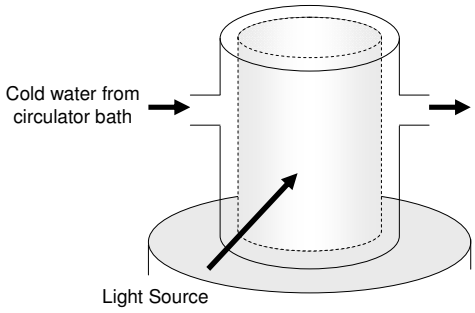

Figure 2.20 The water jacket, through which the visible irradiations were performed.

2.2.10 pH Study of the Photocatalytic Destruction of Methylene Blue and Acid Orange 7 in Solution Using Paste Films

The cell shown in figure 2.21 was used to study the effect of pH on the destruction of each dye using paste films. The cell allowed the soaking solution to be in contact with the paste film through the small window cut in the cuvette. 100 mL solutions of dye at various pH values were prepared using the same concentrations used in section 2.2.9 to allow for *in-situ* monitoring. 3.5 mL of each staining solution was syringed into the assembled cell and allowed to adsorb onto the surface of the film while being continually stirred in the dark for approximately 1 hour. The design of the cell allows both measurement of the solution and the solution + paste film (see figure 2.21(b)) by rotating it in the spectrophotometer. Subtraction of both these spectra (after correcting for the slight increase in path length due to the cut in the cuvette) therefore can allow the spectra of just the paste film to be obtained.

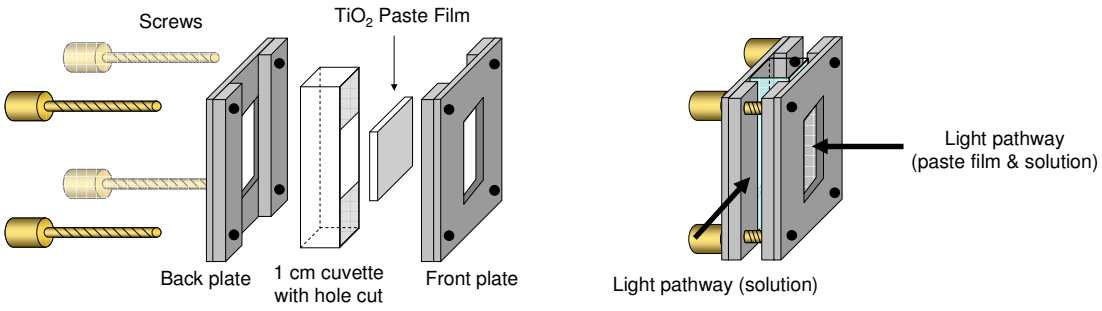

Figure 2.21 (a) The expanded cell showing all the components. **(b)** The assembled cell showing the two ways in which we can monitor the progress of the destruction in the spectrophotometer.

Figure 2.22 below shows the cells being irradiated through the paste film at an intensity of approximately 2 mW cm^{-2} UVA whilst being stirred. Absorbance measurements were taken at regular time intervals to monitor the destruction of the dye. This was done until the solution went completely colourless for both dyes only once. Subsequent runs were monitored over a period of 1 - 2 hours of irradiation and an initial rate was taken.

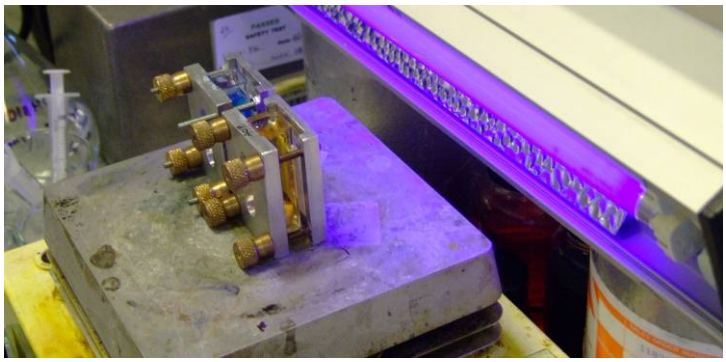

Figure 2.22 Irradiation of both dyes in the pH study of the destruction of the dyes.

As mentioned previously for the destruction using powders, when performing visible light irradiations using the 150 W Xe-arc lamp, a water jacket was used to prevent the solution heating up during the course of the experiment. Figure 2.23 shows the water jacket placed in front of the cell during irradiation, as the cell assembly was to large to fit inside.

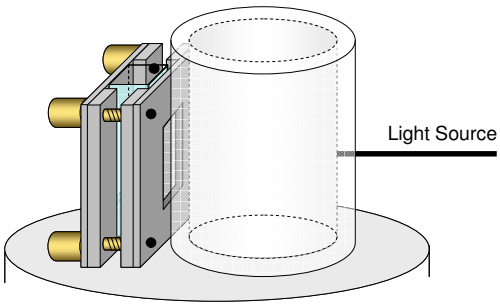

Figure 2.23 The water jacket, through which the visible irradiations were performed.

3 Adsorption and Destruction of Methylene Blue by Semiconductor Photocatalysis

This chapter is focused on the adsorption of methylene blue onto P-25 powder dispersions at a range of pHs and the modelling of this process using a charge distribution multisite complexation model (CD-MUSIC). The extent of adsorption on the semiconductor surface will then be related to its photocatalytic ability.

The modelling of this system will take into account that dye multimers can readily adsorb onto the P-25 surface as well as the monomer species.

3.1 Aggregation of Methylene Blue (MB^+)

The aggregation of thiazine dyes, such as MB^+, has been well studied by groups such as, Ghosh *et al.*[29], who studied the dimerisation and trimerisation of many dyes, including MB^+ via UV/Vis spectrophotometery, and the following equilibria appear to apply:

$$2MB^+ \xrightarrow{K_D} (MB^+)_2 \quad (3.1)$$

$$(MB^+)_2 + MB^+ \xrightarrow{K_{Tr}} (MB^+)_3 \quad (3.2)$$

Ghosh *et al.*[29] report values of 2090 M^{-1} and 3990 M^{-1} for the equilibria constants, K_D and K_{Tr}, and using these values, the fractions of MB^+ in its monomeric, dimeric and trimeric form, i.e. f_M, f_D and f_{Tr}, present in different total dye concentrations, $[MB^+]_{total}$, spanning the range 0 – 1.5 mM, have been calculated and the results of this work are illustrated in figure 3.1.

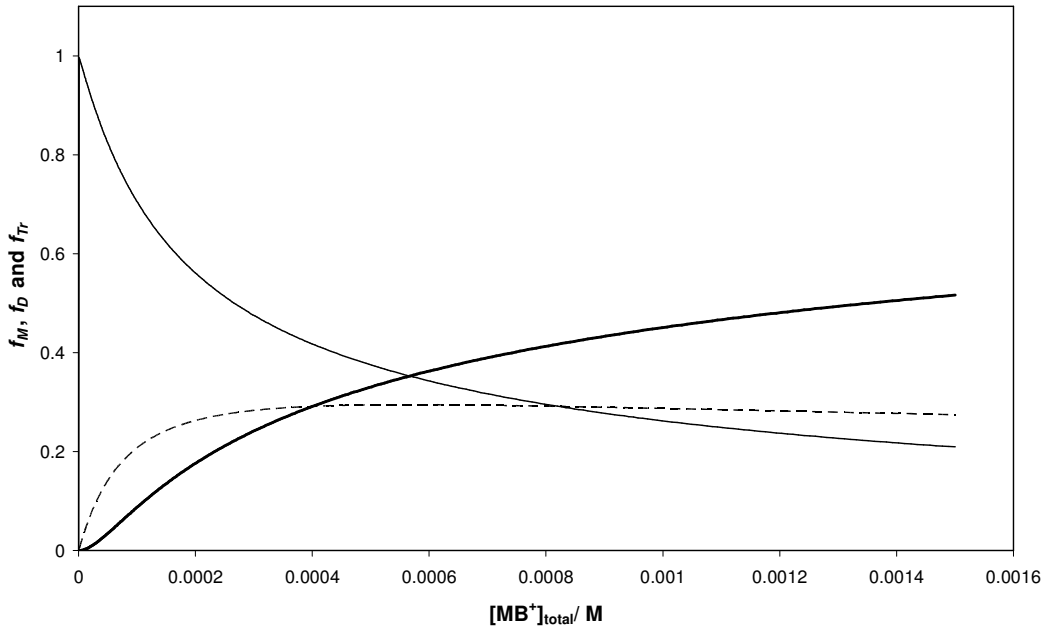

Figure 3.1 Fractions of MB^+, in the form of a monomer (thin solid line), dimer (broken line) and trimer (thick solid line), in solution as a function of the total dye concentration, $[MB^+]_{total}$, calculated using the dimerisation and trimerisation constants reported by Ghosh *et al*.[29]

Thus, at a typical $[MB^+]_{total}$ used for the *in-situ* semiconductor photocatalytic (SPC) studies reported here, where the absorbance of the solution is ca. 1 in a 1 cm cell, i.e. 1.32 x 10^{-5} M, the values of f_M, f_D and f_{Tr} are ca. 0.95, 0.047 and 0.003, respectively. From these values it is clear the level of dimer in solution is not particularly significant at the low $[MB^+]_{total}$ used in our *in-situ* work (1.32 x 10^{-5} M), but more often than not, in *ex situ*-monitored SPC studies, much higher concentrations of MB^+ are used, typically 8x10^{-5} M [3,13,16,30-32] at which f_M, f_D and f_{Tr} are ca. 0.74, 0.19 and 0.07, respectively; and the levels of multimeric dyes species present are significant.

3.2 MUSIC and CD-MUSIC Models

The most commonly used model of the charging behaviour of metal oxides has been the one site/two-pK_a model[33] which assumes a single surface site type which can absorb or desorb a proton, i.e. for TiO_2

$$TiO^- + 2H^+ \overset{K_{a1}}{\rightleftharpoons} TiOH + H^+ \overset{K_{a2}}{\rightleftharpoons} TiOH_2^+ \qquad (3.3)$$

Where, K_{a1}, and, K_{a2}, are the sequential acid association constants for the TiO^- surface species. This simple model reflects the amphoteric nature of the metal oxide, but not the different types of surface site which are known from surface spectroscopy studies.[33-35]

A more recent, and increasing popular, model that takes such species into account is called the multisite complexation (MUSIC) model.[18,33]

P-25 titania has a structure with Ti^{4+}-filled oxygen octahedra. The bulk of the solid is comprised of triply coordinated (Ti_3O^0) where each Ti^{4+} distributes its charge over six neighbouring oxygens giving a bond valence equal to 2/3. On the surface of the P-25, these oxygens may be singly ($TiO^{-4/3}$), doubly ($Ti_2O^{-2/3}$), or triply coordinated (Ti_3O^0) due to missing bonds. It has been shown that, as soon as the $TiO^{-4/3}$ group comes into contact with water it immediately picks up a proton and becomes $TiOH^{-1/3}$.[34] In the case of titania, the MUSIC model identifies singly ($TiOH^{-1/3}$) and doubly ($Ti2O^{-2/3}$) co-ordinated surface groups as responsible for the observed charging behaviour of the titania surface via the following protonation reactions:

$$TiOH^{-1/3} + H^+ \overset{K_{H1}}{\rightleftharpoons} TiOH_2^{+2/3} \qquad (3.4)$$

$$Ti_2O^{-2/3} + H^+ \overset{K_{H2}}{\rightleftharpoons} Ti_2OH^{+1/3} \qquad (3.5)$$

where K_{H1} and K_{H2} are the sequential acid association constants for these two surface species. Other work indicates that these two constants have similar values and so, for simplicity, are usually assumed equal and represented by one parameter, K_H.[18,33] It is also usual to assume that the densities of the singly and doubly co-ordinated sites, $TiOH^{-1/3}$ and $Ti_2O^{-2/3}$, are the same and equal to N_S.[18,33]

The charge of surface complexes are distributed over two electrostatic planes shown in figure 3.2. Hydrated counterions of the background electrolyte have a minimum distance of approach to the surface and so form the diffuse double layer (*ddl*) with its head at 2-plane in this 3-plane system as shown in figure 3.2.

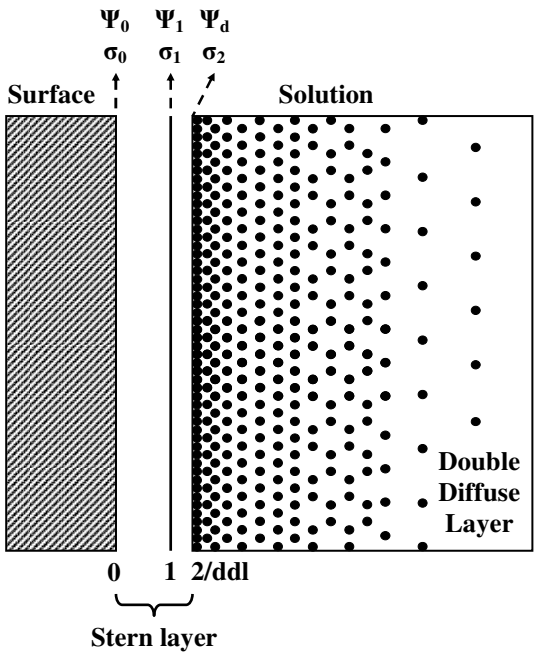

Figure 3.2 Schematic diagram illustrating the basic features of a three plane model of a metal oxide-electrolyte interface with innersphere complex formation at the 1-plane and outersphere complex formation with the counterions at the head of the double diffuse layer in the 2-plane.

The hydrated ions at the 2-plane are usually treated as point charges, which form outersphere, ion-pair complexes that do not form strong chemical bonds with the surface groups. The ion-pair reactions of the surface groups with these hydrated ions at the head of the *ddl* are as follows:

$$TiOH^{-1/3} + C^{+} \overset{K_{C1}}{\rightleftharpoons} TiO^{-1/3}\text{-}C^{+} \quad (3.6)$$

$$TiOH_2^{+2/3} + A^{-} \overset{K_{A1}}{\rightleftharpoons} TiOH_2^{+2/3}\text{-}A^{-} \quad (3.7)$$

$$Ti_2O^{-2/3} + C^{+} \overset{K_{C2}}{\rightleftharpoons} Ti_2O^{-2/3}\text{-}C^{+} \quad (3.8)$$

$$Ti_2OH^{+1/3} + A^{-} \overset{K_{A2}}{\rightleftharpoons} Ti_2OH^{+1/3}\text{-}A^{-} \quad (3.9)$$

where C^+ and A^- are the hydrated cations and anions of the counterions at the head of the *ddl* and K_{C1}, K_{C2}, K_{A1} and K_{A2} are the relevant ion-pair complexation constants. As with K_{H1} and K_{H2}, it is usual to assume that $K_{C1} = K_{C2} = K_C$ and $K_{A1} = K_{A2} = K_A$.[18,33]

The above, simple basic Stern MUSIC model has been used by Bourikas *et al.*[18] to model very effectively the observed primary charging behaviour of titania, including P-25, as a function of pH, for a wide variety of different electrolytes. The results of this work show that with increasing difference between the solution pH and the p.z.c. of P-25 TiO_2 (i.e. $\Delta pH = pH - p.z.c.$) the surface charge either becomes increasingly positive (for increasing negative values of ΔpH) or negative (for increasing positive ΔpH). Figure 3.3 shows plots of surface charge, σ_o, vs. pH for P-25 TiO_2 in solutions of different NaCl concentrations generated using the MUSIC model and the parameters in table 3.1.

Table 3.1 Parameters used in the MUSIC model to generate plots of the charging behaviour of P-25 in the presence of various concentrations NaCl at a range of pH values (at 298 K).

Parameter	Value	Parameter	Value
MUSIC (Basic Stern) model			
C (Fm^{-2})	0.9	$\log K_{Cl}$	-1.1
$\log K_{Na}$	-0.5	N_S (nm^{-2})	5.6
$\log K_H$	6.6	A (m^2/g)	50

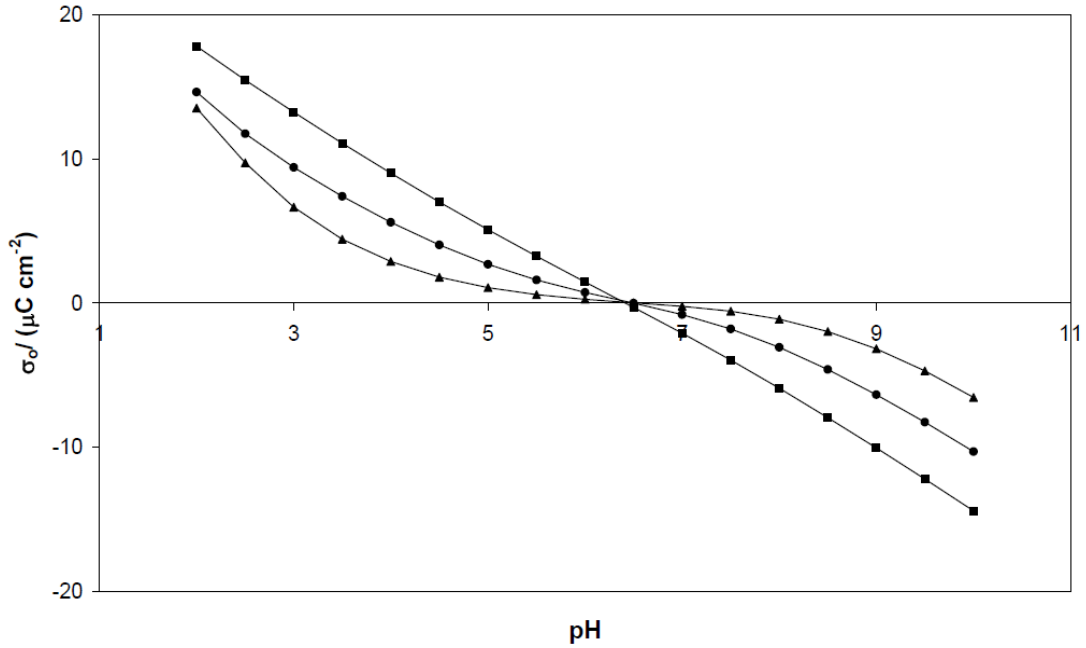

Figure 3.3 Charging behaviour of P-25 titania at various [NaCl] levels as a function of pH, as calculated using the MUSIC model and the parameters listed in table 3.1. The [NaCl] values used were: 0.1 (■), 0.01 (●) and 0.001 (▲) M, respectively.

This model assumes that the tendency of the particles to aggregate – which is greatest at the p.z.c. – does not reduce the effective number of adsorption sites available and this is supported by the work of many workers[33,35] in their excellent fits of the Stern model generated curves to the observed charging behaviour of many oxides, including TiO_2, in well-stirred systems. Although particle size measurements were not performed as part of this work, the absorption spectra of the titania dispersions with and without dye were recorded, since the turbidity of these dispersions, as measured by the absorbance at 800 nm say, provides a reasonable guide to the degree of dispersion of the particles. In our work it was found the absorbance of the P-25 dispersion at 800 nm, with and without the dye (17 mg dm^{-3}) did not vary over the pH range 2 – 10, there by indicating a reasonably consistent dispersion of the titania, with and without dye, at all pHs studied.

Thus, if the adsorption of MB^+ is due mainly to electrostatic attractive forces then it follows the values of, K_L, and, n_o, for MB^+ adsorption should increase with

increasing ΔpH and become increasingly negligible for increasing positive values of ΔpH. Certainly, this simple electrostatic model provides a rationale for the well established observation that 'cationic dyes bind [on metal oxide semiconductor photocatalysts] at pH values greater than the p.z.c., while anionic dyes show the opposite trend'.[9]

The MUSIC model can be extended further to account for surface complexation of strongly binding (inner-sphere) which form between the surface species and a strongly binding species, such as a dye.[18,33]

Unlike the outersphere complexes which are treated as point charges, part of the charge of an innersphere complex is attributed to the surface, i.e. the 0-plane in figure 3.2, while the remaining part resides in the 1-plane at a distance from the surface but before the *ddl*. The capacitance of the basic Stern layer, C, divides into two when inner-sphere complexes are formed, where the inner- and outer-layer capacitances, C_1, and, C_2, are related to C as follows:

$$1/C = 1/C_1 + 1/C_2 \tag{3.10}$$

The charge densities and potentials of the three (0-, 1- and 2-) planes are: σ_0, σ_1 and σ_2 and Ψ_1, Ψ_2 and Ψ_d, respectively (see figure 3.2).

It is generally assumed that the singly co-ordinated surface groups are the most important reactive surface groups for specific adsorption. For simplicity we assume MB^+ and its aggregates form mondentate innersphere complexes with $TiOH^{-1/3}$, so that, for example, the key reaction for the monomer involving MB^+ adsorption at such sites is as follows:

$$TiOH^{-1/3} + MB^+ \overset{K_{MB1}}{\rightleftharpoons} TiOH\text{-}MB^{+2/3} \tag{3.11}$$

In order to test this simple model, the amount of dye adsorbed per g of TiO_2 ($[MB^+]_{ads}$) was determined as a function of pH and the results are illustrated in figure

3.4. The conditions and methods used to obtain this data ($[MB^+]$ = 300 mg dm^{-3}; $[TiO_2]$ = 750 mg dm^{-3}) were as used by Bourikas *et al.*[18] in their recent investigation into the adsorption of the anionic, azo dye Acid Orange 7 on the surface of P-25 titania. These adsorption edge results reveal that the level of $[MB^+]_{ads}$ is negligible at pH $\leq$ 7.5 which is not too surprising. More importantly, above pH 7.5, $[MB^+]_{ads}$ increases almost exponentially with increasing pH and it is possible to simulate the adsorption edge data illustrated in figure 3.4 using a CD-MUSIC programme by assuming: (i) not only monomers, but dimers and trimers of MB^+ are adsorbed onto the surface and (ii) dimer and trimer formation on the surface is promoted by hydroxyl anion association, i.e.

$$TiOH^{-1/3} + 2MB^+ + OH^- \overset{K_{MB2}}{\rightleftharpoons} TiOH((MB^+)_2OH^-)^{+2/3} \qquad (3.12)$$

$$TiOH^{-1/3} + 3MB^+ + 2OH^- \overset{K_{MB3}}{\rightleftharpoons} TiOH((MB^+)_3(OH^-)_2)^{+2/3} \qquad (3.13)$$

Table 3.2 Parameters used in the MUSIC and monomer and multimer dye CD-MUSIC models for methylene blue (at 298 K)

Parameter	Value	Parameter	Value
MUSIC (Basic Stern) model			
C (Fm^{-2})	0.9	$\log K_H$	6.6
$\log K_{Na}$	-0.5	$\log K_{Cl}$	-1.1
N_S (nm^{-2})	5.6		
Monomer/Multimer Dye CD-MUSIC model			
C_1 (Fm^{-2})	1.1	K_{MB1}	7
C_2 (Fm^{-2})	5.0	K_{MB2}	4000
		K_{MB3}	16×10^6
General data			
A (m^2/g)	50	K_D (M^{-1})	2090
K_{Tr} (M^{-1})	3990		

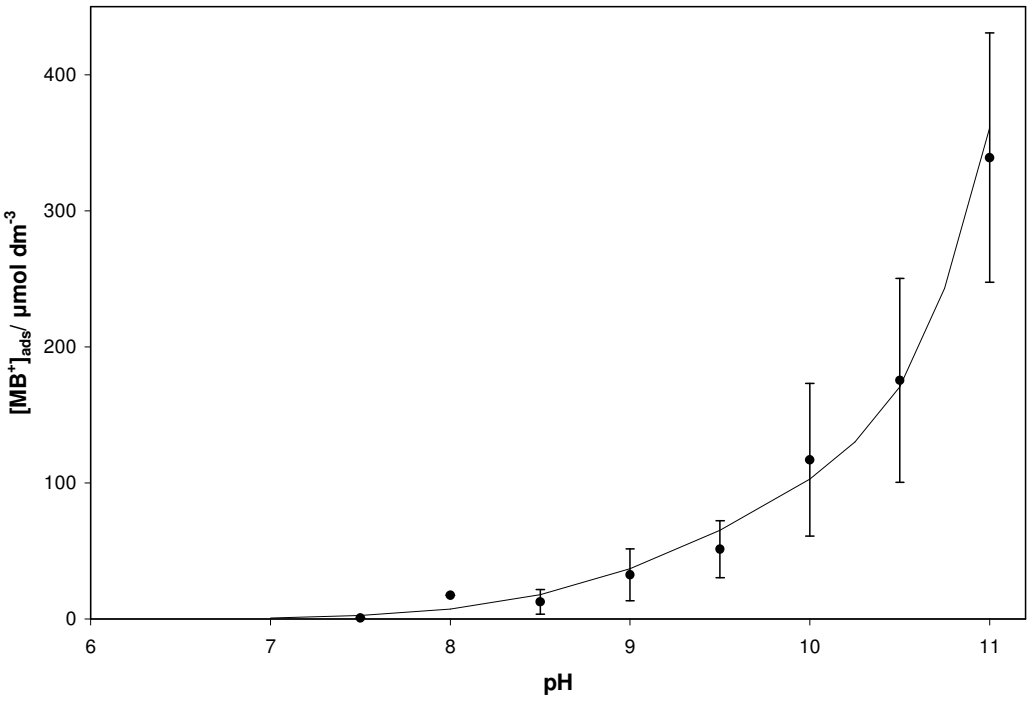

Figure 3.4 Adsorption edge data for MB^+ on P-25 titania measured under *ex situ* conditions ($[TiO_2]$ = 750 mg dm^{-3}) $[MB^+]_{total}$ = 300 mg dm^{-3}. The solid line was those calculated using the CD-MUSIC model and the constants and equations given in table 3.2, Appendix A and table A1, respectively.

Some support of the latter assumption is given by the finding of others who found that the formation of dimmers of thionine (a thiazine dye like MB^+) is enhanced by an association reaction with an anionic species, such as chloride. The anion, presumably reduces the repulsive forces acting between the positively charged thionine molecules in the multimer. Encouragingly, the solid line illustrated in figure 3.4, which was calculated using: (i) the above multimer CD-MUSIC model, (ii) the above reaction equations (3.3) – (3.13), and (iii) the constants and equations given in table 3.2 and A1, shows a good fit to the data. This simple CD-MUSIC model allows the amount of MB^+ adsorbed on titania at different pHs, dye concentrations and ionic strengths to be calculated for a wide variety of conditions. Further details of how the CD-MUSIC model was used to generate the solid line are given in appendix A.

The above CD-MUSIC model can also be used to generate adsorption isotherms for MB^+ as a function of pH, which can be subsequently analysed as if they were Langmuir adsorption curves, so as to generate apparent values of, K_L, and, n_o, as a function of pH, plots of which are shown in figure 3.5. These plots reveal the not too surprising finding that K_L, and, n_o, increase with increasing pH.

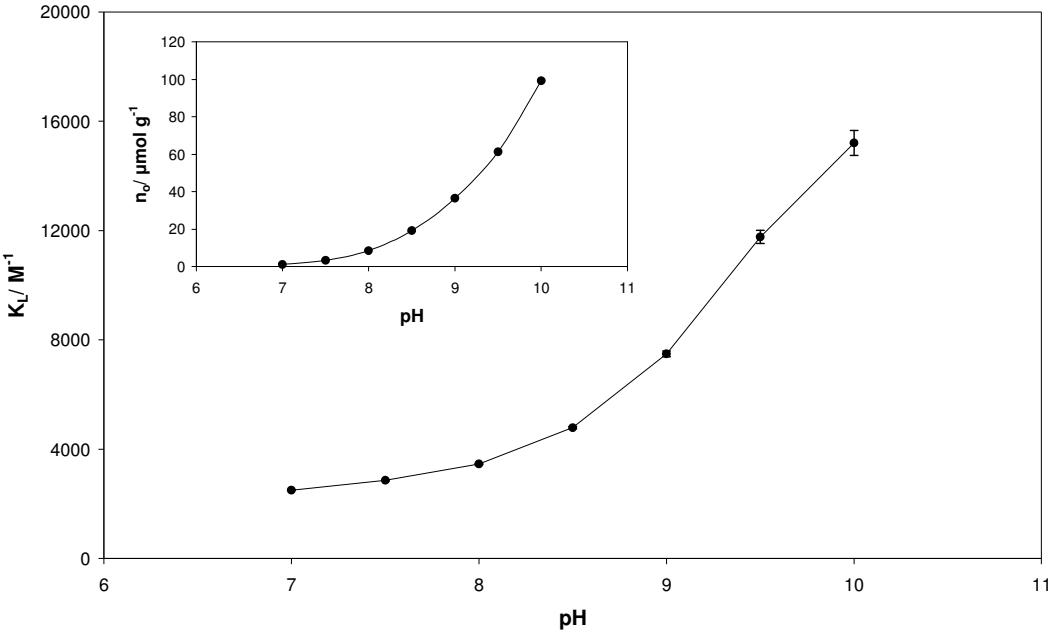

Figure 3.5 Plots of the apparent Langmuir adsorption constant, K_L, and the total number of surface sites available for innersphere complex formation, n_o, (insert plot) as a function of pH. Each K_L, and, n_o, data set was obtained using the multimer CD-MUSIC model to predict the adsorption isotherm at a pH, which was then analysed as if they were Langmuir type isotherms, so as to reveal values for K_L, and, n_o.

As mentioned in the introduction, there does not seem to be any literature looking at the trends in, K_L, and, n_o, for methylene blue as a function of pH so there is no data to make a direct comparison with the results in figure 3.5. If we compare the individual, K_L, values from the literature (listed in table 1.1) we find that the results obtained by Houas *et al.*[3] and *Lachheb et al.*[11] are of the same order of magnitude to the calculated values using the above model, i.e. they quote values of 6.25 x 10^3 M^{-1} and 6.65 x 10^3 M^{-1} respectively at natural pH and the above model predicts, K_L, to be approximately 2.5 x 10^3 M^{-1} at pH 7. The other adsorption constants quoted in table

1.1 are much higher than these values at lower pHs, however these values cannot be directly compared with the above model as they were obtained from photocatalytic studies.

3.3 MB^+ as a Test Dye for Assessing Photocatalyst Activity with UV Light

A series of experiments were carried out under *in-situ* monitoring conditions (i.e. $[TiO_2]$ = 20 mg dm^{-3}; $[MB^+]_{total}$ = 1.32 x 10^{-5} M) in which the initial rates of MB^+ bleaching, r_i (units: absorbance units/min or Abs U min^{-1}) photosensitised by UV excited titania, were measured as a function of pH and the results of this work are illustrated in figure 3.6. It is possibly little surprise that the initial rate of destruction of MB^+ rises from pH 6 with increasing pH, in much the same way that the $[MB^+]_{ads}$ was found to vary with pH (see figure 3.4). Indeed, it seems reasonable that the rate of photocatalysis would be related to $[MB^+]_{ads}$ (calculated using the CD-MUSIC model for the *in-situ* reaction conditions) and so, as illustrated by the insert plot, it is not surprising to note a strong correlation between r_i and $[MB^+]_{ads}$.

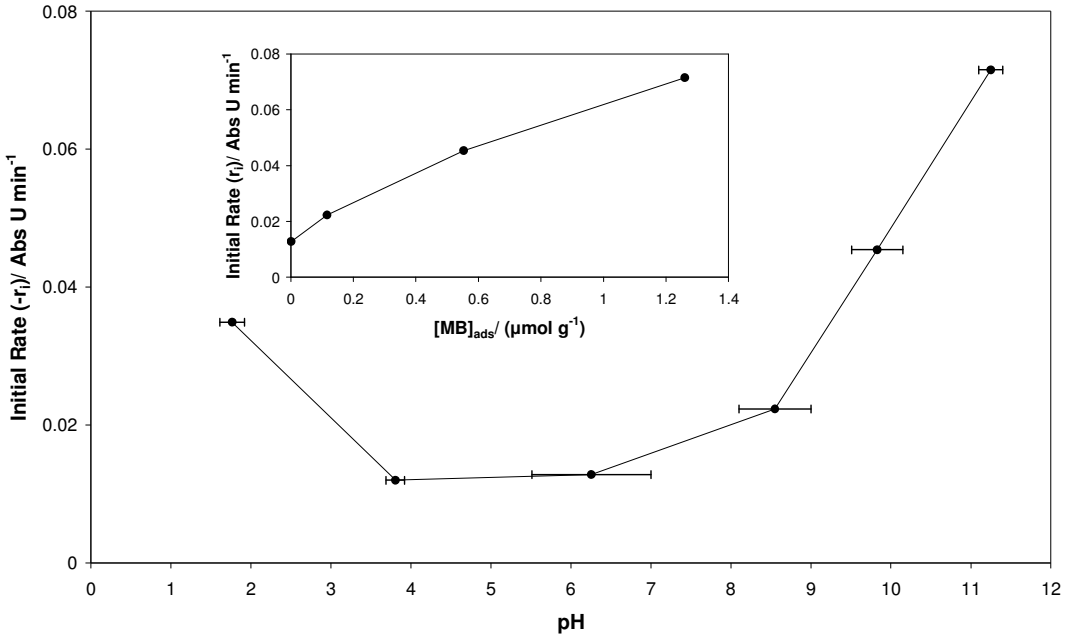

Figure 3.6 Measured initial rate of photobleaching of MB^+ (in units of absorbance units at 660 nm per min, i.e. Abs U min^{-1}) as a function of pH for experiments conducted under *in-situ* conditions ($[TiO_2]$ = 20 mg dm^{-3}; $[MB^+]_{total}$ = 1.32 x 10^{-5} M) using two 8W BLB lamps (UVA: 2 mW cm^{-2}). The insert diagram is a plot of the initial rate data in the main figure vs. the amount of MB^+ adsorbed onto the titania, as calculated using the CD-MUSIC model and constants in table 3.2.

These finding suggest that the rate determining step for the primary oxidation of MB^+ is the reaction between the photogenerated hole and adsorbed MB^+, i.e.:

$$MB^+_{ads} + h^+ \rightarrow MB^{2+\bullet} \qquad (3.14)$$

where $MB^{2+\bullet}$ is an unstable oxidised radical of MB^+, which subsequently decomposes to bleached products. The fact that there is a lower, but still appreciable degree of photobleaching at pHs for which $[MB^+]_{ads}$ is negligible (i.e. at pHs < 7) implies a secondary, less effective, but still significant, mode of photobleaching in operation; this latter process most likely involves indirect hydroxyl radical attack of the free (non-adsorbed) dye, i.e.

$$OH_{ads} + h^+ \rightarrow OH^{\bullet}_{ads} \qquad (3.15)$$

$$OH^{\bullet}_{ads} + MB^+ \rightarrow \text{dye oxidation products} \qquad (3.16)$$

where the dye oxidation products may be $MB^{2+\bullet}$, but could also be a hydroxylated intermediate form of the dye.

So far it has been assumed that at all pHs discussed so far the photo-generated electron is scavenged by dissolved oxygen, i.e.:

$$4e^- + O_2 + 4H^+ \rightarrow 4H_2O \qquad (3.17)$$

It appears likely that at pHs > 4 reaction (3.17) is effectively catalysed by MB^+, since the latter is able to scavenge rapidly the photogenerated electrons via:

$$2e^- + H^+ + MB^+ \rightarrow LMB \qquad (3.18)$$

where: LMB is leuco-methylene blue, a colourless, reduced form of MB^+. That no evidence of LMB is found between pHs 4 – 12 is no surprise, since LMB is known[36] to be very rapidly oxidised by oxygen at these pHs, i.e.:

$$2LMB + 2H^+ + O_2 \rightarrow H_2O + 2MB^+ \qquad (3.19)$$

Thus, the combination of reactions (3.17) and (3.18) results in the effective catalysis of reaction (3.17) by MB^+ at pHs > 4.

The above reactions of the photogenerated holes and electrons provides a ready rationale for most of the observed variation of r_i vs. pH illustrated in figure 3.6 for the photobleaching of MB^+ by UVA-activated P-25 titania. The exception is the observed high rate of photobleaching at pH 2, which is due to the pH-sensitivity of reaction (3.19). In particular, at pH 2 reaction (3.19) is so slow that the observed significant rate of photobleaching of MB^+ is due to a combination of bleaching reactions (3.16) and (3.18), rather than the usual oxidative bleaching reaction (3.16).[15] This 'oxidative-reductive-photobleaching' feature at pH 2 of the TiO_2/MB^+ photocatalytic system was demonstrated by monitoring at all pHs the absorption

spectrum of the reaction solution *after* it was photobleached as a function of time in the dark. Only at pH 2 was any (35%) recovery of the initial absorbance of the MB^+ observed in this 'dark' study of the photobleached solutions; this being due to the slow re-oxidation of LMB at pH 2, i.e. reaction (3.19). Thus, the unusually high rate of photobleaching observed for MB^+ at pH 2, is due to the pH conditions which allow dye photobleaching to occur by both oxidative (reaction (3.16)) and reductive (reaction (3.18)) pathways.[15]

3.4 MB^+ Sensitised Bleaching using Visible Light

As noted earlier, MB^+ can also be photobleached via a dye-sensitised process in which the electronically excited state of the dye, $MB^{+}*$, injects an electron into the conduction band of the titania to produce an oxidised dye radical, $MB^{2+\bullet}$, which is unstable and capable of decomposition into colourless products, i.e.

$$MB^{+}* + TiO_2 \rightarrow MB^{2+\bullet} + TiO_2(e^-) \qquad (3.20)$$

Since MB^+ does not absorb strongly in the UV, this dye-sensitised process is most easily and usually demonstrated using an intense visible light, which in this work was provided by a 150W Xe-arc light. Thus, using the same *in-situ* reaction conditions as described previously, but with the Xe-arc light, combined with a 400 nm cut-off filter, the initial rate of dye photobleaching was measured as a function of pH and the results are also illustrated in 3.7. These results show the rate increases from a small value at pH 6 to a significant rate at pH 11, much like the amount of MB^+ adsorbed on TiO_2 increases with increasing pH (see figure 3.4). In line with this model, the insert diagram in figure 3.7, a plot of r_i values measured using visible light at different pHs versus the multimer CD-MUSIC model-calculated value of $[MB^+]_{ads}$ (under *in-situ* reaction conditions, reveals a clear correlation between the two parameters. This correlation seems appropriate given the nature of the key process, i.e. reaction (3.20), and its implication that only dye molecules that are in direct contact with the surface can undergo photodegradation via this dye-

sensitised route.[37] Note however, at high dye surface concentrations dye excited state annihilation and self-quenching processes are likely to compete with the charge injection process and so decrease the overall efficiency of the dye-sensitised photobleaching process.[37] The latter effect may be responsible for the apparent negative deviation from linearity in the insert plot in figure 3.7, at high vales of $[MB^+]_{ads}$.

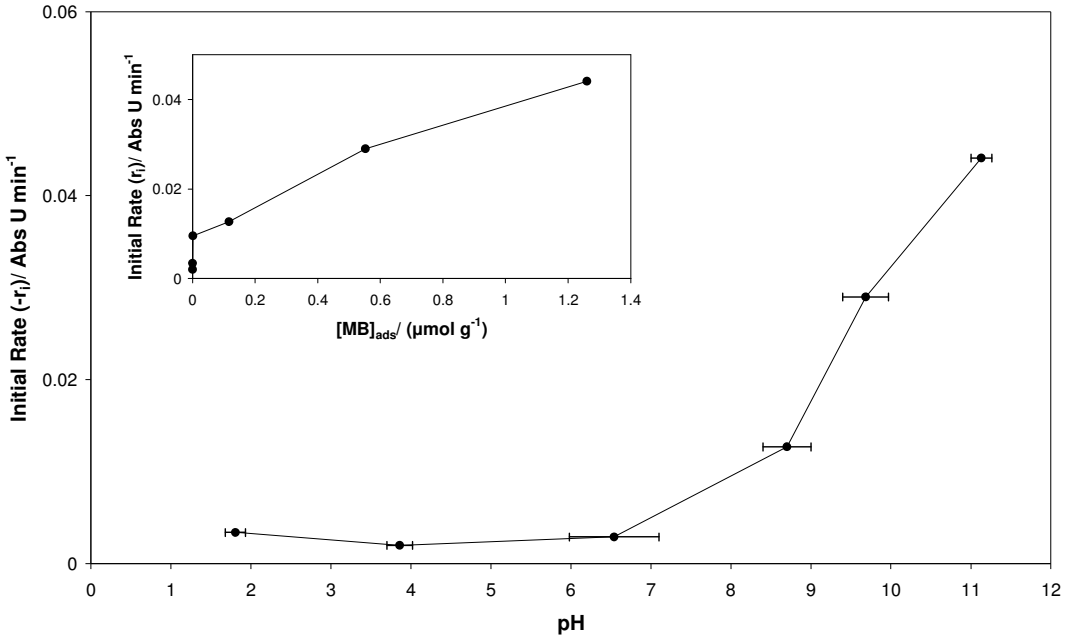

Figure 3.7 Measured initial rate of photobleaching of MB^+ (in units of absorbance units at 660 nm per min, i.e. Abs U min^{-1}) as a function of pH for experiments conducted under *in-situ* conditions ($[TiO_2]$ = 20 mg dm^{-3}; $[MB^+]_{total}$ = 1.32 x 10^{-5} M) using a 150W Xe-arc lamp with a 400 nm filter (i.e. a visible – no UV – light source). The insert diagram is a plot of the initial rate data in the main figure vs. the amount of MB^+ adsorbed onto the titania, as calculated using the CD-MUSIC model and constants in table 3.2.

As mentioned in table 1.1 and in section 1.2.1.2, it is found in the literature that the rate of photobleaching MB^+ generally increases as the pH is increased, just as we have seen for the results of this chapter for both UV and visible irradiations. Although Guillard *et al.*[12] showed an increase in the rate as the pH is increased from pH 3 to pH 9, they had an appreciable rate at pH 3 (~ 0.04 min^{-1}) which was not observed in this work for visible irradiations. Possible reasons for the high rate at

pH 3 could perhaps be due to the use of high concentrations of P-25 (500 mg dm^{-3}) and MB^+ (8.42×10^{-5} M) causing the system to behave differently and/or the use of syringe filters which may have adsorbed some of the dye, giving erroneous readings.

3.5 Conclusions

The observed adsorption of MB^+ on P-25 titania over a range of pH values (pH 2 – 11) is well described using a CD-MUSIC model in which aggregated forms of the dye present in solution, as well as its monomeric form, are adsorbed onto the surface of titania. In this model, the charge on the aggregated adsorbed forms appears modified by co-adsorbed hydroxyl ions.

The rate of bleaching of MB^+, photocatalysed by titania using UV light, appears to *increase* over the pH range 4 – 11 in much the same way the amount of adsorbed MB^+, $[MB^+]_{ads}$, increases, possibly indicating that the rate determining step involves direct hole oxidation of adsorbed MB^+. At pH 2, the rate of UVA dye photobleaching is high due to reductive and oxidative bleaching processes. The initial rate of bleaching of MB^+ via a visible light-driven, dyesensitised process, appears also to correlate with $[MB^+]_{ads}$ at different pHs, indicating that only dye molecules that are in direct contact with the surface can undergo photodegradation via a dye-sensitised route. This work indicates that dye adsorption is an important factor in the observed kinetics of dye photobleaching on titania, using either UVA light, where bleaching is mainly via semiconductor photocatalysis, or visible light, where the main bleaching process is via dye-photosensitisation.

4 Adsorption and Photocatalytic Bleaching of Acid Orange 7 ($AO7^-$) on P-25 Titania

As previously mentioned for methylene blue, the modelling of this system will take into account that dye multimers can readily adsorb onto the P-25 surface as well as the monomer species.

The aggregation of azo dyes, such as $AO7^-$, has been well studied,[29,38-41] including by Ghosh *et al.*[29], who studied the dimerisation and trimerisation of many dyes, including $AO7^-$ via UV/Vis spectrophotometry, and the following equilibria:

$$2AO7^- \overset{K_D}{\rightleftharpoons} (AO7^-)_2 \quad (4.1)$$

$$(AO7^-)_2 + AO7^- \overset{K_{Tr}}{\rightleftharpoons} (AO7^-)_3 \quad (4.2)$$

These workers report values of 1400 M^{-1} and 3500 M^{-1} for the equilibria constants, K_D and K_{Tr} and others[38-40] have reported similar values (e.g. 953, 1030, 1320 M^{-1}) for K_D. Using the values of K_D and K_{Tr} reported by Ghosh *et al.*[29], the fractions of $AO7^-$ in its monomeric, dimeric and trimericform, i.e. f_M, f_D and f_{Tr}, present in different total dye concentrations, $[AO7^-]_{total}$, spanning the range 0 – 1.5 mM, were calculated and the results of this work are illustrated in figure 4.1. Thus, at a typical $[AO7^-]_{total}$ used for *in-situ* SPC studies, where the absorbance of the solution has a value of ca.1 in a 1 cm cell, i.e. 4.86 x 10^{-5} M, the values of f_M, f_D and f_{Tr} are ca. 0.78, 0.1 and 0.02, respectively. From these values it is clear the level of dimer in solution is not insignificant even at this low $[AO7^-]_{total}$. It should also be noted, that the fractions of these aggregated species increases with increasing $[AO7^-]_{total}$, so that at an $[AO7^-]_{total}$ = 8.57 x 10^{-4} M – not atypical of the dye concentrations used in *ex situ* monitored SPC studies – the values of these fractions are increased to: 0.33, 0.27 and 0.40, respectively, which are disturbingly appreciable levels!

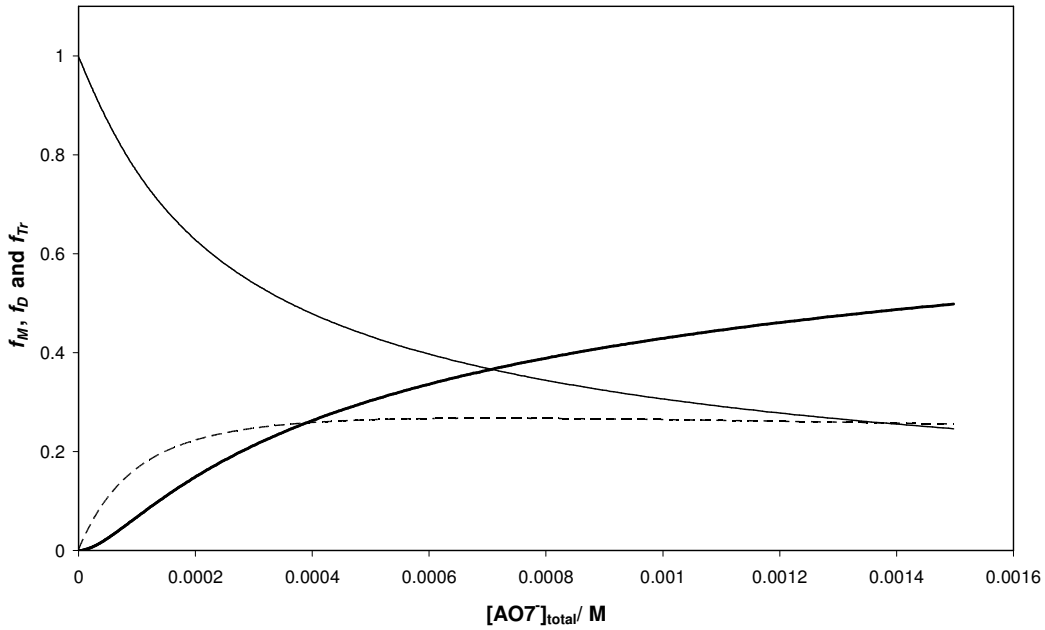

Figure 4.1 Fractions of $AO7^-$, in the form of a monomer (thin solid line), dimer (broken line) and trimer (thick solid line), in solution as a function the total dye concentration, $[AO7^-]_{total}$, calculated using the dimerisation and trimerisation constants reported by Ghosh *et al*.[29]

The MUSIC and CD-MUSIC models have previously been detailed in section 3.2. The parameters used in the MUSIC and monomer and multimer dye CD-MUSIC models for $AO7^-$ are listed in table 4.1.

Table 4.1 Parameters used in the MUSIC and monomer and multimer dye CD-MUSIC models for acid orange 7 (at 298 K)

Parameter	Value	Parameter	Value
MUSIC (Basic Stern) model			
C (Fm^{-2})	0.9	$\log K_H$	6.6
$\log K_{Na}$	-0.5	$\log K_{Cl}$	-1.1
N_S (nm^{-2})	5.6		
Monomer/Multimer Dye CD-MUSIC model			
C_1 (Fm^{-2})	1.1	$K_{AO7\text{-}in}$ (ref. 18)	15.1
C_2 (Fm^{-2})	5.0	$K_{AO7\text{-}in}$ (this work)	14.54
General data			
A (m^2/g)	50	K_D (M^{-1})	1400
K_{Tr} (M^{-1})	3500		

It is generally assumed that only the singly co-ordinated surface groups form innersphere complexes with anions.[18]

There have been many FTIR studies in the literature that support the assumption that $AO7^-$ forms a bidentate innersphere complex via two oxygens of the SO_3 group.[2,17,18] Figure 4.2 shows a FTIR-ATR obtained using P-25 stained in a solution containing 300 mg dm^{-3} of $AO7^-$ and 750 mg dm^{-3} of P-25 at pH 2.

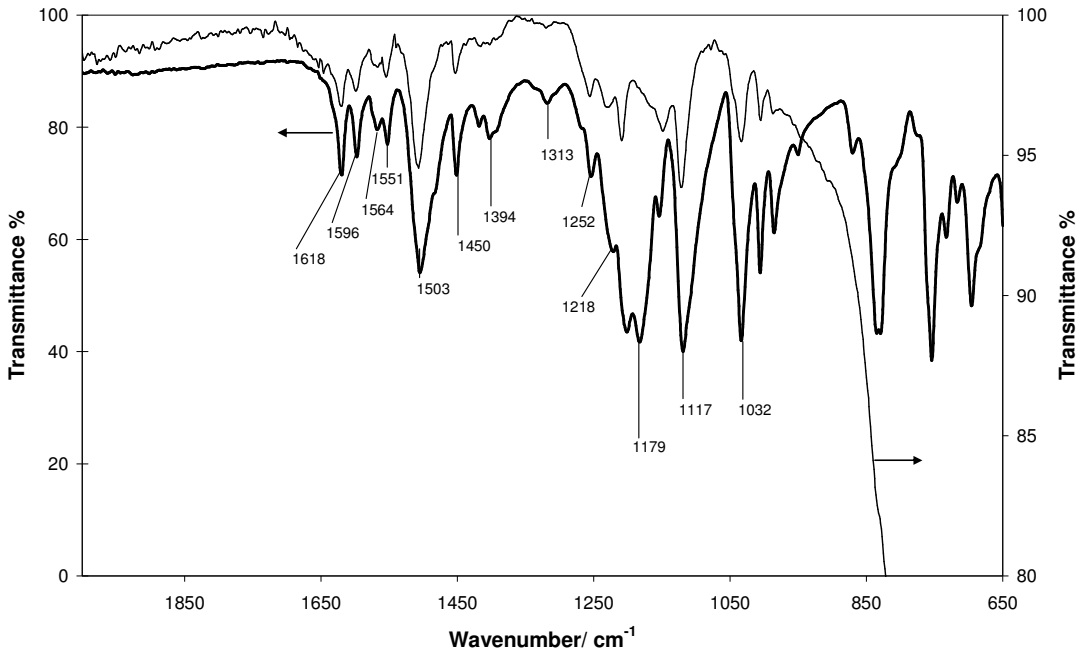

Figure 4.2 FTIR-ATR spectra of $AO7^-$ powder (thick black line) and $AO7^-$ stained P-25 powder (thin black line). The P-25 was stained using 300 mg dm^{-3} of $AO7^-$ and 750 mg dm^{-3} of P-25 at pH 2.

A detailed assignment of the bands in the region of 2000 – 1000 cm^{-1} have reported previously by Stylidi *et al.*[2] The band at 1503 cm^{-1} has been linked to either the -N=N- vibrations or to the aromatic ring vibrations which are interacting with the azo bond. Bands at 1450, 1551, 1564, 1596 and 1618 cm^{-1} are linked to the skeletal vibrations of the aromatic rings. The small peak at 1394 cm^{-1} can be attributed to the OH bending vibrations. Peaks at 1313 cm^{-1} and 1179 cm^{-1} are due to the sulfonate group, $\upsilon_{as}(SO_3)$ and $\upsilon_s(SO_3)$ respectively, and those at 1252 cm^{-1} and 1218 cm^{-1} arise from the tautomer form of the dye and correspond to the vibration stretching modes

of υ(C-N) and υ(N-N) respectively. The bands at 1117 cm^{-1} and 1032 cm^{-1} can be assigned to the coupling between the benzene mode and $\upsilon_s(SO_3)$.

Upon adsorption of the dye onto the P-25 surface, two bands in the FTIR-ATR spectrum disappear at 1313 cm^{-1} and 1179 cm^{-1} which correspond to the sulfonate group. This suggests a strong interaction of the two oxygen atoms of the sulfonate group with the titania surface. Figure 4.3 shows the adsorption mode proposed by Bourikas *et al.*[18] of $AO7^-$ on the surface of P-25.

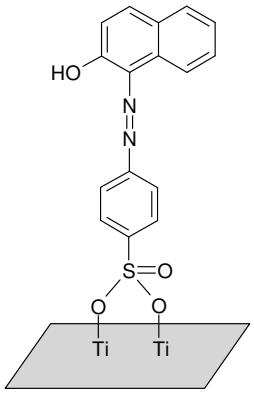

Figure 4.3 The proposed adsorption mode of $AO7^-$ on the surface of P-25 titania.

Thus, assuming $AO7^-$ forms a bidentate innersphere complex with $TiOH^{-1/3}$, as suggested by the work of others,[29,38-41] the key reaction involving $AO7^-$ adsorption at such sites is:

$$2TiOH^{-1/3} + 2H^+ + AO7^- \overset{K_{AO7}}{\rightleftharpoons} Ti_2AO7^{+1/3} + 2H_2O \qquad (4.3)$$

The CD-MUSIC approach, coupled with reactions (3.3) – (3.10), (4.3) and the key model parameters in table 4.1, were used by Bourikas *et al.*[18] (with log $K_{AO7\text{-}in}$ = 15.1, *vide infra*) to generate the solid line fits to their adsorption edge data recorded for $AO7^-$ on P-25 that are illustrated in figure 4.4. Further details of how the CD-MUSIC model was used to generate these curves are given in Appendix A.

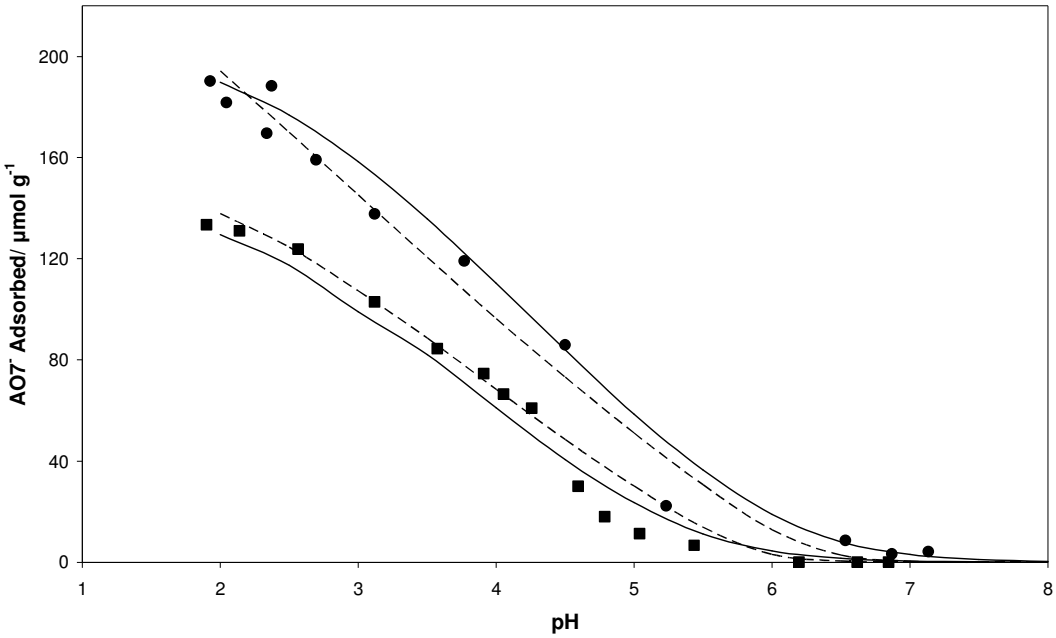

Figure 4.4 Adsorption edge data for $AO7^-$ on P-25 titania measured under *ex situ* conditions ($[TiO_2]$ = 750 mg dm^{-3}) reported by Bourikas *et al.*,[18] for $[AO7^-]_{total}$ values of: 8.56 x 10^{-4} M (●) and 1.43x10^{-4} M (■). The solid lines were those calculated using the CD-MUSIC model (assuming all free and adsorbed dye is monomeric) and the constants given in table 4.1; the curves are identical to those reported earlier by Bourikas *et al.*[18] The broken lines were those calculated using the revised multimer CD-MUSIC model and the constants given in table 4.1.

The above fit to the data is good, but is based on the erroneous, but commonly made, assumption that the dye is monomeric at all the concentrations used to generate the data in figure 4.4. An obvious and simple improvement to this model is to assume that the $TiOH^{-1/3}$ surface species adsorb the monomer, dimer and trimer forms of $AO7^-$ equally well (not including the electrostatic element), i.e. for the relevant adsorption processes:

$$2TiOH^{-1/3} + 2H^+ + (AO7^-)_2 \overset{K'_{AO7}}{\rightleftharpoons} Ti_2(AO7)_2^{-2/3} + 2H_2O \qquad (4.4)$$

$$2TiOH^{-1/3} + 2H^+ + (AO7^-)_3 \overset{K''_{AO7}}{\rightleftharpoons} Ti_2(AO7)_3^{-5/3} + 2H_2O \qquad (4.5)$$

$K'_{AO7} = K''_{AO7} = K_{AO7}$. Note that K_{AO7} is an apparent constant in which the concentrations of surface sites are in units of M. In contrast, in table 4.1, intrinsic

constants are reported, i.e. ones in which the surface sites are expressed as mole fractions, which renders them independent of experimental conditions such as, ρ, the solid solution ratio (in this case [TiO_2] in g dm^{-3}) and A, the specific surface area (m^2 g^{-1}). As a consequence, because it is for a bidentate reaction, K_{AO7} is related to the intrinsic constant, $K_{AO7\text{-}in}$ (in table 3.3) via the following expression:

$$K_{AO7} = \frac{K_{AO7-in}}{\rho A N_S} \tag{4.6}$$

The solid lines illustrated in figure 4.4, showing an improved fit, were generated using: the above revised (multimer) version of the CD-MUSIC model employed by Bourikas *et al.*,[18] the constants given in table 4.1, with a revised value for K_{AO7} ($\log K_{AO7\text{-}in}$ = 14.54), and the values of K_D and K_{Tr} reported by Ghosh *et al.*[29] and given earlier. These lines reveal an encouragingly overall improved fit to the adsorption edge data. The above multimer CD-MUSIC model can also be used to generate adsorption isotherms for $AO7^-$ as a function of pH which can be subsequently analysed as if they were Langmuir adsorption curves, so as to generate apparent values of K_L, and n_o as a function of pH, plots of which are illustrated in figure 4.5. These plots reveal the not too surprising finding that K_L, and n_o increase with increasing negative ΔpH and are negligible for positive values of ΔpH; trends that have been observed by others.[11,20]

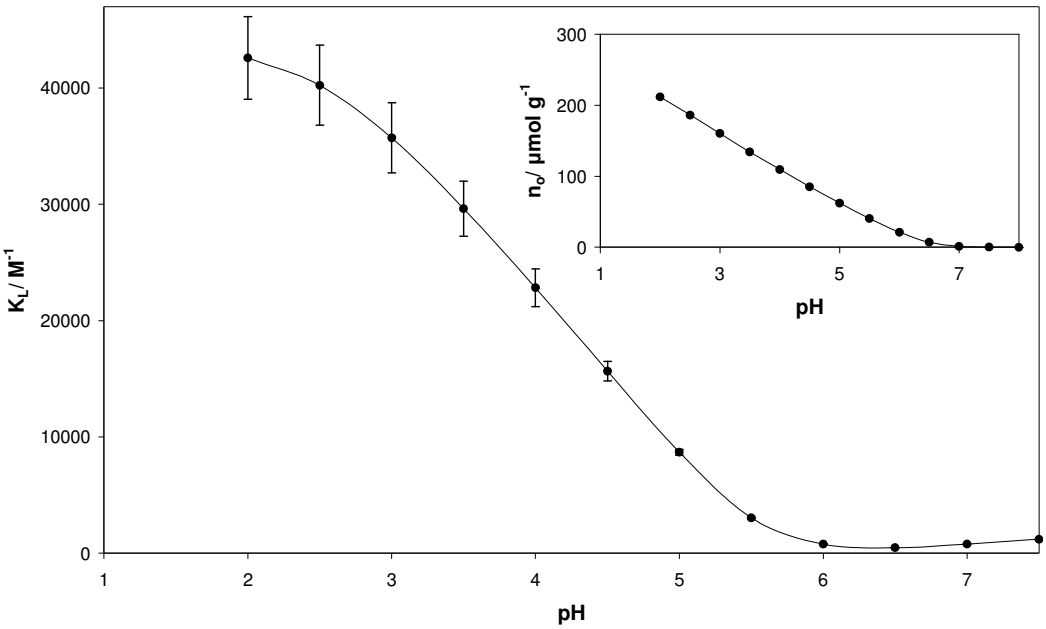

Figure 4.5 Plots of the apparent values of the Langmuir adsorption constant, K_L, (main diagram) and the total number of surface sites available for innersphere complex formation, n_o, (insert diagram) as a function of pH. Each K_L and n_o data set was obtained using the multimer CD-MUSIC model to predict the adsorption isotherm at a pH, which was then analysed as if they were Langmuir-type isotherms, so as to reveal values for K_L and n_o.

The trend observed for, K_L, shown in figure 4.5 is consistent with the trends found in the literature (see table 1.2). The quoted, K_L, values in the literature are however generally much lower than those calculated using the above CD-MUSIC model. The exception being the, K_L, value quoted by Bauer *et al.*[17] of 18000 M^{-1} at pH 6 which seems excessively high considering it is close to the titanias p.z.c. where very little dye should be attracted to the surface. The reasons for the variation in the magnitude of the, K_L, values are unclear. The calculated, K_L, and, n_o, values in figure 3.12 are very similar to those calculated by Bourikas *et al.*[25] (see figure 1.21).

4.1 $AO7^-$ as a Test Dye for Assessing Photocatalyst Activity with UV Light

In a series of experiments carried out under *in-situ* monitoring conditions ($[TiO_2]$ = 20 mg dm^{-3}; $[AO7^-]_{total}$ = 4.86 x 10^{-5} M) the initial rates of $AO7^-$ bleaching, r_i, photosensitised by UV excited titania, were measured as a function of pH and the results of this work are illustrated in figure 4.6. Surprisingly, these results reveal the rate increases by less than a factor of 2 over the pH range 2 to 10 and are not too dissimilar to those reported by others using P-25 TiO_2 as the semiconductor photocatalyst.[22,42] For example, using an *ex situ* method ($[TiO_2]$ = 750 mg dm^{-3}; $[AO7^-]_{total}$ = 8.57 x 10^{-4} M), Verykios *et al*.[22] found the rate of photobleaching under solar-simulator Xe-arc light irradiation to be pH independent over the range pH 2 – 9, but faster at pH 10 – 12. Augugliaro [42] and his co-workers reported, also using an *ex situ* method ($[TiO_2]$ = 200 mg dm^{-3}; $[AO7^-]_{total}$ = 2.86 x 10^{-5} M), that whilst the rate of photobleaching of $AO7^-$ under solar light irradiation dipped at pH 6, at pH 2 and 11 the rates were similar.[42] Note that the results from the above two reports are complicated by the fact that dye bleaching can occur by both semiconductor photocatalysis and dye photosensitisation as solar, or solar simulated, light was used.

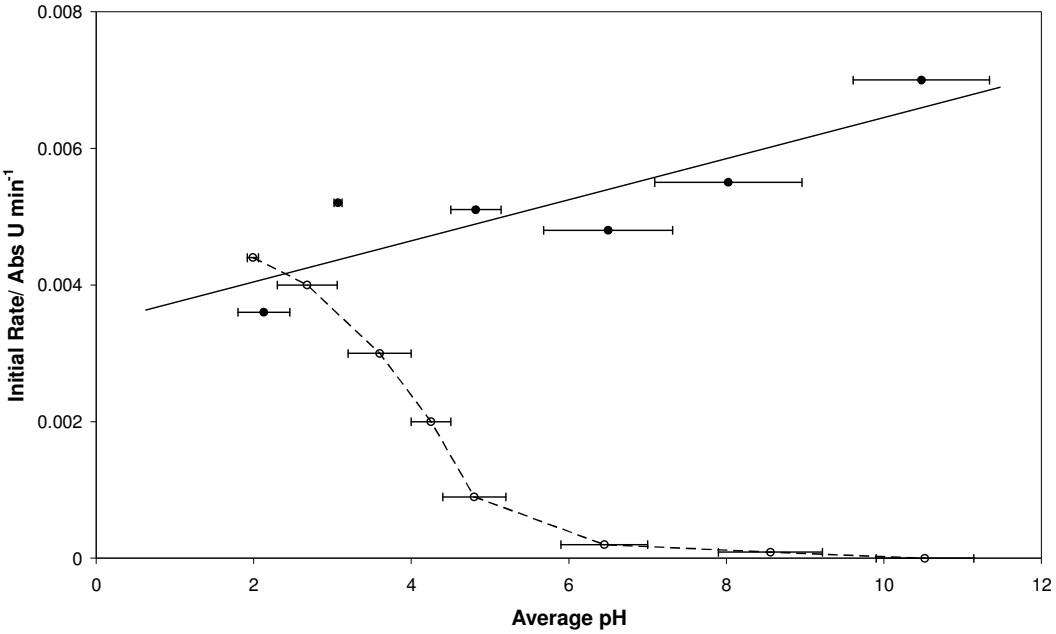

Figure 4.6 Measured initial rate of photobleaching of $AO7^-$ (in units of absorbance units at 484 nm per min, i.e. Abs U min^{-1}) as a function of pH for experiments conducted under *in-situ* conditions ($[TiO_2]$ = 20 mg dm^{-3}; $[AO7^-]_{total}$ = 4.86 x 10^{-5} M), with [NaCl] = 0.01 M, using either: (●) two 8 W BLB lamps (UVA: 2 mW cm^{-2}) or (○) a 180 W Xe-arc lamp with a 400 nm filter (i.e. a visible – no UV – light source).

The multimer CD-MUSIC model reported here can be used to estimate the total fraction of singly co-ordinated sites occupied by the dye, f_{AO7}, as a function of solution pH, under the *ex situ* measurements employed in this work, and the results are illustrated in figure 4.7.

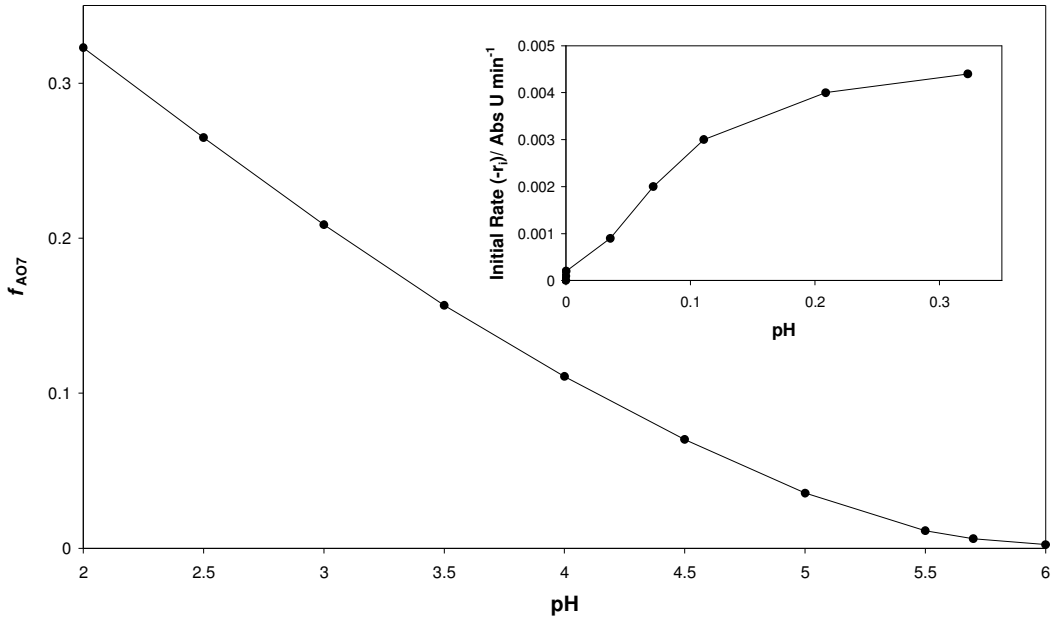

Figure 4.7 Multimer CD-MUSIC model-calculated values of the fraction of singly co-ordinated surface sites on P-25 titania with adsorbed $AO7^-$, f_{AO7}, as a function of pH. The insert plot is of the r_i values from figure 4.6, for visible light versus the value of f_{AO7} at the associated pH.

This plot shows that, as expected, f_{AO7} increases markedly with increasingly negative ΔpH; note also that the model predicts this effect is even more pronounced under *ex situ* monitoring conditions, since f_{AO7} increases significantly with increasing $[AO7^-]_{total}$. The results illustrated in the main figure 4.7 do not provide a ready explanation of the kinetic results illustrated in figure 4.6 for UV irradiation of the $AO7^-/TiO_2$ system, since it would seem reasonable to expect r_i to be related to f_{AO7} (as observed for MB^+). The reasons as to why that this is not the case are unclear. The simplest explanation is that the UV photocatalysed bleaching of $AO7^-$ occurs via the doubly co-ordinated sites, i.e. $Ti_2O^{-2/3}$, since – according to the CD-MUSIC model – dye adsorption (via innersphere complex formation) does not occur at these sites at any pH. However, a number of alternative explanations are also possible. Interestingly, a modest variation in r_i (initial photocatalytic rate) as a function of pH appears a common feature of both anionic and cationic (such as methylene blue) dyes when used to assess the activity of P-25 titania.[11] Clearly, further work is required to ascertain the underlying cause(s) for this notable, apparently common, largely

indifferent variation in rate as a function of pH for anionic and cationic dyes when used to test titania under UV SPC conditions.

4.2 $AO7^-$ Sensitised Bleaching using Visible Light

As noted earlier, $AO7^-$ can also be photobleached via a dye-sensitised process in which the electronically excited state of the dye, $AO7^{-*}$, injects an electron into the conduction band of the titania to produce an oxidised dye radical, $AO7^{\bullet}$, which is unstable and capable of decomposition into colourless products, i.e.

$$AO7^{-*} + TiO_2 \rightarrow AO7^{\bullet} + TiO_2\,(e^-) \qquad (4.7)$$

Since $AO7^-$ does not absorb strongly in the UV, this dye-sensitised process is most easily and usually demonstrated using an intense visible light, such as provided by a Xe-arc light. Thus, using the same in situ reaction conditions as described previously, but with a 180 W Xe-arc light, combined with a 400 nm cut-off filter, the initial rate of dye photobleaching was measured as a function of pH and the results are also illustrated in figure 4.6. These results show the rate increases from a small value at pH 6 to a significant rate at pH 2, much like the fraction of sites occupied by adsorbed dye on the TiO_2 increases with decreasing pH (see figure 4.7). Indeed, the insert diagram in figure 4.7, which shows a plot of r_i values measured using visible light at different pHs versus the multimer CD-MUSIC model-calculated value of f_{AO7}, reveals a clear, if not simple, correlation between the two parameters. This correlation seems appropriate given the nature of the key process, i.e. reaction 4.7, and its implication that only dye molecules that are in direct contact with the surface can undergo photodegradation via such a dye-sensitised route.[37] Note however, at surface coverages approaching or exceeding a monolayer, as might be expected using high dye concentrations, dye excited state annihilation and self-quenching processes can compete with the charge injection process and so decrease the efficiency of dye-sensitised photobleaching.[37] The latter effect may be responsible

for the apparent negative deviation from linearity in the insert plot at high values of r_i versus f_{AO7}.

4.3 Conclusions

The observed adsorption of $AO7^-$ on P-25 titania over a range of pH values (pH 2 – 8) is well described using a CD-MUSIC model which accounts for dye aggregation in solution and subsequent adsorption of these aggregates. The model predicts the apparent dark Langmuir adsorption constant, K_L, and the number of adsorption sites, n_o, increases with decreasing pH, as has been observed by others.[9,40]

The rate of bleaching of $AO7^-$, photocatalysed by titania using UV light, appears to increase modestly (by a factor < 2) over the pH range 2 – 10, despite the fact that $AO7^-$ adsorption on P-25 titania is not significant above pH 6 and increases almost linearly and markedly below pH6, covering ca. 32% of the singly co-ordinated surface sites at pH 2 under *in-situ* experimental conditions ($[TiO_2]$ = 20 mg dm^{-3}; $[AO7^-]_{total} = 4.86 \times 10^{-5}$ M). The reasons for the lack of a strong dependency of initial rate of photobleaching upon f_{AO7} remain unclear. In contrast, the initial rate of bleaching of $AO7^-$ via a visible light-driven, dye-sensitised process, appears to correlate to some degree with f_{AO7} at different pHs, as expected given that the reaction mechanism implies only dye molecules that are in direct contact with the surface can undergo photodegradation via a dye-sensitised route.

5 Adsorption and Destruction of Acid Orange 7 on Titania Paste Films

Previously, chapters 3 and 4 have looked at the adsorption and destruction of dye on P-25 powder. This section will briefly look at these processes using titania paste films. The paste was prepared and cast as detailed in sections 2.2.2 and 2.2.3. Paste films allow the straightforward generation of adsorption isotherms as there is no need for filtering and/or centrifuging and the mass of semiconductor is constant for each measurement. In this set of experiments, the dark Langmuir adsorption constant, K_L, and the number of adsorption sites, n_o, was experimentally determined as detailed in the introduction (section 1.2).

Adsorption isotherms for $AO7^-$, using a range of concentrations of staining solutions (5 – 700 mg dm^{-3}) for each pH were obtained using the procedure detailed in section 2.2.6. In order to accurately determine the amount of dye adsorbed, the stained disk was submerged in 100 mL of 0.001 M NaOH. This inverted the charge of the titania surface and repelled the dye into solution. The absorbance of the solution was then measured to calculate the number of moles of dye adsorbed on the paste film. This was then divided by the average mass of titania on each paste film (c.a. 2.6 mg) to give a value of micromoles per gram of catalyst. This method was preferred as, at high concentrations of staining solution, measuring the change in absorbance of the staining solution would involve applying appropriate dilutions to ensure the dye was mainly monomeric to accurately determine how much dye was adsorbed.

One nice quality about paste films is the fact that the spectrum of the adsorbed dye can easily be obtained by recording the absorption spectra of the film using a spectrophotometer. Thus, figure 5.1 shows the spectra of the wet paste films after soaking for 1 hour in concentrations ranging from 20 mg dm^{-3} to 700 mg dm^{-3} of $AO7^-$ at pH 2. The spectra of a dilute (mostly monomeric) solution of 1 x 10^{-5} M $AO7^-$ in pH 2 HNO_3 is shown by the broken line in figure 5.1, where λ_{max} is at 484 nm. The shape of the spectra of the stained films indicate the adsorption of species other than the monomer, i.e. multimers, as the λ_{max} of the spectra has shifted down towards 400 nm. This is evident even at low concentrations suggesting that the

decision to include the adsorption of multimer species for the modelling of the adsorption of dyes on P-25 is justified. However, the shift in the λ_{max} of the adsorbed dye could be due to the possibility that the inner sphere complex of the dye with the semiconductor surface may have a different spectrum than that of dye monomers and multimers. Another possibility to note could be that the azo form of $AO7^-$ (λ_{max} 430 nm)[43] could be stabilised somehow upon adsorption, hence the shift in the spectra is due to the dominance of the azo over the hydrazone form (λ_{max} 484 nm).[43]

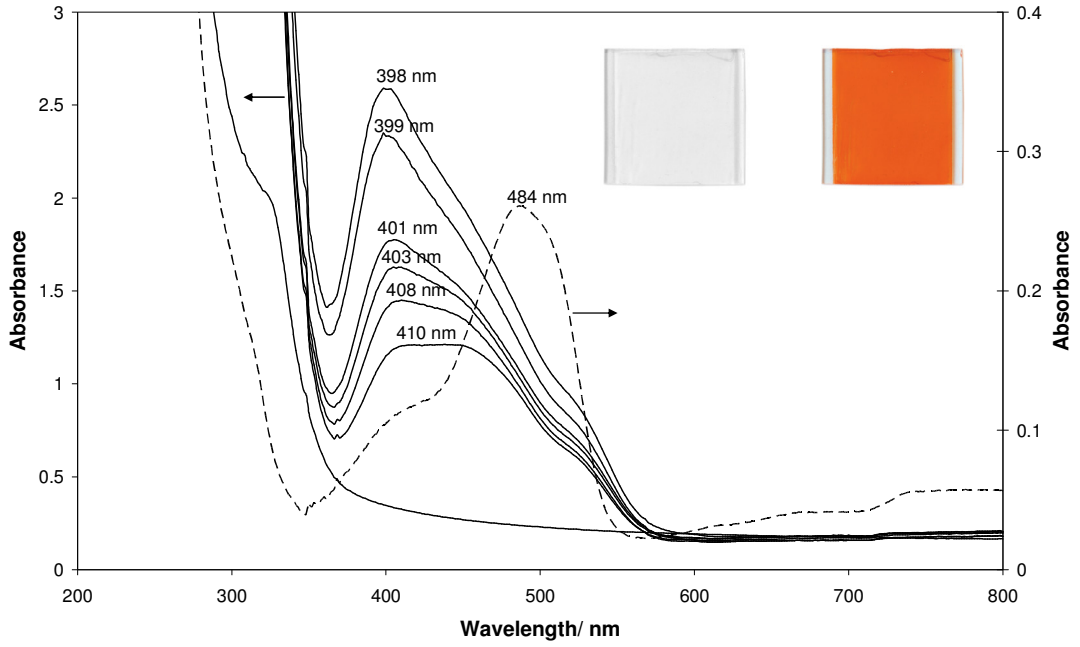

Figure 5.1 The solid lines show the increasing adsorption spectra of stained paste films using; 20, 40, 90, 300, 500 and 700 mg dm^{-3} $AO7^-$ staining solutions at pH 2. The broken line shows a dilute (1 x 10^{-5} M) solution of $AO7^-$ which is mostly monomeric. The inserted picture shows a paste film before and after being stained in 300 mg dm^{-3} of $AO7^-$. The λ_{max} values are given above each spectra.

Adsorption isotherms were generated with and without the use of 0.01 M background electrolyte (NaCl). The isotherms generated without NaCl present are shown in figure 5.2 and those generated using NaCl are shown in figure 5.3. The same paste films were used for all concentrations at each pH for each dye to ensure that variation in performance between films did not affect the results as the mass of titania and the porosity would be constant.

The Langmuir adsorption isotherms in figures 5.2 and 5.3 were analysed as detailed in section 1.2 to determine, K_L, and, n_o, values. These values are tabulated in table 5.1.

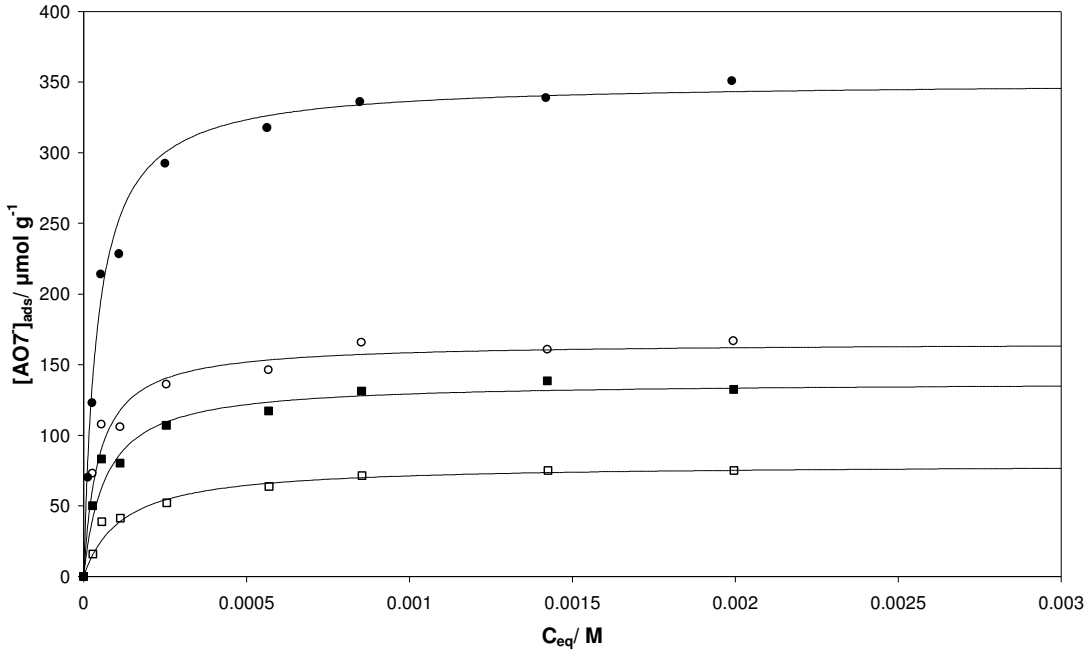

Figure 5.2 Adsorption isotherms for acid orange 7 on paste films at various pH values; (●) pH 2, (○) pH 3, (■) pH 4 and (□) pH 5, with no NaCl present. The solid 'best fit' lines were generated by inserting the determined, K_L, and, n_o, from double reciprocal plots (as detailed in section 1.2) into equation 1.7.

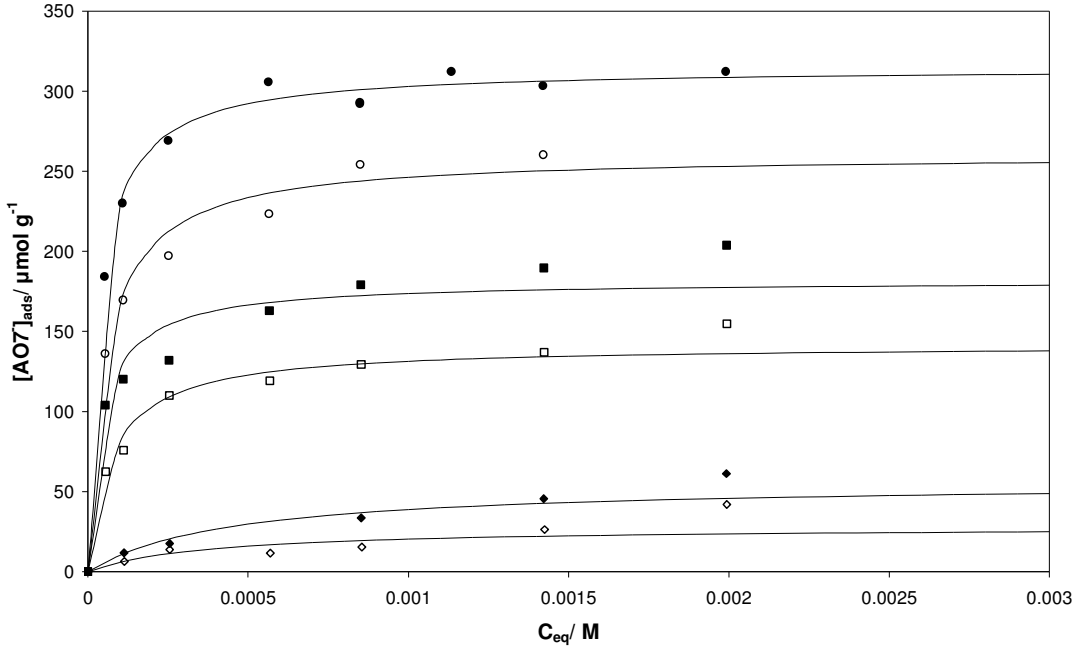

Figure 5.3 Langmuir adsorption isotherms for acid orange 7 on paste films at various pH values; (●) pH 2, (○) pH 3, (■) pH 4, (□) pH 5, (♦) pH 5.5 and (◊) pH 6, containing 0.01 M NaCl. The solid 'best fit' lines were generated by inserting the determined, K_L, and, n_o, from double reciprocal plots (as detailed in section 1.2) into equation 1.7.

Table 5.1 K_L, and, n_o, values determined from double reciprocal plots of the data in figures 3.15 and 3.16 for acid orange 7 (with and without background electrolyte).

	With NaCl		No NaCl	
pH	**K_L/ M^{-1}**	**n_o/ µmol g^{-1}**	**K_L/ M^{-1}**	**n_o/ µmol g^{-1}**
2	26903	313	23906	350
	(1 x 10^3)	(3)	(2 x 10^3)	(21)
3	21131	251	21943	166
	(2 x 10^3)	(10)	(2 x 10^3)	(8)
4	22123	182	15225	138
	(4 x 10^3)	(11)	(2 x 10^3)	(9)
5	14329	136	8564	80
	(2 x 10^3)	(8)	(2 x 10^3)	(13)
5.5	2270	56		
	(5 x 10^2)	(12)		
6	2647	28		
	(1 x 10^3)	(9)		

Figures 5.4 and 5.5 show plots of the trends in, K_L, and, n_o, for acid orange 7 using the values listed in table 5.1. Both plots show, K_L, and, n_o, decrease as the p.z.c. of the titania is approached (pH 6.6) as previously noted for the powder work in section 3.2.

A surprising finding in this work is the fact that no significant difference between, K_L, and, n_o, was observed when adding background electrolyte. Figure 3.3 showed how the charging behaviour of the titanias' surface is influenced by the presence of NaCl, suggesting there would be some noticeable difference in the adsorption of the dyes. It is not clear why the presence of NaCl does not influence greatly the variation in, K_L, versus pH illustrated in figure 5.4.

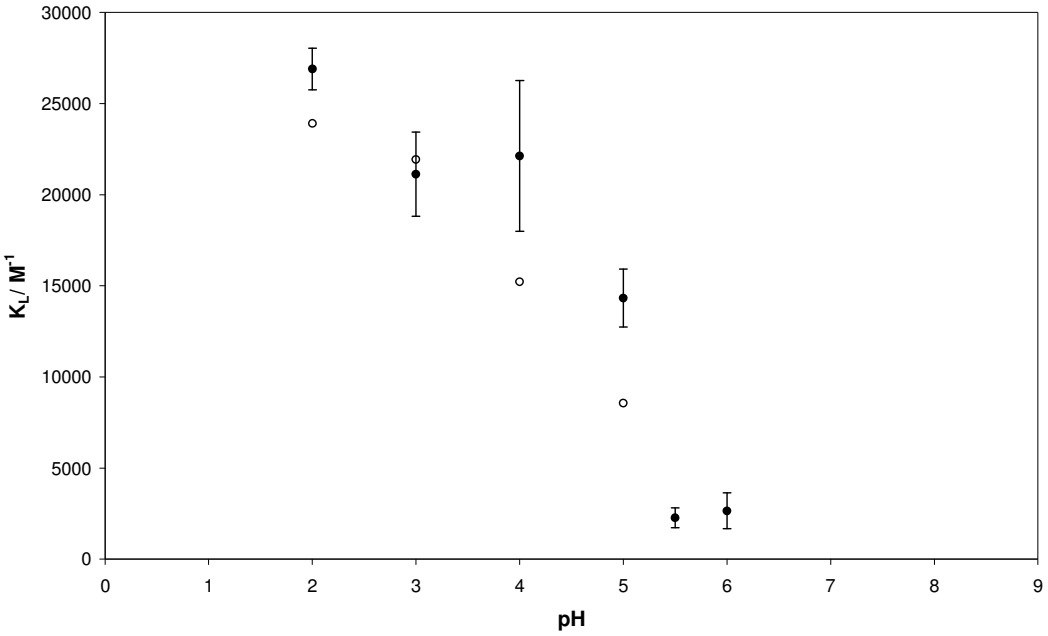

Figure 5.4 Observed trends in adsorption constant, K_L, for acid orange (●) with and (○) without 0.01 M NaCl.

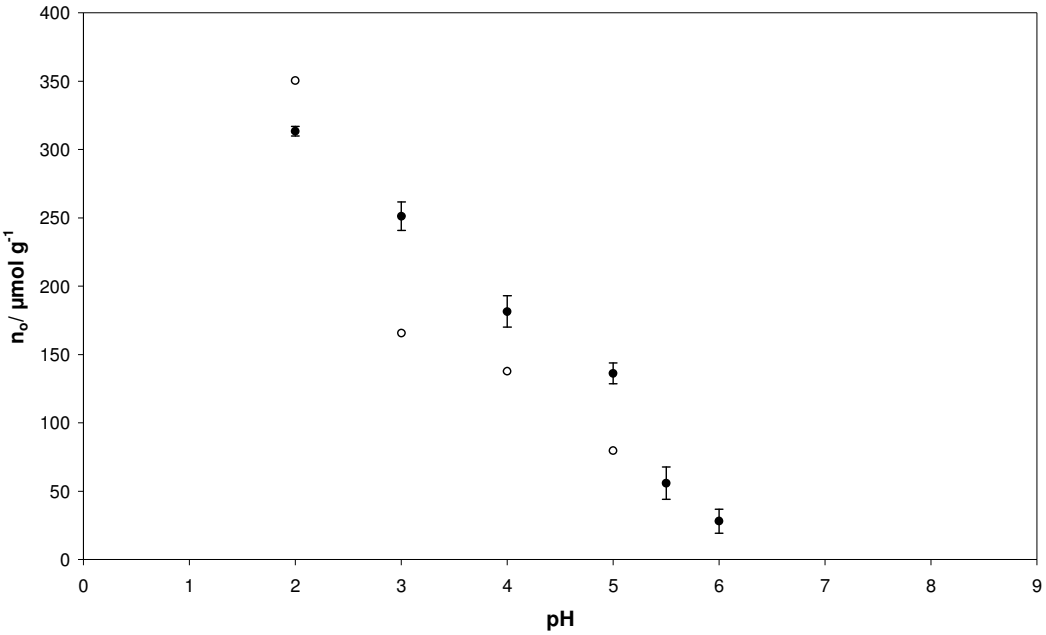

Figure 5.5 Observed trends in maximum number of adsorption sites, n_o, for acid orange 7 (●) with and (○) without NaCl.

5.1 FTIR Spectra of $AO7^-$ Stained Paste Films

Since normal borosilicate glass would cut out the transmission in the fingerprint region in an FTIR study of the adsorption of $AO7^-$, calcium fluoride disks were used to support the paste film. Figure 5.6 shows the same changes in the IR bands as observed for the P-25 powder adsorption study.

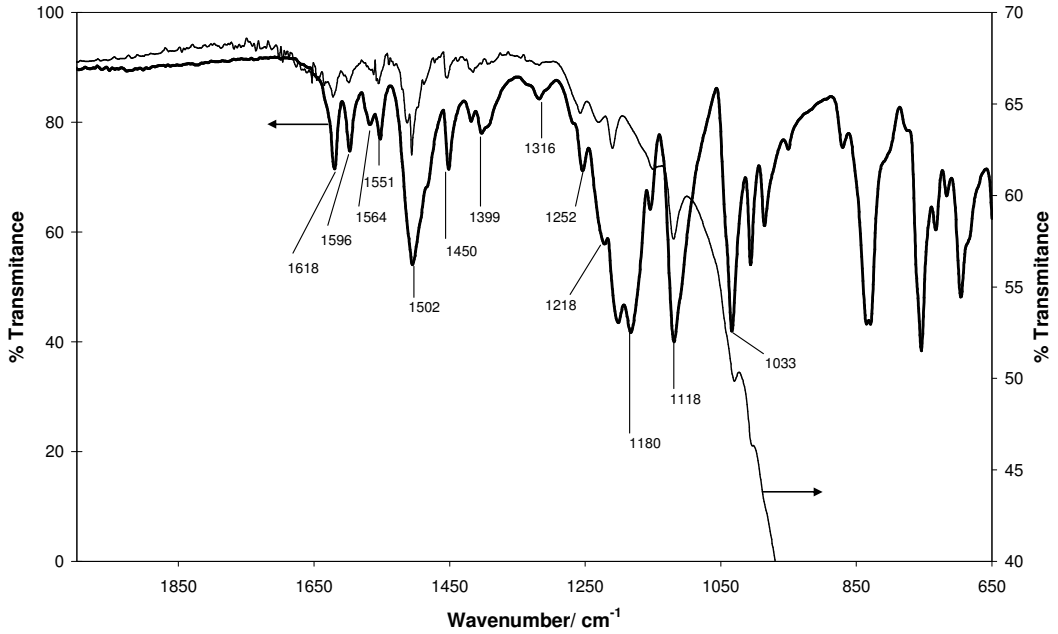

Figure 5.6 FTIR spectra of $AO7^-$ powder (thick black line) and $AO7^-$ stained paste film (thin black line) using 300 mg dm^{-3} of $AO7^-$ at pH 2.

A detailed assignment of the bands in the region of 2000 – 1000 cm^{-1} have reported previously by Stylidi *et al.*[2] The band at 1502 cm^{-1} has been linked to either the -N=N- vibrations or to the aromatic ring vibrations which are interacting with the azo bond. Bands at 1450, 1551, 1564, 1596 and 1618 cm^{-1} are linked to the skeletal vibrations of the aromatic rings. The small peak at 1399 cm^{-1} can be attributed to the OH bending vibrations. Peaks at 1316 cm^{-1} and 1180 cm^{-1} are due to the sulfonate group, $\upsilon_{as}(SO_3)$ and $\upsilon_s(SO_3)$ respectively, and those at 1252 cm^{-1} and 1218 cm^{-1} arise from the tautomer form of the dye and correspond to the vibration stretching modes of υ(C-N) and υ(N-N) respectively. The bands at 1118 cm^{-1} and 1033 cm^{-1} can be assigned to the coupling between the benzene mode and $\upsilon_s(SO_3)$. As observed with the P-25 powder in section 3.2, upon adsorption of the dye onto the P-25 surface, two bands in the FTIR spectrum disappear at 1316 cm^{-1} and 1180 cm^{-1} which correspond to the sulfonate group. This suggests a strong interaction of the two oxygen atoms of the sulfonate group with the titania surface. Despite the different nature of the titania this implies the adsorption of $AO7^-$ is similar for both powder dispersions and supported paste films.

5.2 Destruction of $AO7^-$ on Paste Films

All irradiations in this section were carried out under *in-situ* monitoring conditions (i.e. $[AO7^-]_{total} = 4.86 \times 10^{-5}$ M) in which the initial rates of dye bleaching, r_i (units: absorbance units min^{-1} or Abs U min^{-1}) photosensitised by UV excited titania, were measured as a function of pH. The results of this work are illustrated in figure 5.7. Blank experiments (i.e. without TiO_2) show no bleaching of colour at the extremes of pH (pH 2 and pH 10) showing that $AO7^-$ is very UV stable.

Compared with the results of the P-25 powder irradiations, the same trend is observed, i.e. the rate increases by less than a factor of 2 over the pH range 2 to 10. The paste films however provide a slightly slower rate of photodegradation (by a factor of < 2). As mentioned previously, these findings are not too dissimilar to those reported by Verykios *et al.*[22] and Augugliaro *et al.*[42], whose results are shown in figures 5.8 and 5.9 respectively. Verykios *et al.*[22] found the rate of photobleaching under solar-simulator Xe-arc light irradiation to be pH independent over the range pH 2 – 9, but faster at pH 10 – 12. Augugliaro [42] and his co-workers reported that whilst the rate of photobleaching of $AO7^-$ under solar light irradiation dipped at pH 6, at pH 2 and 11 the rates were similar. The above two reports are complicated by the fact that dye bleaching can occur by both semiconductor photocatalysis and dye photosensitisation as solar, or solar simulated, light was used.

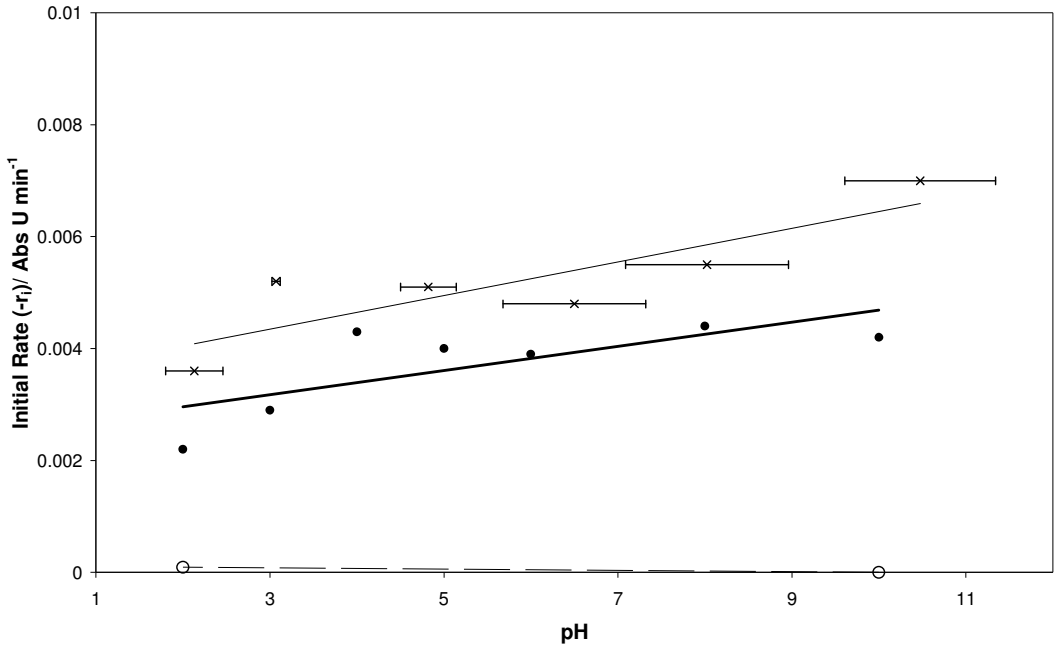

Figure 5.7 Measured initial rate of UVA photobleaching of $AO7^-$ using paste films (●) (in units of absorbance units at 484 nm per min, i.e. Abs U min^{-1}) as a function of pH for experiments conducted under *in-situ* conditions ($[AO7^-]_{total}$ = 4.86 x 10^{-5} M), using two 8 W BLB lamps (UVA: 2 mW cm^{-2}). Blank irradiations for $AO7^-$ (○) show the dye is UV stable. The results for the P-25 powder UVA irradiations (×) from section 3.2.1 are shown as a comparison to the paste films.

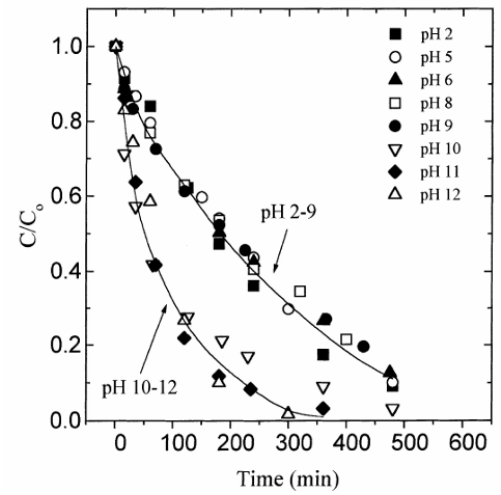

Figure 5.8 Effect of the initial pH on the decolourisation of aqueous solutions of acid orange 7 where $[AO7^-]$ = 300 mg dm^{-3} and $[TiO_2]$ = 750 mg dm^{-3}.[22]

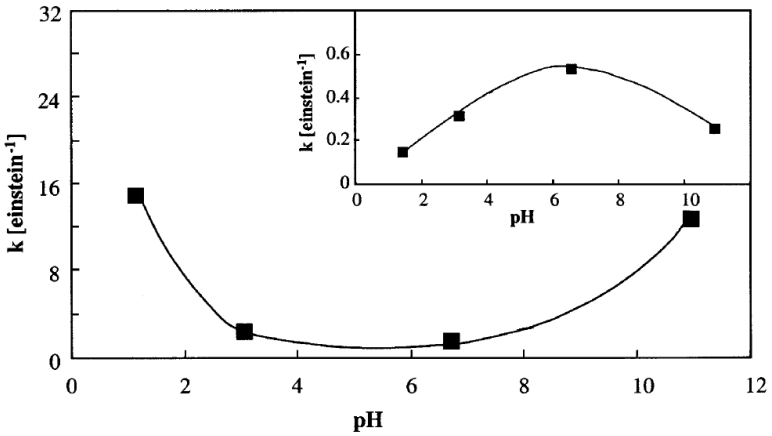

Figure 5.9 Rate constant values for the degradation of $AO7^-$ versus pH and corresponding rate constant values of TOC reduction (in the inset). Where $[AO7^-]$ = 2.86 x 10^{-5} M and $[TiO_2]$ = 200 mg dm^{-3}.

The visible light photobleaching of $AO7^-$ (shown in figure 5.10) shows a steady linear increase of the rate as the pH is lowered (i.e. $[AO7^-]_{ads}$ is increased) with the only outlier at pH 2 where the rate drops. The drop could possibly be due to screening as a result of the large concentration of dye adsorbed, preventing the visible light getting to the dye in direct contact with the surface. Blank irradiations show very little colour depletion over the pH range studied. The surprising finding from the visible irradiations of the paste films is that at pH 6 and above there is still an appreciable rate of destruction although there is very little dye adsorbed on the surface. The reason for this is unclear. This is not the case with the P-25 irradiations which is also shown in figure 3.22, where the rate drops almost to zero at pH 6 and above.

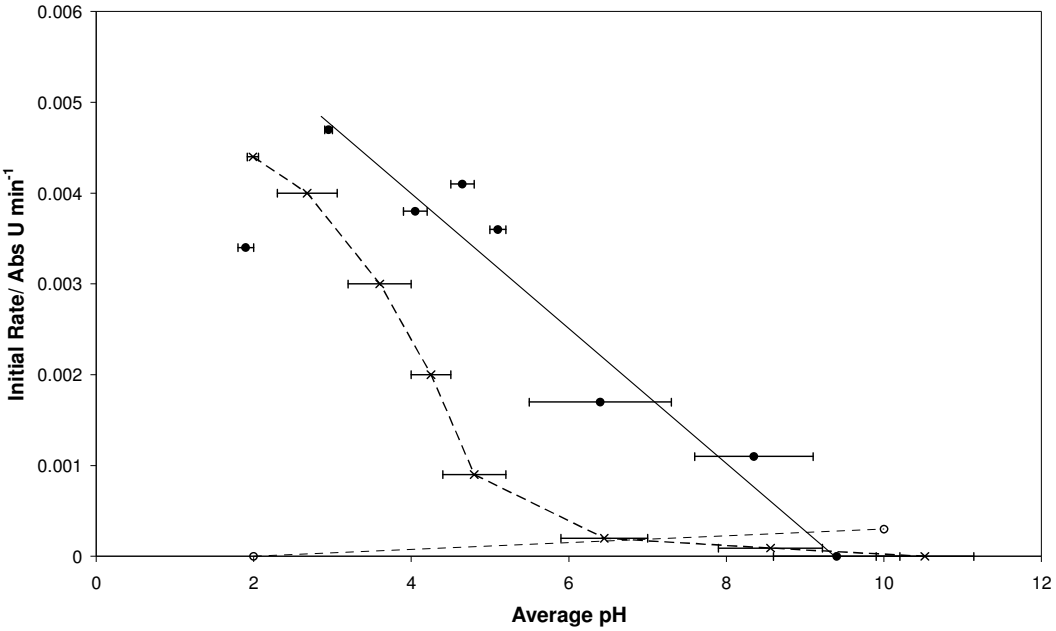

Figure 5.10 Measured initial rate of photobleaching of $AO7^-$ (●) (in units of absorbance units at 484 nm per min, i.e. Abs U min^{-1}) as a function of pH for experiments conducted under *in-situ* conditions ($[AO7^-]_{total}$ = 4.86 x 10^{-5} M) using a 150 W Xe-arc lamp with a 400 nm filter (i.e. a visible – no UV – light source). The blank irradiations (○) show very little colour loss over the pH range (pH 2 – 10). The results for the P-25 powder visible irradiations (×) from section 3.2.1 are shown as a comparison to the paste films.

5.3 Conclusions

It was observed for $AO7^-$ that, as the pH is decreased from pH 6 to pH 2, $[AO7^-]_{ads}$ increases and subsequently, K_L, and, n_o, increases, which is expected due to the increasing positive charge on the titania surface as the pH becomes more acidic. Above pH 6 the amount of $AO7^-$ adsorbed becomes negligible.

As observed for the P-25 dispersions, the rate of bleaching of $AO7^-$, photocatalysed by titania paste films using UV light, appears to increase modestly (by a factor < 2) over the pH range 2 – 10. The system is complicated by the fact that the depletion of colour can also occur through a dye-sensitised process, so the reason for this lack of a strong dependency remains unclear. The initial rate of bleaching using visible light

however showed a significant dependence on the amount of dye adsorbed as the rate increased as the pH became more acidic. This is to be expected as the dye has to be in direct contact with the semiconductor surface in order to inject an electron.

6 Further Work

The multimer CD-MUSIC model should be used to model the adsorption of the dyes on paste films as well as on P-25 titania. The experimentally determined trends in, K_L, and, n_o, for paste films are very similar to those generated for P-25 powder dispersions, suggesting that there should be no problem in fitting calculated curves to the data.

Further work should be carried out for methylene blue on paste films. Initial experiments found some strange trends in the destruction rates which should be investigated further.

Different sources/forms of titania could also be investigated to see if they perform differently. As there is a wide range of other metal oxide semiconductors available, an interesting study could be performed using different semiconductors with different p.z.c.'s to see if the same trends are observed but shifted with respect to the p.z.c.

7 Appendix A

Tables A1 and A2 (below) defines the formation of each species in terms of the following components (columns): dissolved species, surface species and electrostatic components. The latter are defined in terms of the expression exp(-$F\Psi_i/RT$), with i = 0, 1 and 2 for the corresponding planes (see figure 3.2). The species concentrations are calculated using the coefficients in tables A1 and A2, where, reading across the table, the general expression for the species concentration, S (units: M) is:

$$[S] = \Pi [C_K]^{nk} \, 10^{\log K} \tag{A1}$$

Where C_k is the component's concentration (units: M), including electrostatic components, exp(-$F\Psi_i/RT$), surface components ($TiOH^{-1/3}$ and $Ti2O^{-2/3}$) and solution components. The coefficients n_k are in the rows. The final column comprises the relevant expressions for the logarithms of the intrinsic reaction equilibrium constants with, where appropriate, concentration terms of known components.

Briefly the equations in the CD-MUSIC model can be solved using the parameters in tables 3.2 and 4.1 and the functions generated using tables A1 and A2 for MB^+ and $AO7^-$ respectively. Thus, it can be shown for titania that:

$$\Sigma_1 = (\rho A / F)(\sigma + N_S) \tag{A2}$$

For a given pH, a set of potentials, Ψ_0, Ψ_1 and Ψ_d (=Ψ_2) are chosen so that a value for Σ_1 and then σ_0 (via equation A2) can be calculated.

Similarly, the summations:

$$\Sigma_2 = (\rho A / F)\sigma_1 \tag{A3}$$

And

$$\Sigma_3 = (\rho A / F)\sigma_2 \tag{A4}$$

Allow values for σ_1 and σ_2 to be calculated. However, these values must also be related to each other via the following electrostatic equations:

$$\sigma_0 = C_1(\psi_0 - \psi_1) \tag{A5}$$

$$\sigma_0 + \sigma_1 = C_2(\psi_1 - \psi_2) \tag{A6}$$

$$\sigma_0 + \sigma_1 + \sigma_2 + \sigma_{ddl} = 0 \tag{A7}$$

Where

$$\sigma_{ddl} \text{ (units } \mu\text{C cm}^{-2}) = -11.72c^{1/2}\sinh(zF\psi_d / RT) \tag{A8}$$

Where c is the background electrolyte concentration. Thus, for any pH, by varying the values of Ψ_0, Ψ_1 and Ψ_d (= Ψ_2) eventually a unique set of values for these potentials can eventually be obtained which generate σ_0, σ_1, σ_2 and σ_{ddl} values (via equations: A2 – A4 and A8, respectively) that are the same as those generated using eqns A5 and A6 and which also satisfy the need for overall electroneutrality, i.e. equation A8. In this work the optimisation process was carried out using an in-house written, macro incorporated in Excel. Others[18,34] use the significantly faster and equally effective ECOSAT program for calculating chemical equilibria. Both approaches generate the same data sets for both basic Stern (i.e. MUSIC) and three plane (CD-MUSIC) model calculations.

In applying the CD-MUSIC model it is assumed monomers, dimers and trimers of MB^+ present in solution adsorb onto the surface of the titania, and co-adsorbed hydroxyl ions modify the charge of the aggregated forms as indicated by reactions (3.12) and (3.13). In running the model the following were used: the surface species rows in table A1, along with the knowledge of the total dye concentration and the fraction of that which is in solution in monomeric form (from figure 3.1) and the values of the various constants, such as K_{MB1}, K_{MB2} and K_{MB3}, given in table 3.2.

In applying the CD-MUSIC model as proposed by Bourikas and his co-workers,[16] where $AO7^-$ is assumed to be monomeric in solution and adsorb onto the surface as such, the last 2 surface species rows in table A2 are not applicable and the value of

$K_{AO7\text{-}in}$ used is given in table 4.1. In extending this model to allow for the monomers, dimers and trimers of $AO7^-$ present in solution to adsorb equally well onto the surface of the titania, all surface species rows in table A2 are used, along with the knowledge of the total dye concentration and the fraction of that which, in solution, is in monomeric form (from figure 4.1) and the revised value of $K_{AO7\text{-}in}$ given in table 4.1.

Table A1 Surface speciation for the adsorption of MB^+ on the surface of P-25 titania

	Dissolved Component				**Surface Component**		**Electrostatic Component**			
Surface Species	**H^+**	**Na^+**	**Cl^-**	**$AO7^-$**	**$TiOH^{-1/3}$**	**$Ti_2O^{-2/3}$**	$e^{-F\Psi_0/RT}$	$e^{-F\Psi_1/RT}$	$e^{-F\Psi_2/RT}$	$\log K$
$TiOH^{-1/3}$	0	0	0	0	1	0	0	0	0	0
$Ti_2O^{-2/3}$	0	0	0	0	0	1	0	0	0	0
$TiOH_2^{+2/3}$	1	0	0	0	1	0	1	0	0	$\log K_H$
$Ti_2OH^{+1/3}$	1	0	0	0	0	1	1	0	0	$\log K_H$
$TiOH^{-1/3}$–Na^+	0	1	0	0	1	0	0	0	1	$\log K_{Na^+}$
$Ti_2O^{-2/3}$–Na^+	0	1	0	0	0	1	0	0	1	$\log K_{Na^+}$
$TiOH_2^{+2/3}$–NO_3^-	1	0	1	0	1	0	1	0	-1	$\log K_{NO_3^-} + \log K_H$
$Ti_2OH^{+1/3}$–NO_3^-	1	0	1	0	0	1	1	0	-1	$\log K_{NO_3^-} + \log K_H$
$TiOH\text{-}MB^{+2/3}$	2	0	0	1	2	0	1.5	-0.5	0	$\log K_{MB1}$
$TiOH((MB^+)_2OH^-)_2^{+2/3}$	2	0	0	2	2	0	1.5	-1.5	0	$\log K_{MB2} + \log K_W + \log K_D$
$TiOH((MB^+)_3(OH^-)_2)_2^{+2/3}$	2	0	0	3	2	0	1.5	-2.5	0	$\log K_{AO7} + 2\log K_W + \log(K_D K_{Tr})$
Sum							Σ_0	Σ_1	Σ_2	

Table A2 Surface speciation for the adsorption of $AO7^-$ on the surface of P-25 titania

	Dissolved Component				Surface Component		Electrostatic Component			
Surface Species	H^+	Na^+	Cl^-	$AO7^-$	$TiOH^{-1/3}$	$Ti_2O^{-2/3}$	$e^{-F\Psi_0/RT}$	$e^{-F\Psi_1/RT}$	$e^{-F\Psi_2/RT}$	$\log K$
$TiOH^{-1/3}$	0	0	0	0	1	0	0	0	0	0
$Ti_2O^{-2/3}$	0	0	0	0	0	1	0	0	0	0
$TiOH_2^{+2/3}$	1	0	0	0	1	0	1	0	0	$\log K_H$
$Ti_2OH^{+1/3}$	1	0	0	0	0	1	1	0	0	$\log K_H$
$TiOH^{-1/3}$–Na^+	0	1	0	0	1	0	0	0	1	$\log K_{Na^+}$
$Ti_2O^{-2/3}$–Na^+	0	1	0	0	0	1	0	0	1	$\log K_{Na^+}$
$TiOH_2^{+2/3}$–Cl^-	1	0	1	0	1	0	1	0	-1	$\log K_{Cl^-} + \log K_H$
$Ti_2OH^{+1/3}$–Cl^-	1	0	1	0	0	1	1	0	-1	$\log K_{Cl^-} + \log K_H$
$Ti_2AO7^{1/3}$	2	0	0	1	2	0	1.5	-0.5	0	$\log K_{AO7}$
$Ti_2(AO7)_2^{-1/3}$	2	0	0	2	2	0	1.5	-1.5	0	$\log K_{AO7} + \log K_D$
$Ti_2(AO7)_3^{-4/3}$	2	0	0	3	2	0	1.5	-2.5	0	$\log K_{AO7} + \log(K_D K_{Tr})$
Sum							Σ_0	Σ_1	Σ_2	

8 References

1. A. Mills, S-K Lee, J. Photochem. Photobiol A: Chem. 152 (2000) 233–247.
2. M. Stylidi, D.I. Kondarides, X.E. Verykios, Appl. Catal. B 40 (2003) 271–286.
3. A. Houas, H. Lachheb, M. Ksibi, E. Elaloui, C. Guillard, J.M. Herrmann, Appl. Catal. B. 31 (2001) 145–157.
4. M.A. Brown, S.C. De Vito Crit. Rev. Environ. Sci. Technol. 23 (1993) 249–324.
5. http://www.iso.org/iso/iso_catalogue/catalogue_tc/catalogue_detail.htm?csnumber=31807 (Accessed: October 2010).
6. C. Guillard, E. Puzenat, H. Lachheb, A. Houas, J.M. Herrmann, Int. J. Photoen. 7 (2005) 1–9.
7. http://www.pilkingtonselfcleaningglass.co.uk/how-it-works/ (Accessed: July 2010)
8. http://www.iso.org/iso/iso_catalogue/catalogue_tc/catalogue_detail.htm?csnumber=46019 (Accessed: October 2010).
9. K. Rajeshwar, M.E. Osugi, W. Chanmanee, C.R. Chenthamarakshan, M.V.B. Zanoni, P. Kajitvichyanukul, R. Krishnan-Ayer, J. Photochem. Photobiol., C 9 (2008) 171–192.
10. H. Yoneyama, Y. Toyoguchi, H. Tamura, J. Phys. Chem. 76 (1972) 3460–3464.
11. H. Lachheb, E. Puzenat, A. Houas, M. Ksibi, E. Elaloui, C. Guillard, J.M. Herrmann, Appl. Catal. B. 39 (2002) 75–90.
12. C. Guillard, H. Lachheb, A. Houas, M. Ksibi, E. Elaloui, J.M. Herrmann, J. Photochem. Photobiol A: Chem. 158 (2003) 27–36.
13. T. Zhang, T. Oyama, A. Aoshima, H. Hidaka, J. Zhao, N. Serpone, J. Photochem. Photobiol A: Chem. 140 (2001) 163–172.
14. S. Lakshmi, R. Renganathan, S. Fujita, J. Photochem. Photobiol A: Chem. 88 (1995) 163–167.
15. A. Mills, J. Wang, J. Photochem. Photobiol A: Chem. 127 (1999) 123–134.
16. R.W. Matthews, J. Chem. Soc., Faraday Trans. 1, 85 (1989) 1291–1302.
17. C. Bauer, P. Jacques, A. Kalt, Chem. Phys. Lett. 307 (1999) 397–406.
18. K. Bourikas, M. Stylidi, D.I. Kondarides, X.E. Verykios, Langmuir 21 (2005) 9222–9230.

19. J. Bandara, J.A. Mielczarski, J. Kiwi, Langmuir 15 (1999) 7670–7679.
20. G. Li, X.S. Zhao, M.B. Ray, Sep. Purif. Technol. 55 (2007) 91–97.
21. K. Vinodgopal, D.E. Wynkoop, P.V. Kamat, Environ. Sci. Technol. 30 (1996) 1660–1666.
22. F. Kiriakidou, D.I. Kondravides, X.E. Verykios, Catal. Today 54 (1999) 119–130.
23. I.K. Konstantinou, T.A. Albanis, Appl. Catal., B, 49 (2004) 1–14.
24. K. Wang, J. Zhang, L. Lou, S. Yang, Y. Chen, J. Photochem. Photobiol., A: Chem.165 (2004) 201–207
25. K. Bourikas, Private Communication.
26. http://www.molecularinfo.com/MTM/UV.pdf (Accessed: August 2010).
27. http://las.perkinelmer.co.uk/content/TechnicalInfo/TCH_FTIRATR.pdf (Accessed August 2010).
28. A. Mills, N. Elliott, G. Hill, D. Fallis, J.R. Durrant R.L. Willis Photochem. Photobiol. Sci. 2 (2003) 591–596.
29. A.K. Ghosh, P. Mukerjee, J. Am. Chem. Soc. 92 (22) (1970) 6408–6412.
30. X. Yan, T. Ohno, K. Nishijima, R. Abe, B. Ohtani, Chem. Phys. Lett. 429 (2006), 606–610.
31. R.F.P. Nogueira, W.F. Jardim, J. Chem. Educ. 70 (1993), 861–862.
32. P. Reeves, R. Ohlhausen, D. Sloan, K. Pamplin, T. Scoggins, C. Clark, B. Hutchinson, D. Green, Sol. Energy 48 (1992), 413–420.
33. P. Venema, T. Hiemstra, W.H. Van Riemsdijk, J. Colloid Interface Sci. 181 (1996), 45–59.
34. K. Bourikas, T. Hiemstra, W.H. Van Riemsdijk, Langmuir 17 (2001), 749–756.
35. T. Hiemstra, W.H. Van Riemsdijk, J.Colloid Interface Sci. 179 (1996) 488–508.
36. O. Impert, A. Katafias, P. Kita, A. Mills, A. Pietkiewicz–Graczyk, G. Wrzeszcz, Dalton Trans. 3 (2003), 348–353.
37. K.R. Gopidas, P.V. Kamat, J. Phys. Chem. 93 (1989), 6428–6433.
38. B. Simončič, J. Špan, Dyes Pigm. 26 (1994) 257–276.
39. K.M. Kale, E.L. Cussler, D.L. Evans, J. Phys. Chem. 84 (1980) 593–598.
40. B. Milicevic, G. Eigenmann, Helv. Chim. Acta 14(1964) 1039-1043.

41. R.L. Reeves, M.S. Maggio, S.A. Harkaway, J. Phys. Chem. 83 (18) (1979) 2359–2368.
42. V. Augugliaro, C. Baiocchi, A.B. Prevot, E. García-López, V. Loddo, S. Malato, G. Marcí, L. Palmisano, M. Pazzi, E. Pramauro, Chemosphere 49 (2002) 1223–1230.
43. C. Bauer, P. Jacques, A. Kalt, J. Photochem. Photobiol., A: Chem. 140 (2001) 87–92.